ISSN 1857–9027
e-ISSN 1857–9949

МАКЕДОНСКА АКАДЕМИЈА НА НАУКИТЕ И УМЕТНОСТИТЕ

ОДДЕЛЕНИЕ ЗА ПРИРОДНО-МАТЕМАТИЧКИ И БИОТЕХНИЧКИ НАУКИ

MACEDONIAN ACADEMY OF SCIENCES AND ARTS

SECTION OF NATURAL, MATHEMATICAL AND BIOTECHNICAL SCIENCES

ПРИЛОЗИ
CONTRIBUTIONS

39

(1)

СКОПЈЕ – SKOPJE
2018

Publisher: Macedonian Academy of Sciences and Arts

*

Printed by: Vinsent Grafika, Skopje

*

Number of copies: 300

*

June 2018

Published twice a year
The Contributions, Sec. Nat. Math. Biotech. Sci. is indexed in:
Chemical Abstracts, Mathematical Reviews, Google Scholar, EBSCO and DOAJ

http://manu.edu.mk/contributions/NMBSci/

Прилози, Одд. прир. мат. биотех. науки, МАНУ	Том	Бр.	стр.	Скопје
	39	1	1–78	2018
Contributions, Sec. Nat. Math. Biotech. Sci., MASA	Vol.	No.	pp.	Skopje

TABLE OF CONTENTS

С О Д Р Ж И Н А

ПРИЛОЗИ, Одделение за природно-математички и биотехнички науки, МАНУ, том **39**, бр. 1, стр. 5–14 (2018)
CONTRIBUTIONS, Section of Natural, Mathematical and Biotechnical Sciences, MASA, Vol. **39,** No. 1, pp. 5–14 (2018)

Received: November 7, 2017
Accepted: December 12, 2017

ISSN 1857–9027
e-ISSN 1857–9949
UDC: 520-1:528.94]:75.05
DOI: 10.20903/csnmbs.masa.2018.39.1.115

Review

ASTRONOMERS AS SKETCHERS AND PAINTERS: THE EYE – THE HAND – THE UNDERSTANDING[1]

Dieter B. Herrmann

Leibniz-Sozietät der Wissenschaften zu Berlin, Berlin, Germany

e-mail: post@dbherrmann.de

Today we are accustomed to seeing the objects of the universe in magnificent digital pictures vividly before our eyes. But before the invention of photography, the art of painting and drawing played an important role in scientific research. Those who were powerful astronomers of this art had the advantage. This article substantiates this thesis by means of selected examples. The drawings and the related discoveries of Galileo Galilei (1564–1642), Johannes Hevelius (1611–1687), Tobias Mayer (1723–1762), Johann Heinrich Mädler (1794–1874), Julius Schmidt (1825–1884), Giovanni Schiaparelli (1835–1910), Eugenios Antoniadi (1870–1944), William Parsons alias Lord Rosse (1800–1867), Ernst Wilhelm Leberecht Tempel (1821–1889), Etienne Trouvelot (1827–1895) and Walter Löbering (1895–1969) and showed their most important drawn observation documents. It can be seen that thanks to their art and the associated highly developed ability to perceive it, astronomers' drawings have made astounding discoveries that others have been denied. Finally, some thoughts on the role of drawn or painted astronomical motifs in the present are developed.

Key words: astronomy; painters; photography; Galileo Galilei; Johannes Hevelius; Tobias Mayer; Johann Heinrich Mädler; Julius Schmidt; Giovanni Schiaparelli; Eugenios Antoniadi; Lord Rosse; Ernst Wilhelm Tempel; Etienne Trouvelot; Walter Löbering

INDRODUCTION

In many respects, art and science are a mismatched couple. And yet, time and again artists have used their own means to reflect on the objects of science, while scientists have drawn inspiration from the artists' ideas and used them for scientific purposes. Now, if visual artist and scientist are the *same person*, something very special can happen - and this is what this article is about. Our focus here is on astronomers as painters at the service of astronomical research, but also on painters as astronomers.

IT ALL BEGAN WITH GALILEI

Due to his training at the Florence Academy of Arts, Galileo Galilei obtained research findings that he probably would not have gained without the skills he acquired during his artistic studies. The importance of Galilei's artistry for his scientific insights has recently been mapped out for the first time in the compelling in-depth study [1] by the Berlin-based art historian Horst Bredekamp. It is well known that Galilei was one of the first persons to use a telescope to observe the moon and other astronomical objects. He sketched in ink what he saw, using his trained eye and hand, and later engraved his observations in copper. What is more, Galilei drew the correct conclusions from what he saw. This is shown most clearly in the following quote from his letter to Antonio de Medici dated January 7, 1610: "Indeed one can clearly see that the moon surface in fact is not even, smooth or clear… but rather rough and uneven…, that it is full of elevations and indentations similar to but much

[1]Shortened version of a lecture presented by the author on April 15, 2013 at the Macedonian Academy of Science and Arts in Skopje. Translated from the German version into English by Judith Blank

bigger than the mountains and valleys dispersed over the earth's surface". [2]

His three-dimensional interpretation of light-dark phenomena as mountainous landscapes is far from trivial, as shown by the example of the Englishman Thomas Harriot who observed the moon by telescope even *before* Galilei without identifying what he saw as mountains and valleys.

Figure 1. Galilei statue in Florence (photo: author)

Figure 2. Ink drawing of the moon by Galilei 1610 (photo: Deutsches Museum, München)

FROM HEVELIUS TO FAUTH

However, Galilei was not an exception. Also in later centuries, astronomers used the art of sketching for their research.

When Johannes Hevelius decided to draw up a large map of the full moon, he learned that his friend Gassendi in Paris was pursuing the same project with the help of an experienced drawer and copper engraver. Hevelius set out his plans to Gassendi who wrote back that Hevelius should be the one to complete the work since he was observer, sketcher and engraver in one person. Hevelius' lunar map prevailed until the arrival of Tobias Mayer.

In an autobiographical outline, Mayer gives a detailed account of how he started to become interested in sketching and painting at a very early age. Having set his eyes upon a painting of the crucified Christ, he would copy it again and again, until achieving a decent reproduction. [3] But this self-study was more than a transient passion; rather, it was to accompany him for the rest of his life. Later he also became concerned with the question of colour mixing when using natural colours, giving lectures and even publishing an academic paper about this topic.

Undoubtedly, his talent and experience in drawing and painting became particularly evident in the field of lunar cartography. Besides, Mayer – and in this respect he surpassed his predecessors – not only sketched what he saw but also used a special procedure to measure the position of individual objects on the moon, making his representations of the moon even more valuable compared to other portrayals published by then - a typical example for the combination of art and science. Eventually, his work resulted in a 19.4-cm-diameter moon map which was found in his estate after his death and finally published by Georg Christoph Lichtenberg in 1775.

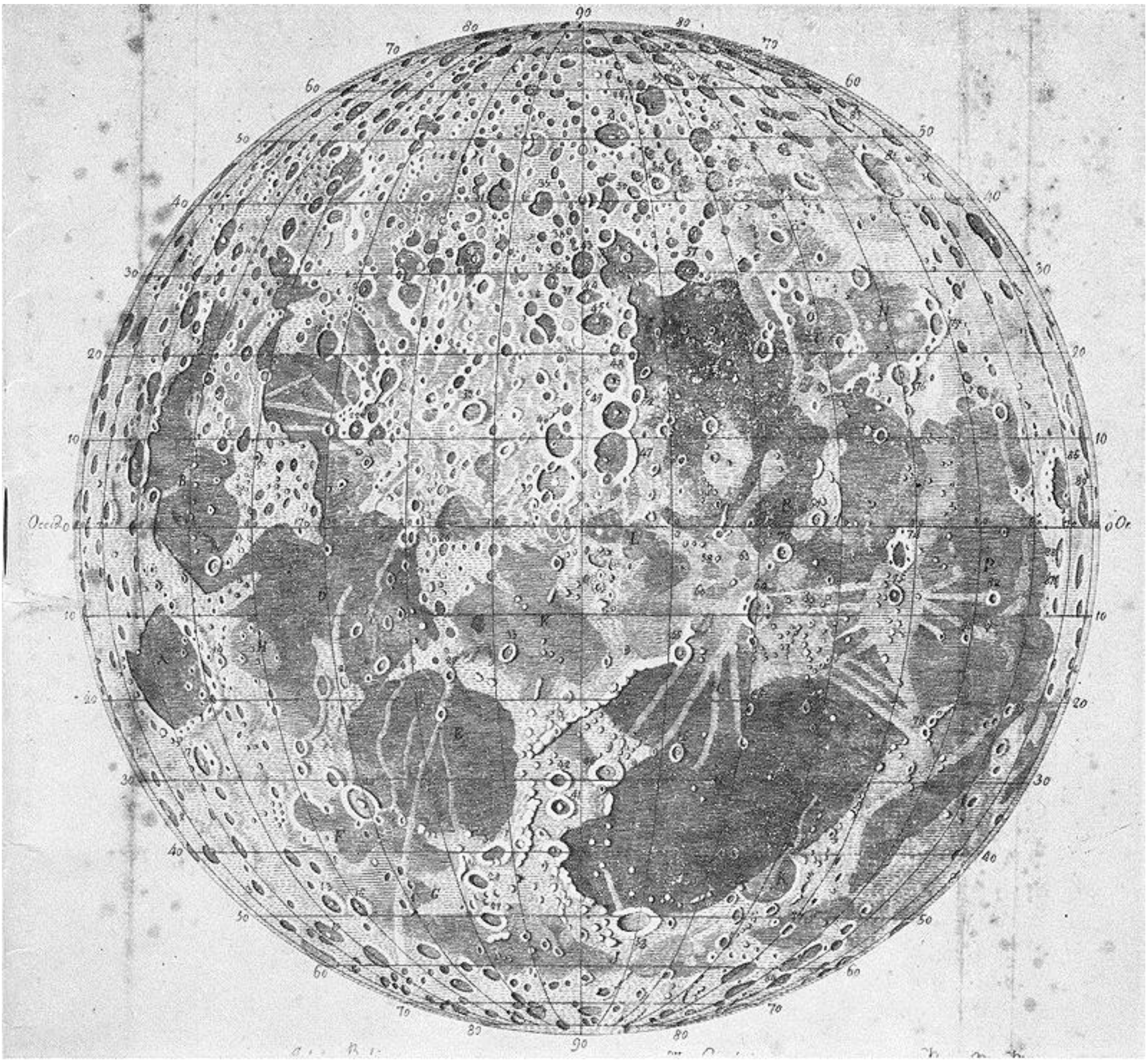

Figure 3. Tobias Mayer's moon map (author's archives)

The Berlin-born astronomer Johann Heinrich Mädler is also known for his great accomplishments in the field of lunar cartography. It is fair to assume that his talent for drawing and his artistically trained eye played an important role here. For Mädler, before starting his career as astronomer, had worked as calligraphy teacher in Berlin and had published a textbook on the art of calligraphy as early as in 1827. He had also put to press several other publications on this topic [4]. Surely this must have furthered his eye-hand coordination beyond usual standards.

We also know that the author of the largest and probably finest moon map of the 19th century, Julius Schmidt, had a special gift for drawing. His obituary reads: "With his keen eyes for the more subtle nuances of shape, tints of light and colour and his exquisite sketching talent, he soon recognised the scientific value of his observations…" [5] Unfortunately, we have not been able to establish whether or not Schmidt had ever had any training in this field. Also as an astronomer he was self-taught, but this in no way impaired his career which culminated in his appointment as director of the Observatory of Athens. The results of his research, in particular his moon map measuring almost 2 metres in diameter, are considered outstanding achievement in the field of lunar cartography.

SKETCHES TRIGGER MARS FEVER

One of the astronomers whose drawings caused a lively scientific debate that was to last for decades was Giovanni Schiaparelli. As is well known, he observed Mars during the planet's approach to the Earth in 1877, discovering and sketching many thin straight lines some of which extending over several thousand kilometres. Schiaparelli referred to them as "canali", thinking at first of natural watercourses on the planet. He at once discovered forty formations of this type. Many of these lines intersect in darker, surface-like formations that at the time none other than E.C. Pickering mistook for water. Many observations by others seemed to *confirm* the "canal" thesis. While in the end, with improving observation techniques, the "canals" turned out to be an illusion, they must have been visible to good observers, considering the stage of development of the instrumentation technology at the time. Schiaparelli's talent for observing and drawing had to do with the fact that initially he had studied "civil engineering" at the University of Turin. Architectural studies at the time would have included classes in descriptive geometry, perspective drawing with light and shadow, as well as training in artistic imagination and cartography [6].

At least the Martian canals acted as a powerful stimulus to Mars research. The last advocates of this hypothesis published their opinions as recently as in the 1940s. It was not until the age of space travel with the pictures of the Martian surface taken by Mariner 4 (1965) that the excitement over Martian canals received its death blow.

Figure 4. Schiaparelli and "his" Mars canals on an Italian stamp (2010)

CONQUERING EVEN GREATER DISTANCES

We are well acquainted with the drawings of astronomical objects far out there in space made by the Irish nobleman, telescope builder and astronomer Lord Rosse long before the discovery of extragalactic worlds by Hubble in the 20th century. Little is known about Rosse's life, so we do not know whether he ever studied drawing or had a special talent for drawing. However, any competent art historian can easily see the quality of his eye and hand on the basis of the sketches themselves. Lord Rosse's main contribution to astronomy is his discovery of the structures of extragalactic objects, obtained by observations with the 72-in mirror "Leviathan" that he himself had built. Admittedly, the true nature of the drawn objects remained a mystery to Rosse. His probably best known representation is the one of the M 51 nebulae in Canes Venatici. This object had already been drawn by John Herschel, but Herschel saw much less than Lord Rosse. In the history of astronomy, it has generally been argued that this was due to the larger size of Lord Rosse's instrument. Of course the size of "Leviathan" with its 72-in mirror played an important role in the discovery of detailed structures. However, the combination of Rosse's eye, hand and the large telescope would seem to have been crucial for his breaking into new ground in science. Rosse did not rely on observation techniques alone, but he understood very well the importance of the artist's eye and of his ability of portraying what he saw. This is also reflected in the fact that he employed the trained artist Samuel Hunter specifically to assist him as observer and drawer.

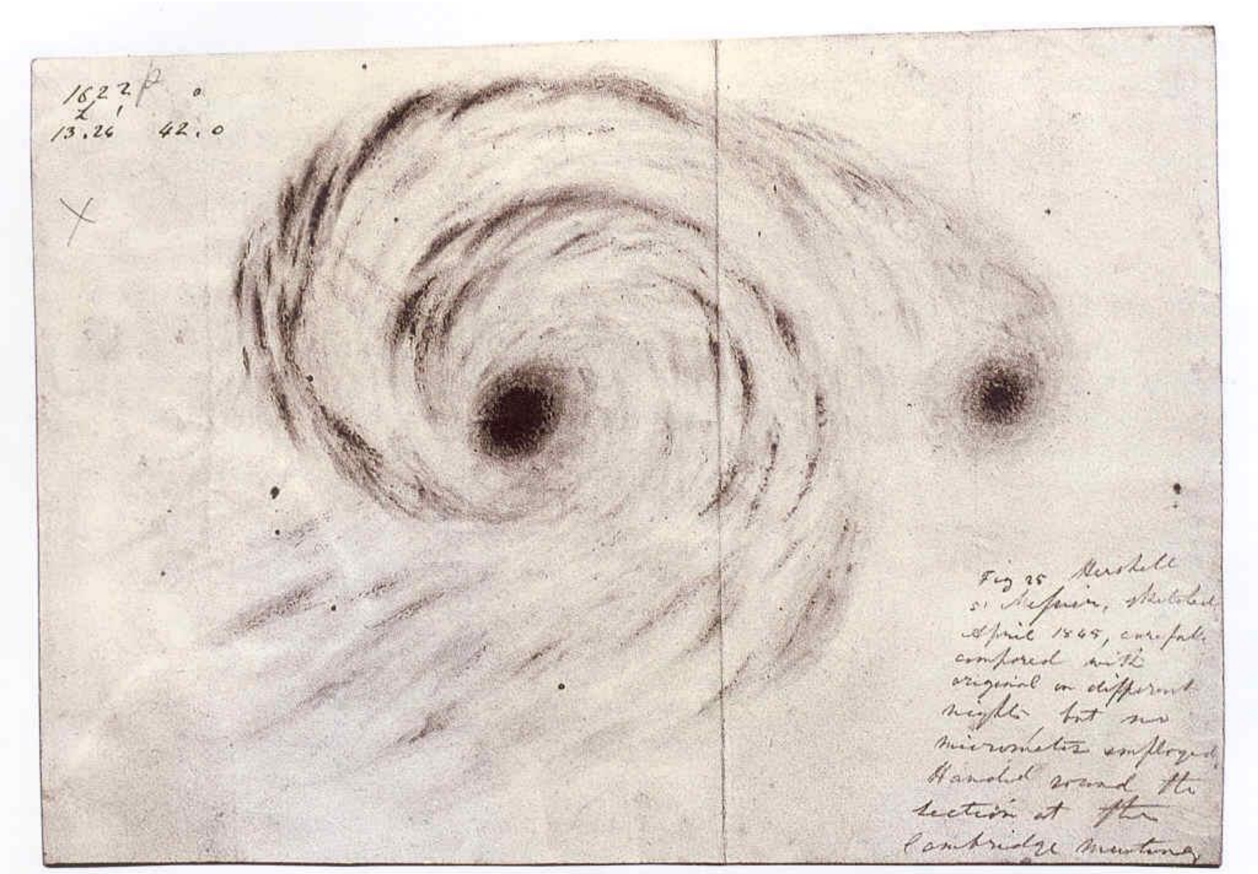

a)

b)

Figure 5. a) Drawing of the M 51 object by Lord Rosse (source: Wikipedia);
b) Picture of M 51 (Hubble Space Telescope)

In his contribution to "Astronomical Notes" in 1888, Hermann Carl Vogel compared Rosse's drawings with lithographs from photos, claiming that the photos made using the recently developed silver bromide-gelatine dry plates showed much more details than Rosse's drawings [7]. Vogel had more confidence in photography than in drawing and the more the nebula drawings of others resembled photographs, the more he valued them. But if we compare modern images of M 51 with Rosse's drawings, we see immediately that Rosse's drawings were much closer to reality than the photos taken in 1888.

Our next example is Ernst Wilhelm Leberecht Tempel who was born in Niedercunnersdorf, Saxony. Tempel had trained as a lithograph, so there is no mistaking his qualifycations as precise observer and drawer. He had also lived in Venice where he was admired for his detailed renderings for botanists and natural scientists. After astronomy had caught his interest, he became extremely successful also in this field. He discovered 21 comets and 5 minor planets, including the one he referred to as "Maximiliana". His numerous, finely-structured drawings of nebulous objects and his discovery of a reflection nebula around the star Merope in the Pleiades cluster made him famous among experts.

The surrealist graphic artist, painter and sculptor Max Ernst was so impressed by Tempel's life story and achievements that he dedicated to him his graphic cycle "Maximiliana". Tempel was a master in seeing details and translating what he saw into drawings and lithographs, and it must have been these abilities that fascinated the artist Ernst. Even back then, Ernst, who in his "Maximiliana" also included some of his own surrealist drawings to honour Tempel, foresaw that the importance of drawings for astronomy would decline with the technical development of photography.

A very special case of the hand-eye phenomenon in astronomy is that of the Frenchman Étienne Trouvelot. He made a name for himself in astronomy, even though he had never formally studied this field. He also ranks as a drawer and painter, probably also without ever having had any formal training. After Louis Napoléon's 1851 coup, Trouvelot left France where until then he had been engaged in political activities on behalf of the Republicans. In the US, he joined the Natural History Society and published several articles on entomology. In 1870, his delicate drawings of polar lights attracted the attention of the director of the Harvard College Observatory, Joseph Winslock. This was the beginning of a typical American career. Winslock recruited him for Harvard where Trouvelot worked as a drawer. His drawings were published in the Observatory publications. As a result, other observatories invited him to observe and draw using also their instruments. These drawings gave rise to studies on sunspots, planets and the moon, some at the Washington 26-in refractor - with its 26-in aperture one of the world's largest refractors at the time. The total number of pictures reached about 7000. Trouvelot's astronomical drawings and paintings were printed and exhibited like an artist's works. But his keen eye also spotted details that caused a stir in scientific circles. For instance, in 1887 Trouvelot discovered radial structures within the Saturn ring system whose existence was definitely demonstrated only some 100 years later by the Voyager space probe [8]. In 1882, Trouvelot returned to France where he was immediately hired to work at the Meudon Observatory near Paris. There, he produced hundreds of drawings, especially of prominences and other phenomena on the solar surface. His observations of solar spots revealed details that could be photographed only much later using modern technical means in the light in specific spectral ranges.

A similar career as astronomical drawer (without being an astronomer) was that of Walther Löbering [9]. He had completed formal studies at the Dresden Academy of Arts and had then settled down near Plauen in Fasendorf, Vogtland. There, he worked as an artist, but also as a teacher at the Plauen national art school. At the beginning of the 20s, he turned to astronomy, in particular to the planet Jupiter that he observed using mainly a 10-in reflector telescope. Löbering created a wealth of drawings of Jupiter's changeable atmospheric phenomena, drafting rotation maps and exploring in particular the Great Red Spot (GRS). Later, he built a small observatory and regularly published his observations in "Astronomical Notes", "Die Himmelswelt" and in the magazine "Die Sterne". In 1954, the German Academy of Sciences awarded him the Leibniz Medal for his extraordinary achievements apart from his actual professional activity. Finally, in Löbering's death year, a summary of all his observations between 1926 and 1964 made it into the Leopoldina treatises (the society is today referred to as national academy of Germany) [10].

As a painter, he expressly stated that in the Jupiter sketches he proceeded as if he was drawing portraits - portraits in which, nevertheless, some details needed to be verified by measuring the "objects".

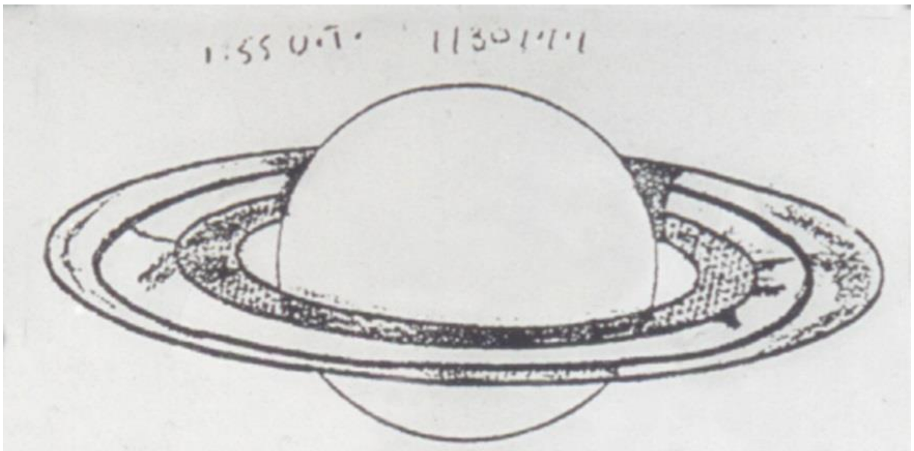

a)

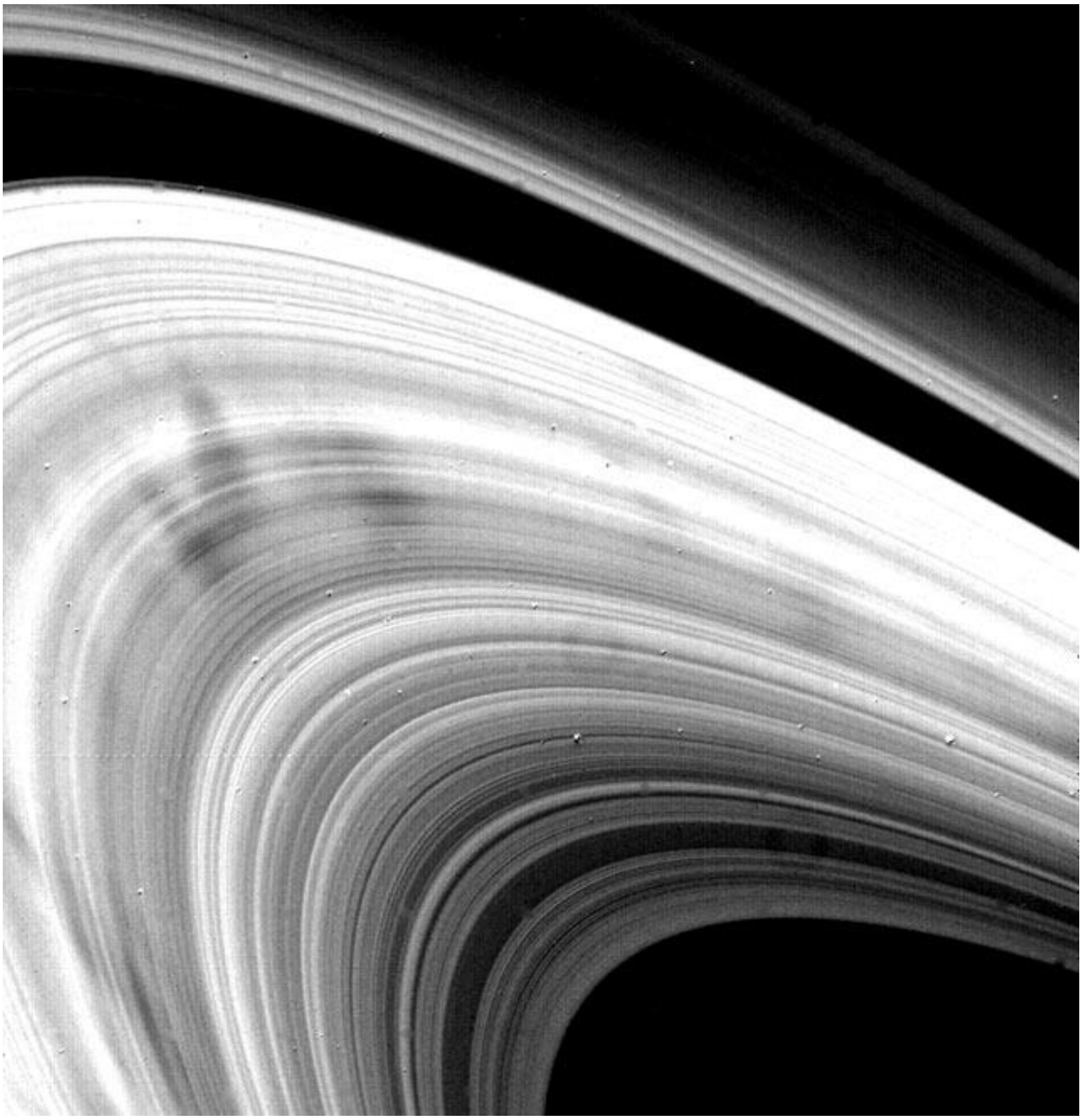

Figure 6. a) Drawing of the radial structures within the Saturn ring system by Trouvelot;
b) Photos of the radial structures by Voyager 1 (1980)

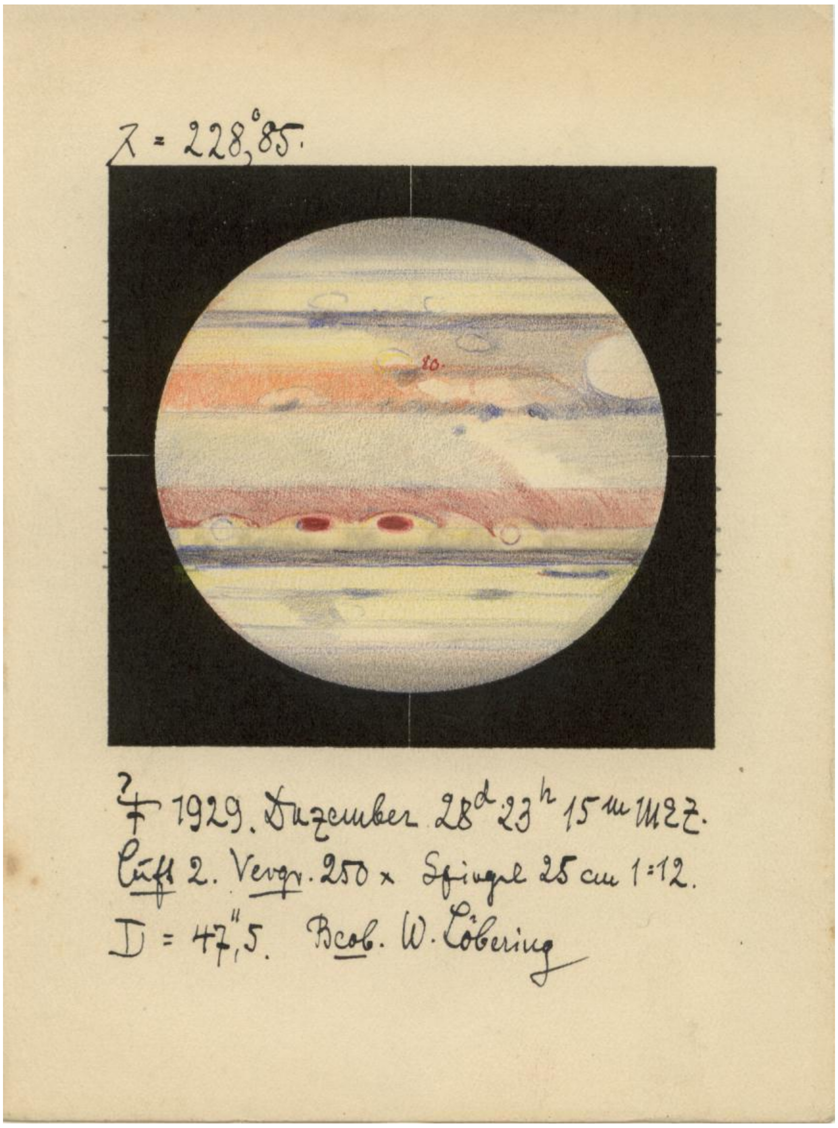

Figure 7. Drawing of Jupiter by Walter Löbering (archives of the Archenhold Observatory, Berlin)

For the exploration of Jupiter it is interesting that Löbering’s observations indicated a left-turning vortex within the GRS. However, this observation was ignored by most of the scientific community. But the rotation profiles recorded later by the Voyager space probes indeed confirmed the GRS’s left-turning vorticity. Löbering, with his painter’s eye and hand, and B.M. Peek (1958) [11], who analysed amateur observations made over decades by the British Astronomical Association, were the only ones to notice [12].

END OF AN ERA

With photography and the ensuing development of electron-optical image converters, drawers at the telescope had to take a backseat. This is not negative but a sign of progress. Because today, no drawer however gifted in observing would be able to perceive and record the wealth of information captured by the gigantic telescopes of our time, not to mention non-optic wavelength ranges.

However, there is no denying that over more than two centuries the drawers and painters among astronomers played a significant role in research. Galilei was their earliest ancestor. Certainly, none of the discoveries made later by drawing astronomers shook the world view the way Galilei’s drawings did.

Even today, visual representations are essential to astronomical research, in particular false-colour images of digitalised observation files. But much of what we know cannot be photographed. Since Camille Flammarion’s popular books with their fascinating pictures, drawers and painters have tried to translate this knowledge into pictures.

Today, Flammarion's spiritual grandchildren and great-grandchildren are those artists that work at ESA, ESO or NASA creating much sought-after "artist's impressions" that help us imagine foreign planets, remote areas of the universe and other breath-taking phenomena. These representations of research findings are probably not very different from real photographs, if only we could take pictures of them.

REFERENCES

[1] H. Bredekamp, *Galilei. Der Künstler. Die Sonne. Der Mond. Die Hand*, Akademie-Verlag, Berlin, 2007.

[2] Ibid, p. 104

[3] E. G. Forbes, *Tobias Mayer (1723-1762). Pioneer of enlightened science in Germany*, Göttingen, 1980, p. 20.

[4] H. Eelsalu, D. B. Herrmann, *Johann Heinrich Mädler (1794-1874),* Akademie-Verlag, Berlin 1985, pp.11 and 83 f.

[5] Krüger, Obituary (Johann Friedrich Julius Schmidt), *Astronomische Nachrichten*, **106** no. 2577–78, (1884), p. 9.

[6] A. Ferrari, Between two Halley's comet visits, *Memorie della Società Astronomica Italiana,* **82,** N2 (2011), 233.

[7] H. C. Vogel, Ueber die Bedeutung der Photographie zur Beobachtung von Nebelflecken, *Astronomische Nachrichten* **119** (1888), pp. 337.

[8] R. Koppmann: Die Entdeckung der Planetensonden, *Sterne und Weltraum*, **22** (1983), pp. 342 – 346.

[9] G. Loibl, Jupiter und der Kunstmaler – zum Gedenken an Walther Löbering, *VdS, Journal für Astronomie*, **36** (2011), pp. 60.

[10] W. Löbering, Jupiterbeobachtungen von 1926-1964, *Nova Acta Leopoldina, New Series*, **14** (1969), no. 190.

[11] B. M. Peek, *The Planet Jupiter*, London, 1958.

[12] E. Mädlow, letter addressed to the author on November 11, 1983

АСТРОНОМИТЕ КАКО СКИЦИРАЧИ И СЛИКАРИ: ОКОТО – РАКАТА – РАЗБИРАЊЕТО

Dieter B. Herrmann

Leibniz-Sozietät der Wissenschaften zu Berlin, Berlin, Germany

Денес сме навикнати пред нашите очи да гледаме објекти од универзумот во прекрасни дигитални слики. Но, пред откривањето на фотографијата, уметноста на сликање и цртање одигра значајна улога во научните истражувања. Оние астрономи што биле силни во оваа уметност имале предност. Статијава ја поткрепува оваа теза со помош на избрани примери. Цртежите и поврзаните откритија на Галилео Галилеј (1564–1642), Јоханес Хевелиј (1611–1687), Тобијас Мајер (1723–1762), Јохан Хајнрих Медлер (1794–1874), Јулиј Шмит (1825–1884), Џовани Шкипарели 1835–1910), Еугениос Антониади (1870–1944), Вилијам Парсонс алијас Лорд Роуз (1800–1867), Ернст Вилхелм Леберет Темпел (1821–1889), Етјен Троувелот (1827–1895) и Волтер Леберинг (1895–1969) ги покажаа најважните документи за набљудување. Може да се види дека благодарение на нивната уметност и поврзаните високо развиени способности за тоа да го согледаат, цртежите на астрономите создадоа зачудувачки откритија кои другите ги негираа. Конечно, сега се развиваат некои погледи за улогата на нацртаните или насликани астрономски мотиви.

Клучни зборови: астрономија; сликари; фотографија; Galileo Galilei; Johannes Hevelius; Tobias Mayer; Johann Heinrich Mädler; Julius Schmidt; Giovanni Schiaparelli; Eugenios Antoniadi; Lord Rosse; Ernst Wilhelm Tempel; Etienne Trouvelot; Walter Löbering

ПРИЛОЗИ, Одделение за природно-математички и биотехнички науки, МАНУ, том **39**, бр.1, стр. 15–21 (2018)
CONTRIBUTIONS, Section of Natural, Mathematical and Biotechnical Sciences, MASA, Vol. **39,** No. 1, pp. 15–21 (2018)

Received: April 3, 2018
Accepted: May 31, 2018

ISSN 1857–9027
e-ISSN 1857–9949
UDC: 537.226.1:539.23.083
DOI: 10.20903/csnmbs.masa.2018.39.1.116

Original scientific paper

A MODEL BASED METHOD FOR COMPARING THE PROPERTIES OF SOME METAL-Ta_2O_5/SiO_2-Si STRUCTURES

Nenad Novkovski[1,2]

[1]Institute of Physics, Faculty of Natural Sciences and Mathematics, Ss. Cyril and Methodius University, Skopje, Republic of Macedonia
[2]Research Center for Environment and Materials, Macedonian Academy of Sciences and Arts, Skopje, Republic of Macedonia

e-mail: nenad@iunona.pmf.ukim.edu.mk

Oxygen annealed radio frequency (RF) reactively sputtered and thermally grown (thermal) Ta_2O_5 films on silicon were comparatively studied by using combination of *C-V* and *I-V* measurements and the previously developed comprehensive model for the metal-Ta_2O_5/SiO_2-Si structures. Dielectric properties of separate layers were extracted by comparing the experimental and the theoretical results. It is found that the net leakage properties of the Ta_2O_5 layer are significantly better in the case of RF than thermal, particularly in the case of the Au gate. Excessive growth of the SiO_2 layer of about 0.3 nm in the case of RF films leads to an unwanted increase of the equivalent oxide thickness. Appropriate interface engineering is required in order to prevent the SiO_2 excessive growth during the oxygen annealing. Such a growth can reduce the beneficial effects of the annealing on the net properties of Ta_2O_5 films obtained by RF.

Key words: high permittivity dielectrics; conduction in dielectrics; leakage currents model

INTRODUCTION

Ta_2O_5 films are nowadays extensively investigated for various applications, such as coatings for gravitational-wave detectors [1], multilayer stacked electrode in organic light-emitting diodes [2], resistive switching memories [3], gapless-type atomic switches [4], photocatalysts [5] etc. Ultrathin Ta_2O_5 films are particularly important as a new dielectric material for DRAM capacitors, because of their outstanding properties [6–9], such as high dielectric permittivity, high breakdown fields and low leakage current densities. The oxygen anneal of RF sputtered Ta_2O_5 films at high temperatures is found to be highly beneficial for their insulating properties [10, 11]. It significantly increases the dielectric constant, reduces the fixed charge Q_f (as low as 10^{10} cm^{-2}), reduces the leakage currents, and increases the breakdown field [8]. Pure oxygen ion assisted deposition provides similar improvements [12]. The fabrication of the insulating layer in the case of thermal growth [9] and RF-sputtering followed by oxygen anneal [8] is accompanied by unintentional formation of a silicon dioxide layer, and hence the insulating film has to be treated as a stacked layer. In [13, 14] we proposed and used a comprehensive model describing the leakage currents of thus obtained Ta_2O_5/SiO_2 stacked layers. It has been later generalized for different similar structures [15].

In the present work we study comparatively the RF-sputtered and thermally grown tantalum pentoxide films on silicon by using the model described in [14], in order to compare the impact of the discussed technologies on the properties of separate layers.

EXPERIMENTAL

Chemically cleaned p-type (100) 15 Ω·cm Si wafers were used as substrates. Some of the Ta_2O_5films were deposited at 220 °C by radio frequency (RF) reactive sputtering of 99.99 % pure Ta in a gas mixture of Ar and O_2. Other films were obtained by RF-sputtering of a Ta target in Ar atmosphere followed by thermal oxidation in dry O_2 at 600°C (thermal). All the films were subsequently annealed in dry oxygen at 900 °C for 30 min. The thickness of Ta_2O_5 and the refractive index were measured by ellipsometry (λ = 632.8 nm). The obtained thickness was d_{tp} = 50 nm. The refractive index was typically 2.1, approximately equal to the generally adopted value 2.2.

Metal-Insulator-Semiconductor (MIS) capacitors with two different gate electrodes (Al and Au) were formed. Al and Au electrodes were deposited by thermal evaporation. Au electrodes were deposited onto the Ta_2O_5 film using shadow mask technique. The corresponding gate electrode area is 1.96×10^{-3} cm^2. The MIS capacitors for the Al top electrodes were defined using photolithography and have the active areas of 2.5×10^{-3} cm^2.

High frequency (1 MHz) *C-V* characteristics were measured by a HP 3284 A LCR-meter. For the quasi-static measurements a HP 4140 B picoammeter/voltage source was used, at a voltage ramp rate of 0.1V/s.

I–V characteristics were measured by a HP 4140 A picoammeter DC voltage source. Current was measured in steps of 0.1V, with a hold time of 5 s, allowing for the obtainment of negligible displacement current, as it was confirmed by reversing the voltage range of the measurement. Repeated measurements in the ranges used in this work gave practically the same results, proving that the charge trapping during these measurements does not affect significantly the film properties.

THEORY (SECTION III)

The conduction mechanisms that are considered are:

1. For the SiO_2 layer, hopping conduction along with direct tunneling through a trapezoidal barrier or Fowler-Nordheim tunneling through a triangular barrier, depending on the electric field in the layer (E_{so}). Tunneling current can be created by the electrons or the holes. The barrier for the tunneling of holes is substantially higher than the barrier for electrons. Different carriers from the silicon substrate produce this current: electrons in the case of gate positively biased and holes in the case of gate negatively biased. Hence, the current depends upon the gate polarity.

2. For tantalum pentoxide, Poole–Frenkel mechanism, that is bulk-limited, thus independent on the polarity.

Direct tunneling current density through the SiO_2 layer (J_{DT}) is given by the following expression:

$$J_{\mathrm{DT}} = \frac{q^2}{8\pi h\Phi} E_{\mathrm{so}}^2 \exp\left(-\frac{8\pi\sqrt{2m^* q\Phi^3}}{3hE_{\mathrm{so}}} \left(1 - \left(1 - \frac{d_{\mathrm{so}}}{\Phi} E_{\mathrm{so}} \right)^{3/2} \right) \right) \tag{1}$$

and Fowler-Nordheim tunneling current density by

$$J_{\mathrm{FN}} = \frac{q^2}{8\pi h\Phi} E_{\mathrm{so}}^2 \exp\left(-\frac{8\pi\sqrt{2m^* q\Phi^3}}{3hE_{\mathrm{so}}} \right), \tag{2}$$

where q is the electron charge, h is the Planck's constant, m^* is the effective tunneling mass of carriers in SiO_2, d_{so} is the thickness of SiO_2 layer, Φ is the tunneling barrier height, and E_{so} is the electric filed in SiO_2 layer.

Total leakage current density through the SiO_2 layer (J_{so}) is given by

$$J_{\mathrm{so}} = \sigma_{\mathrm{hc}} E_{\mathrm{so}} + \begin{cases} J_{\mathrm{DT}} & E_{\mathrm{so}} < \dfrac{d_{\mathrm{so}}}{\Phi} \\ J_{\mathrm{FN}} & E_{\mathrm{so}} > \dfrac{d_{\mathrm{so}}}{\Phi} \end{cases}, \tag{3}$$

where σ_{hc} is the hopping conductivity in the SiO_2 layer.

The voltage drop on the SiO_2 layer (V_{so}) is:

$$V_{\mathrm{so}} = E_{\mathrm{so}} d_{\mathrm{so}}. \tag{4}$$

Leakage current density due to the Poole-Frenkel mechanism in the Ta_2O_5layer (J_{tp}) is given by the following expression:

$$J_{\mathrm{tp}} = \sigma_{\mathrm{tp}} E_{\mathrm{tp}} \exp\left(\frac{1}{kT} \sqrt{\frac{q^3}{\pi\varepsilon_0 K_{\mathrm{T}}}} \sqrt{E_{\mathrm{tp}}} \right), \tag{5}$$

where E_{tp} is the electric field in the Ta_2O_5 layer, σ_{tp} is temperature-dependent defect-related constant having dimensions of conductivity, k is the Boltzmann constant, ε_0 is the dielectric constant of vacuum and $K_T = n^2$ is the optical frequency dielectric constant (n is the refractive index) of Ta_2O_5.

The voltage drop on the Ta_2O_5layer (V_{tp}) is given by:

$$V_{tp} = E_{tp} d_{tp}\,, \tag{6}$$

where d_{tp} is the thickness of the Ta_2O_5 layer.

The two quantities that are computed simultaneously here are the oxide voltage:

$$V_{ox} = V_{tp} + V_{so} = d_{tp}E_{tp} + d_{so}E_{so}\,, \tag{7}$$

and the current density in steady state

$$J = J_{tp} = J_{so}\,. \tag{8}$$

Current density $J = J_{so}$ was computed for given field E_{so} in the silicon dioxide, then the field in Ta_2O_5 layer was computed as inverse function of current of $J_{tp} = J$ and the oxide voltage determined with the use of the expression (6). Following typical values were used in computations: $m_e^* = 0.61$ m_0– effective electron mass in SiO_2 (m_0 denotes the mass of free electron), $m_h^* = 0.51$ m_0 – effective hole mass in SiO_2 and $K_T = 4.84$.

The voltage on the insulating stacked layer (V_{ox}) was calculated by using relations involving the flatband voltage (V_{fb}),the gate voltage (V_g) and voltage drop in the semiconductor (φ_s) [16]

$$V_{ox} = V_g - V_{fb} - \varphi_s\,. \tag{9}$$

The voltage drop in the semiconductor (φ_s) has been computed solving numerically the following equation [15]:

$$E_{so} = \pm\frac{\varepsilon_s}{\varepsilon_{so}}\sqrt{\frac{2kTp_0}{\varepsilon_s\varepsilon_0}\left[\left(\exp\left(-\frac{q\varphi_s}{kT}\right)+\frac{q\varphi_s}{kT}-1\right)+\frac{n_i^2}{p_0^2}\left(\exp\left(\frac{q\varphi_s}{kT}\right)-\frac{q\varphi_s}{kT}-1\right)\right]}\,, \tag{10}$$

where ε_s is the relative permittivity of Si (11.9), ε_{so} is the relative permittivity of SiO_2 (3.9), ε_0 is the permittivity of vacuum, n_i is the intrinsic concentration of carriers in Si (1.45×10^{10} cm^{-3}) and p_0 is the steady state majority carrier (holes) concentration in p-type Si.

RESULTS AND DISCUSSION

The high-frequency (1 MHz) *C-V* characteristics for all the considered samples are shown in Figure 1. It is visible that the capacitances in accumulation for RF samples are lower than those for thermal ones. The entire characteristics for RF are shifted towards the right compared to the thermal. Applying the standard procedures used for MOS structures, the equivalent oxide thickness (d_{eq}) [17], the fixed charge density (Q_f) [18] and the interface state density at midgap (D_{itm}) [19]were computed. The results are shown in Table 1. Equivalent thicknesses of the RF films are significantly higher than those of the thermal ones. Fixed charge is positive in the case of the thermal films and negative in the case of RF. The interface state densities are of order of 10^{12} eV^{-1}cm^{-2} and are significantly lower in the case of RF than thermal. Fixed charges of thermal films are about 4×10^{11} cm^{-2}, that is less positive than the value obtained for the films without oxygen anneal, 1.2×10^{12} cm^{-2} [15]. RF films with the fixed charge of about -1.5×10^{12} cm^{-2} manifest similar shift toward the negative values compared to the unanealed RF films ($Q_f = 6 \times 10^{11}$ cm^{-2}) [15]. The oxygen annealing leads in some cases to negative values of Q_f. It is certain that not only positively charged defects are reduced, but an important amount of negatively charged defects is created. This can be explained by the crystallization of the Ta_2O_5 layer, leading to broken bonds at the Ta_2O_5/SiO_2 interface [20]. We have shown that the oxygen anneal at lower temperatures (600 ÷ 850 °C) leads to very low fixed charges (as low as 10^{11} cm^{-2}) [8]. Therefore, increasing the annealing temperature to 900 °C or above can have harmful effects on the fixed charge.

Table 1. Parameters extracted from the *C-V* characteristics

Growth	Gate	d_{eq} (nm)	Q_{ox} (cm^{-2})	D_{itm} (eV^{-1}cm^{-2})
RF-sputtered	Al	8.7	-1.4×10^{12}	1.2×10^{12}
	Au	9.2	-1.6×10^{12}	2.0×10^{12}
Thermal	Al	8.3	4×10^{11}	4.0×10^{12}
	Au	8.4	6×10^{11}	3.0×10^{12}

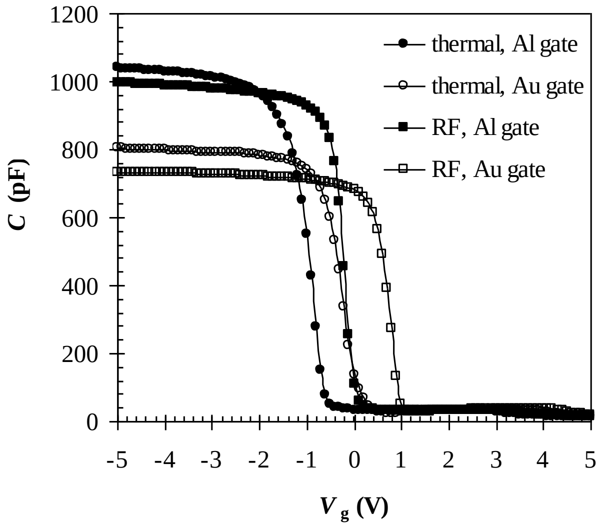

Figure 1. *C-V* characteristics of the MOS capacitors with areas of 0.0025 cm^2 (Al gates) and 0.00196 cm^2 (Au gates) containing thermally grown and RF-sputtered Ta_2O_5 films

The leakage current characteristics shown in Figures 2 and 3 were analyzed by using the model described in the Section III. Few of the parameters were fitted to obtain the matching between the theoretical and experimental results. These are the parameters influenced by the technological processes and not those that are accurately determined in the literature, listed in Section III. The parameters extracted by fitting the theoretical to the experimental results are given in Table 2.

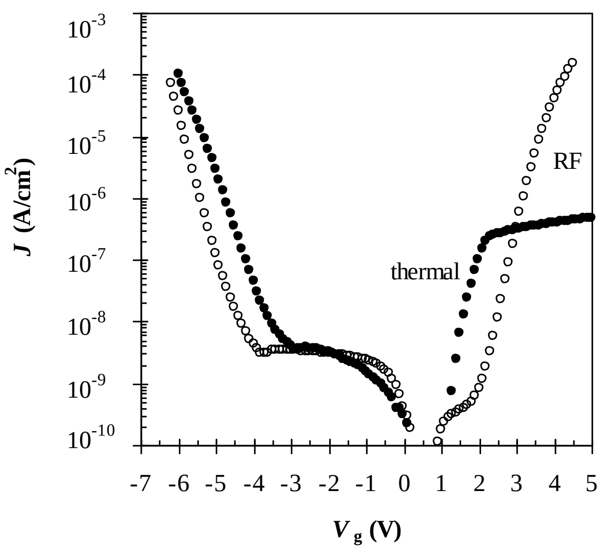

Figure 2. Leakage currents for MOS capacitors with Al gate containing thermally grown and RF-sputtered Ta_2O_5 films

Very good agreement between the theoretical and experimental results in the entire measurement region is obtained (Figure 4), justifying the use of the proposed model in the analysis. Saturated part for the positive gate is due to the strong inversion and is not described by this model.

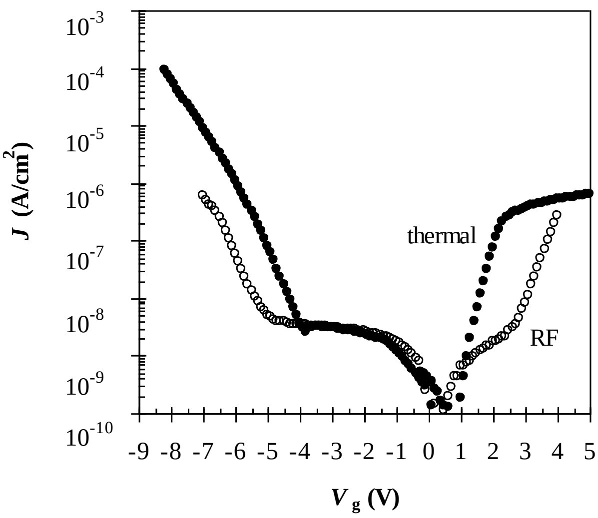

Figure 3. Leakage currents for MOS capacitors with Au gate containing thermally grown and RF-sputtered Ta_2O_5 films

The interfacial SiO_2 layer thickness for thermal films is about 2.7 nm, while for RF it is from 0.3 nm to 0.5 nm higher. Compared to the total thickness (50 nm) it is a very small value, but its contribution to the equivalent oxide thickness is significant. Barriers are practically equal to those for SiO_2 films from literature [13]. There are some differences between the values of the SiO_2 layer hopping conductivity for different samples, but they are comparable to the measurement error and can be disregarded. Thus, we can conclude that the quality of the SiO_2 layer is practically the same for both processes and both gate materials.

The parameter σ_{tp} is the most influenced by the technology and the gate material, which describes the net leakage properties of the Ta_2O_5 layer. In the case of Al gate, σ_{tp} is 3 times lower for RF than thermal films, while for Au gate, it is 10 times lower for RF than thermal. In [13] we explained the difference between Al and Au gates by the creation of defects due to the reactivity of Al with Ta_2O_5. In the case of non-reactive Au gate, the obtained value of σ_{tp} can be considered as intrinsic for the insulating material. Thus, the leakage factor for RF films is an order of magnitude lower than for thermal. In the case of Al gate, the difference between the RF and thermal films is less marked, because the majority of the defects responsible for the leakage are created by the reaction of the Al gate with the film and not during the growth of the insulating layer.

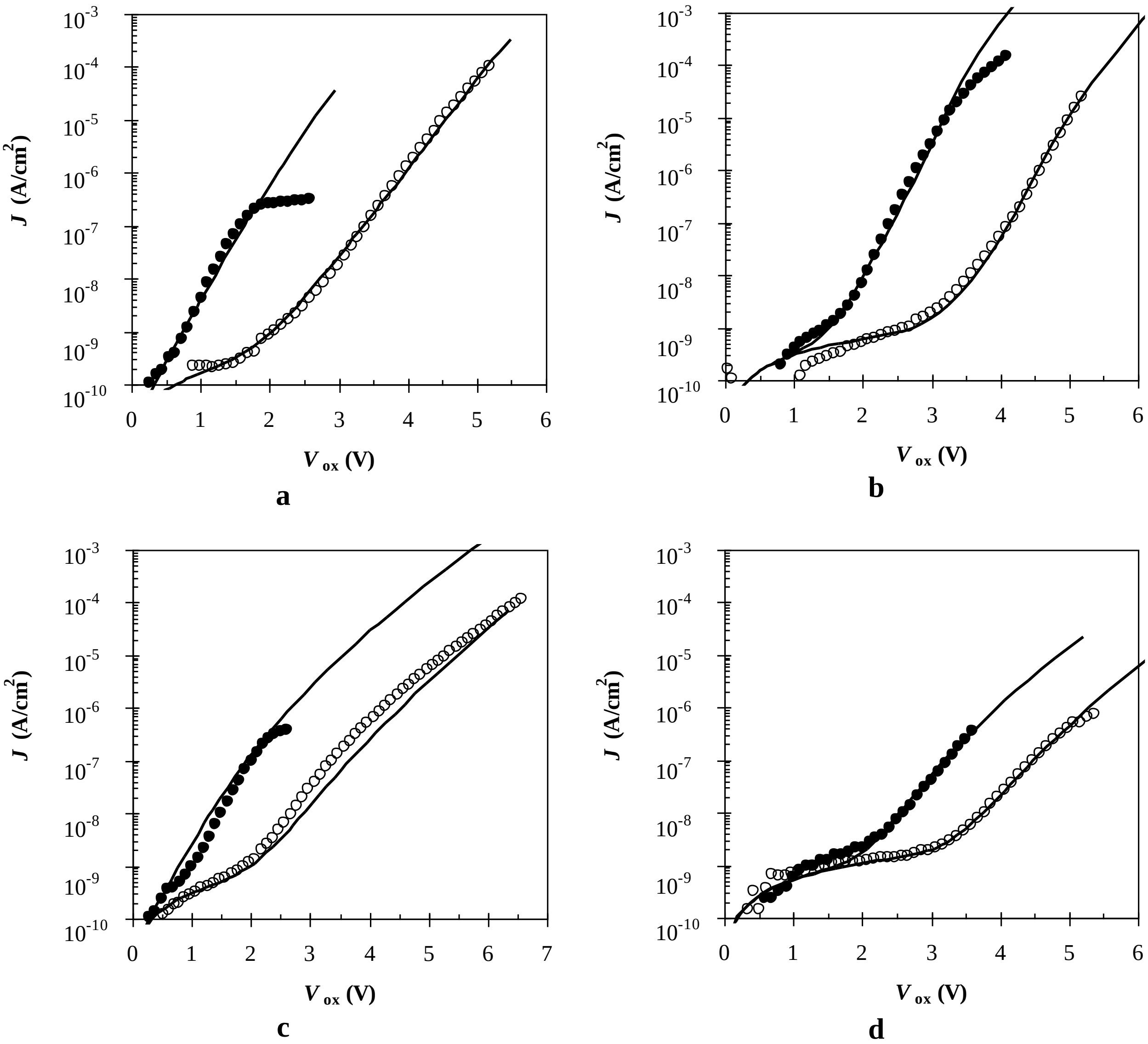

Figure 4. Experimentally obtained leakage currents versus oxide voltage for positive (closed circles) and negative gate (open circles) compared to the theoretical computations: **a)** thermally grown, Al gate, **b)** RF-sputtered, Al gate, **c)** thermally grown, Au gate, **d)** RF-sputtered, Au gate

Table 2. Parameters extracted from the *I-V* characteristics

Growth	Gate	d_{so} (nm)	σ_{hc} (Ω^{-1}cm^{-1})	σ_{tp} (Ω^{-1}cm^{-1})	Φ_e (eV)	Φ_h (eV)
RF-sputtered	Al	3.02	9.0×10^{-17}	2.5×10^{-11}	3.15	4.70
	Au	3.20	1.8×10^{-16}	5.9×10^{-15}	3.15	4.30
Thermal	Al	2.70	6.0×10^{-17}	8.2×10^{-11}	3.15	4.70
	Au	2.75	6.0×10^{-17}	6.6×10^{-14}	3.15	4.70

Using the measured total thickness values (d) and the obtained values for the SiO_2 layer thickness (d_{so}) and the equivalent oxide thickness (d_{eq}), the effective oxide dielectric constant (ε_{ef}) and the net dielectric constant of the Ta_2O_5 layer (σ_{tp}) were computed. Their values are given in Table 3. All the values are close to these reported in literature [15]. The values obtained for Al gate are slightly higher than these for Au gate, for both RF and thermal.

Table 3. Effective dielectric constant of the stack (ε_{ef}) and net dielectric constant of the tantalum pentoxide layer (σ_{tp}).

Growth	Gate	ε_{ef}	σ_{tp}
RF-sputtered	Al	22.5	34.8
	Au	21.1	32.3
Thermal	Al	23.5	34.8
	Au	23.2	34.4

CONCLUSIONS

Based on the use of a comprehensive model for leakage current in metal-Ta_2O_5/SiO_2-Si structures it has been found thatthe oxygen anneal of RF-sputtered films leads to significantly better net leakage properties of the Ta_2O_5 layer, compared to the thermally grown. However, the thickness of the interfacial SiO_2 layer for RF films is about 0.4 nm higher than this for thermal. Therefore, appropriate interface engineering in required in order to benefit from the outstanding net Ta_2O_5 layer without compromising the equivalent oxide thickness.

The use of the model of comparative analysis in description of the properties of separate layers, as is demonstrated in this work, provides in deep insight into the properties of the materials with reduced number of technological experiments compared to direct approach. Therefore, it is to be used in directed search of the technological solutions for materials with required properties.

Acknowledgement:The author is exceptionally grateful to Prof. Elena Atanassova from the Institute of Solid State Physics, Bulgarian Academy of Sciences, for providing the samples of very high quality studied in this work.

REFERENCES

[1] A. Amato, G. Cagnoli, M. Canepa, E. Coillet, J. Degallaix, V. Dolique, D. Forest, M. Granata, V. Martinez, C. Michel, L. Pinard, High-Reflection Coatings for Gravitational-Wave Detectors: State of The Art and Future Developments, *J. Phys.: Conf. Ser.*, **957** (2018), pp. 012006-1–012006-7.

[2] J. Sohn, Y. Kwon, Y. Lee, C. Lee, Light outcoupling efficiency enhancement in organic light-emitting diodes using a multilayer stacked electrode with sol-gel processed Ta_2O_5. *Opt. Exp.*, **25**(2017), pp. 27886–27895.

[3] S. Ryu, S.K. Kim, B. J. Choi, Resistive switching of Ta_2O_5-based self-rectifying vertical-type resistive switchingmemory, *J. Elec. Mat.***47** (2018), pp.162–166.

[4] Yuki Shigeoka, TsuruokaTohru, Hasegawa Tsuyoshi, The rate limiting process and its activation energy in the forming process of a Cu/Ta_2O_5/Pt gapless-type atomic switch, *Jap. J. Appl. Phys.*, **57** (2018), pp. 035202.

[5] S. Sathasivam, B. A. Williamson, A. Kafizas, S. A. Althabaiti, A. Y. Obaid, S. N. Basahel, D. O. Scanlon, C.J. Carmalt, I. P. Parkin, Computational and experimental study of Ta_2O_5thin films, *The J. Phys. Chem.*C,**121**(2017), pp. 202–210.

[6] U. Schroeder, K. Cho, S. Slesazeck, Materials for DRAM Memory Cell Applications, in *Thin Films On Silicon: Electronic and Photonic Applications***8** (2017), pp. 369–401.

[7] A. P. Huang, P. K. Chu, Improvement of interfacial and dielectric properties of sputtered Ta_2O_5 thin films by substrate biasing and the underlying mechanism, *J. Appl. Phys.*, **97** (2005), pp. 114106-1–114106-5.

[8] E. Atanassova, N. Novkovski, A. Dimitrova, M. Pecovska-Gjorgjevich, Oxygen annealing modification of conduction mechanism in thin rf sputtered Ta_2O_5 on Si. *Solid St. Electron.*, **46** (2002), pp.1887–1898.

[9] E. Atanassova, A. Paskaleva, N. Novkovski, and M. Georgieva, Conduction mechanisms and reliability of thermal Ta_2O_5–Si structures and the effect of the gate electrode, *J. Appl. Phys.*, **97** (2005), pp. 094104-1–094104-11.

[10] L. Wang, H. Liu, Y. Jiang, X. Yang, D. Liu, Y. Ji, F. Zhang, D. Chen, Effects of hot-isostatic pressing and annealing post-treatment on HfO_2 and Ta_2O_5 films prepared by ion beam sputtering, *Optik-International Journal for Light and Electron Optics*, **142** (2017), pp. 33–41.

[11] M. C. Sekhar, N. N. K. Reddy, H.S. Akkera, B. P. Reddy, V. Rajendar, S. Uthanna, S.H. Park, Role of interfacial oxide layer thickness and annealing temperature on structural and electronic properties of Al/Ta_2O_5/TiO_2/Si metal–insulator–semiconductor structure, *J. All. Comp.*, **718** (2017), pp.104–111.

[12] J. Han, Q. Zhang, W Fan., G. Feng, Y. Li, A. Wei, R. Hu, Q. Gu, The characteristics of Ta_2O_5 films deposited by radio frequency pure oxygen ion assisted deposition (RFOIAD) technology, *J. Appl. Phys.*, **121**(2017), pp. 065302-1–065302-9.

[13] N. Novkovski and E. Atanassova, Injection of holes from the silicon substrate in Ta_2O_5 films grown on silicon, *Appl. Phys. Lett.*, **85** (2004), pp. 3142–3144.

[14] N. Novkovski, E. Atanassova, A comprehensive model for the *I–V* characteristics of metal-Ta_2O_5/SiO_2-Si structures, *Appl. Phys.*, A, **83** (2006), pp. 435–445.

[15] N. Novkovski, Physical modeling of electrical and dielectric properties of high-κ Ta_2O_5 based MOS capacitors on silicon, *FactaUniversitatis, Series: Electronics and Energetics*, **27** (2014), pp. 259–273.

[16] K. Maitra, N. Bhat, Analytical approach to integrate the different components of direct tunneling current through ultrathin gate oxides in *n*-channel metal–oxide–semiconductor field-effect transistors, *J. Appl. Phys.*, **93** (2003), 1064–1068.

[17] E. Atanassova, T. Dimitrova, Thin Ta_2O_5 layers on Si as an alternative to SiO_2 for high density DRAM applications, in *Handbook of surfaces and interfaces of materials*, Edited by Hari Singh Naiwa, Volume 4: *Solid thin films and layers*, Academic Press, San Diego, (2001),pp. 439–479.

[18] S. M. Sze and K. K. Ng, *Physics of Semiconductor Devices*, 3rd Edition, John Wiley & Sons, New York,2007.

[19] D. K. Schroder, *Semiconductor Material and Device Characterization*, 3rd Edition, John Wiley & Sons (2006).

[20] E. Atanassova, A. Paskaleva, Challenges of Ta_2O_5 as high-κ dielectric for nanoscale DRAMs, *Microelectronics Reliability*, **47** (2007), pp. 913–923.

МОДЕЛЕН МЕТОД ЗА СПОРЕДБА НА СВОЈСТВАТА НА СТРУКТУРИ ОД ТИПОТ МЕТАЛ-Ta_2O_5/SiO_2-Si

Ненад Новковски

Институт за физика, Природно-математички факултет, Универзитет „Св. Кирил и Методиј“, Скопје, Република Македонија
Истражувачки центар за животна средина и материјали, Македонска академија на науките и уметностите, Скопје, Република Македонија

Филмови од Ta_2O_5 врз силициум добиени со високофреквенциско реактивно распрашување и термички третирани во кислород (РФ) и филмови од Ta_2O_5термички израснати (thermal) се проучувани компаративно со употреба на *C-V* and *I-V* и претходно развиениот сеопфатен модел за структури метал-Ta_2O_5/SiO_2-Si. Преку споредба на експерименталните со теориските резултати сеопределени диелектричните својства на одделните слоеви. Најдено е дека чистите својства за протекување низ слоевите од Ta_2O_5се значајно подобри во случајот на РФ отколку кај термички израснатите филмови, особено во случајот на горната електрода од Au. Додатниот пораст на слојот од SiO_2за околу 0,3 nm во случај на РФ-филмовите води до несакан раст на еквивалентната дебелина на оксидот. Потребно е да се направи соодветно нагодување на интерфејсот со цел да се избегне претеранпораст на SiO_2,едновремено користејќи ги подобрените чисти својства на филмовите од Ta_2O_5 добиени со РФ.

Клучни зборови: диелектрици со висока пермитивност; спроводливост низ диелектрици; модел за струите на протекување

ПРИЛОЗИ, Одделение за природно-математички и биотехнички науки, МАНУ, том **39**, бр.1, стр. 23–30 (2018)
CONTRIBUTIONS, Section of Natural, Mathematical and Biotechnical Sciences, MASA, Vol. **39,** No. 1, pp. 23–30 (2018)

Received: April 12, 2018
Accepted: June 1, 2018

ISSN 1857–9027
e-ISSN 1857–9949
UDC: 620.3:678.4]:539.124-14
DOI: 10.20903/csnmbs.masa.2018.39.1.117

Original scientific paper

ELECTRON SPIN RESONANCEON HYBRID NANOCOMPOSITES BASED ON NATURAL RUBBER

Aleksandra Ivanoska-Dacikj[1*], Gordana Bogoeva-Gaceva[1, 2], Srećko Valić[3, 4]

[1]Research Center for Environment and Materials, Macedonian Academy of Sciences and Arts, Skopje, Republic of Macedonia
[2]Faculty of Technology and Metallurgy, Ss. Cyril and Methodius University, 1000 Skopje, Republic of Macedonia
[3]Department of Chemistry and Biochemistry, School of Medicine and Centre for Micro and Nano Science and Technologies, University of Rijeka, Rijeka, Croatia
[4]Rudjer Bošković Institute, Zagreb, Croatia

e-mail: aivanoska@manu.edu.mk

Electron spin resonance (ESR) was used as a new method to analyze the synergy between two nanofillers different by nature, form and rigidity dispersed in natural rubber matrix. Natural rubber (NR) nanocomposites loaded with fixed amount of carbon nanotubes (2 parts per hundred of rubber parts; phr) and various amounts of expanded organically modified montmorillonite (EOMt, 4–20 phr) were investigated. The dependence of the double integral of the resonance spectra on the amount of EOMt present in the natural rubber was established. Its decrease with an increaseof the amount of EOMt confirmed the synergy between these two nanofillers. Also DMA temperature sweep measurements were performed and the cluster-cluster aggregation (CCA) model was used to assess the apparent filler networking energy. The obtained results suggest that the presence of the EOMt above a critical amount strengthens the hybrid-filler networking.

Keywords: electron spin resonance; carbon nanotubes; organo-montmorillonite; rubber nanocomposites

INTRODUCTION

The electron spin resonance (ESR) spectroscopy is a powerful technique for the investigation of carbon-based materials. The appearance of the carbon nanotubes ESR spectra is affected by a lot of factors and that is why different information on the carbon nanotubes ESR line shape could be found in literature. Some authors reported [1, 2] symmetric line shapes (mostly Lorentzian) while others reported asymmetric Dysonian line shapes [3]. The resonance spectrum of isolated carbon nanotubes should represent a symmetrical Lorentzian or Gaussian shape. On the other hand, agglomerated nanotubes are characterized by interconnected conducting domains of the order of 1 to 100 microns [4, 5] and such structures are characterized by resonance spectra presenting a Dysonian like shape.

Although many ESR investigations on carbon nanotubes have been reported [3, 6–14], only a few ESR studies on carbon nanotubes dispersed in polymeric matrices have been published [8, 11, 13, 14]. In these studies, based on the appearance of the ESR spectra on individual and agglomerated carbon nanotubes, it was concluded that, if the dispersion of the nanotubes is good, the resonance line will present a symmetrical shape, and if the nanotubes are aggregated and there is not a good dispersion in the polymer matrix a Dysonian-like resonance shape will appear [8].

In our recent publication [13] we investigated NR based hybrid nanocomposites that contained 6 phr multiwalled carbon nanotubes (MWCNT) and various quantities of EOMt. The obtained ESR spectra had a symmetrical Lorentzian shape for all nanocomposites, indicating good dispersion of the MWCNT throughout the NR matrix, regardless of the EOMt presence and quantity. We found a sharp decrease in the double integral of the resonance spectra when EOMt quantities higher than 12 phr were added in the matrix. The double integral of the resonance spectrum in ESR spectroscopy is proportional to the spin concentration [15]. This suggested that, above a certain amount of EOMt in the matrix, a synergism engenders between EOMt and MWCNT, resulting in a sharp spin concentration decrease in the samples. The synergism between these two nanofillers was also reported in some previous works [16–19], manifested by their better dispersion in some solvents and polymer matrices, but this was for the first time demonstrated by changes in the ESR spectra of the MWCNT in dependence of the EOMt concentration in the nanocomposites.

Motivated by this fact, we wanted to confirm that this kind of changes in the ESR spectra of MWCNT, initiated by the presence of EOMt, are repetitive and could also be observed for different concentrations of MWCNT in the NR matrix. With this in mind, we performed the ESR investigations on NR samples that contain much lower concentration (2 phr) of carbon nanotubes and the same concentrations of EOMt as in our previous work (4–20 phr). The appearance of the carbon nanotubes ESR spectra was analyzed and the dependence of the double integral of the resonance spectra on the amount of EOMt in the NR matrix was established. The cluster-cluster aggregation (CCA)-model [20], which is one of the fundamental micro-mechanical concepts of non-linear viscoelasticity of filled rubber, based on fractal approaches of filler networking, was used to assess the filler networking energy, which could be considered as additional indicator of fillers synergy.

EXPERIMENTAL

Materials

The NR-compounds were based on a Standard Malaysian Rubber (SMR 10). The organo-montmorillonite (OMt) used was Nanofil 15 supplied from Süd-Chemie AG Moosburg, Germany. Distearyl dimethylammonium chloride (QUAT) was used as an organic modifier. The specific gravity of this OMt was 1.8 gcm^{-3} with an average particle size of 25 μm. Carbon nanotubes, NC7000, a multiwall carbon nanotubes (MWCNT) produced by catalytic carbon vapor deposition (CCVD) process, were supplied by NANOCYL S. A. (Belgium). They were 90% pure containing 10% metal oxides and had an average diameter of 9.5 nm and an average length of 1.5 μm. The stearic acid was purchased from ACROS Organics, Geel, Belgium with 97% purity. The vulcanizing accelerators N-tert-Butyl-2-benzothiazolesulfenamide (TBBS) and N-cyclohexyl-2-benzothiazolesulfenamide (CBS) were provided from Rhein Chemie Rheinau GmbH, Mannheim, Germany. Sulfur (S), N-(1,3-Dimethylbutyl)-N'-phenyl-p-phenylenediamine (6PPD) and zinc oxide (ZnO) used in this study were of industrial grade.

Preparation of the rubber nanocomposites

The commercial OMt was first expanded by intercalation of stearic acid in the interlayer space prior to its incorporation in the rubber matrix [21]. This preparation is described in detail in reference [18]. The preparation of the hybrid rubber nanocomposites containing expanded OMt and MWCNT was performed in two steps, in an internal mixer (Haake Rheomix) and in an open two roll mill (Polymix 110 L, size: 203 × 102 mm Servitec GmbH, Wustermark, Germany). The formulations of NR compounds expressed as parts per hundred of rubber (phr) are shown in Table 1. The procedure is fully described in reference [18].

Table 1. Formulation of different NR compounds

Sample code	NR*	MWCNT	EOMt
NR/h200	100	2	0
NR/h222	100	2	4
NR/h244	100	2	8
NR/h266	100	2	12
NR/h288	100	2	16
NR/h21010	100	2	20

*Mass of the ingredients was taken in parts per hundred of rubber (phr). The ingredients which amounts were kept constant in all compounds were ZnO 5 phr, stearic acid 2 phr, 6PPD 1 phr, CBS 1.5 phr, TBBS 0.2 phr and S 1.5 phr.

The test samples were molded and cured to 2 mm plates by compression molding (150 kN) on an electrically heated hydraulic press at 150 °C. The rubber samples were vulcanized up to their respective optimum cure time (t_{90}), previously determined with a vulcameter (Scarabaeus, Langgöns, Germany), and then stored for 24 hours before the tests were performed.

Characterization

Electron spin resonance (ESR) measurements were performed on a Varian E-109 spectrometer operating at 9.29 GHz, equipped with a Bruker ER 041 XG microwave bridge and a Bruker ER 4111 VT temperature unit. Spectroscopic parameters were: microwave power 10.0 mW, modulation amplitude 0.1 mT, scan range 10 mT and scan time 60 s. The measurements were performed at room temperature.

Dynamic mechanical analysis was performed using a dynamic mechanical thermal spectrometer (Gabo Qualimeter, Ahlden, Germany, model Eplexor 2000N) in the tension mode. Temperature sweep analysis was carried out using a constant frequency of 10 Hz in a temperature range from – 80 °C to + 80 °C. For the measurement of the complex modulus (*E**), a static tensile load of 1% pre-strain was applied and then the samples were oscillated with a dynamic strain of 0.5%. The measurements were performed with a heating rate of 2 Kmin^{-1} under liquid nitrogen flow.

RESULTS AND DISCUSSION

The ESR spectrum of 2 phr MWCNT incorporated in the NR based nanocomposite, NR/h200, at room temperature is presented in Figure 1.

A narrow, symmetrical and intense line is observed, reminiscent of the ESR spectrum of pristine CNT [22].

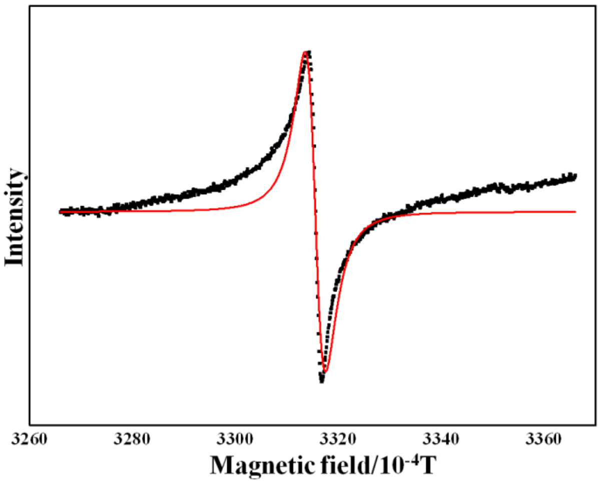

Figure 1. The ESR spectrum of 2 phr MWCNT incorporated in NR based nanocomposite (NR/h200), at room temperature

For a random distribution of CNT the resonance spectrum presents a symmetrical Lorentzian or Gaussian shape. The obtained spectrum was fitted by a Lorentzian line shape [23]:

$$I = 16I_0 \frac{\left(\dfrac{H-H_R}{H_{PP}/2}\right)}{\left(3+\left(\dfrac{H-H_R}{H_{PP}/2}\right)^2\right)^2} \qquad (1)$$

where I_0 is the intensity of the resonance line, H_{PP} is the resonance line width and H_R is the resonance field.

The solid line in Figure 1 represents the best fit obtained by using Equation (1). The agreement between the recorded spectrum and the theoretical shape in the peak region is good. In composite materials, if nanotubes are well dispersed throughout the matrix below the electrical percolation threshold, the resonance line will also have a symmetrical Lorentzian shape [8]. Here, the good agreement between the theoretical Lorentzian shape and the recorded resonance spectrum proves the good dispersion of the nanotubes within the NR matrix. This finding coincides with the finding in our previous investigation [18], in which transmission electron microscopy (TEM) was used as a method to estimate the dispersion of the nanofiller system in these samples. This again confirms that the predispersion of MWCNT in ethanol and the high viscosity of the rubber, which causes occurrence of strong shearing forces during the process of mixing, are sufficient to induce the separation of the individual CNT from their aggregates and to successfully form nanocomposites [18, 21].

To investigate, in this case (a lower quantity of MWCNT in the nanocomposites), the influence of the EOMt content on the resonance line position (*g*-factor) and the double integral, ESR measurements were performed on all samples. The ESR spectra of NR-nanocomposites containing 2 phr MWCNT but different quantities of EOMt (0, 4, 8, 12, 16, 20 phr), normalized to the sample weight, are shown in Figure 2.

All lines have the same Lorentzian shape, which proves that the good dispersion of the nanotubes within the NR matrix is not disrupted by the presence of EOMt, regardless of its quantity within investigated concentration range.

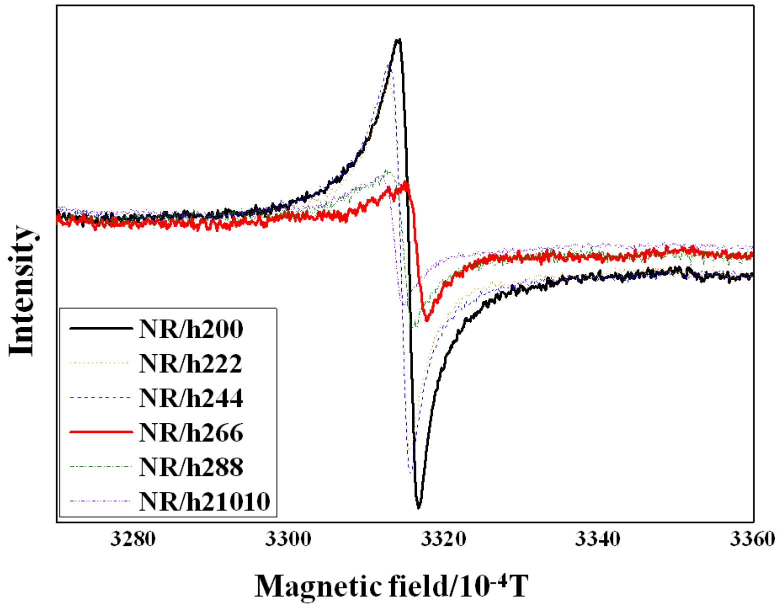

Figure 2. ESR spectra, normalized to the sample weight, of NR-nanocomposites with 2 phr MWCNT and different contents of EOMt, measured at room temperature

Chiparaet al. [8] found the position of the resonance line of carbon nanotubes dispersed in epoxy resin to be located near the free electron *g*-factor value. Their investigations showed the temperature independence of the *g*-factor, which led them to the conclusion that the resonance spectrum of CNT in epoxy resin composites originates from the uncoupled electronic spins delocalized over the carbon nanotubes.

For an uncoupled electronic spin (s = 1/2) the *g*-factor is:

$$g = \frac{h\nu}{\beta H_R} \tag{2}$$

where h is the Planck's constant, β is the Bohr magneton of the electron, ν is the frequency of the microwave field and H_R is the value of the external magnetic field at which the resonance is observed.

Assuming that the resonance spectra of the MWCNT incorporated in the NR-based nanocomposites originate from the uncoupled electronic spins delocalized over the CNT, we calculated the *g*-factor according to Equation (2). These values are presented in Table 2 along with the values of the double integral obtained from the data presented in Figure 2.

The *g*-factor values (Table 2) for all samples are close to the free electron *g*-factor value (g_0 = 2.0023) [24, 25] and are only slightly changing with the presence of EOMt and its quantity.

Table 2. Double integral of the resonance spectra, normalized to weight, and *g*-factor values for all NR nanocomposites

Sample code	*g*-factor	Double integral / m (mg)
NR/h200	2.0029	1507
NR/h222	2.0035	1211
NR/h244	2.0036	1416
NR/h266	2.0023	630
NR/h288	2.0036	581
NR/h21010	2.0040	544

On the other hand, the established dependence of the double integral of resonance spectra on the amount of EOMt showed a sharp decrease when EOMt quantities higher than 8 phr are introduced into the matrix. Intrinsically this is the same amount of EOMt as found in our previous study, but in this case the decrease is even more pronounced. Solid lines in Figure 2 indicate the resonance spectra of the sample containing only MWCNT (NR/h200) and that with additional 12 phr EOMt (NR/h266) where the sharp decrease in the double integral of the resonance spectra occurs. Since the double integral of the resonance spectrum in ESR spectroscopy is proportional to the spin concentration [15], this suggests that above a certain concentration of EOMt a synergism engenders between EOMt and MWCNT, resulting in a sharp spin concentration decrease in the samples.

It is interesting to see how this synergism influences the filler networking, which is determined by the morphological arrangement of the filler particles and formation of joints by filler-filler bonds. Hence, to assess the filler-networking energy of the hybrid nanofillers for different MWCNT/EOMt-ratios, the cluster-cluster aggregation (CCA) model was used. This model is based on the assumption of geometrical arrangements of sub-units resulting from the kinetical cluster-cluster aggregation [26]. According to this model the temperature or frequency dependence of the elastic modulus of the CCA clusters is governed by the immobilized, glassy polymer between adjacent filler particles and is determined by that of a glassy polymer. In the high temperature range, well above the bulk glass transition temperature of the polymer system, an Arrhenius temperature behavior for the elastic modulus is expected, which is typically found in polymers in the glassy state. This Arrhenius like behavior, in a somewhat different interpretation, could be understood by referring it to the transition of the glassy polymer bridges between adjacent filler particles of the filler network, i.e., the apparent filler networking energy. In Figure 3 the relationships between the natural logarithm of storage modulus, ln(E') of the different NR based composites and the inverse temperature, far above the glass-rubber transition region ($10^3 T$ ~ 3.4 to 2.8 K^{-1}; corresponding T ~ 20 °C to 80 °C), are presented. These results are obtained from the DMA temperature sweep measurements. If the Krause assumption [27] that the dynamic modulus is proportional to the number of sub unites (e.g., filler aggregates) is used, then the straight lines obtained have a slope E_c/R, where E_c is the activation energy or, in our case, filler networking energy, and R is the gas constant.

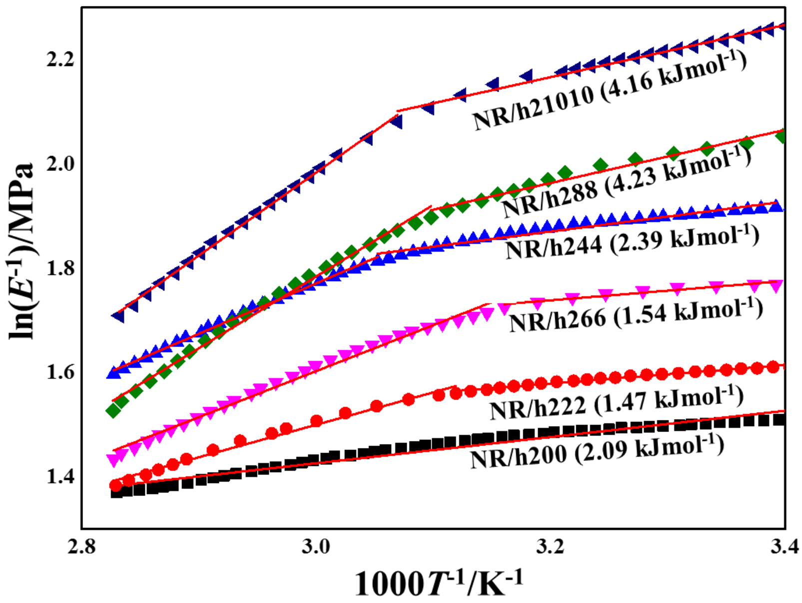

Figure 3. Natural logarithm of storage modulus as a function of reciprocal absolute temperature for the different NR nanocomposites

For the NR/h200 nanocomposite containing only MWCNT there is only one linear relationship between ln(E') and the inverse temperature. For the composites containing the hybrid nanofiller there are two distinct mechanisms with different activation energies. Similar behavior of NR nanocomposites was found in our previous study [13]. Based on the obtained results, we can conclude that the linear relationship that occurs below ~60 °C (but still well above the bulk glass transition temperature of the polymer system) corresponds to the apparent filler networking energies and the other, occurring above ~60 °C, is connected to melting of the stearic acid, used to expand the galleries of OMt layers. The filler networking energies for the different ratios of MWCNT and EOMt are calculated from the slopes and are presented in Figure 3.

The filler networking energy for the nanocomposite containing only MWCNT is 2.09 kJ/mol. The addition of EOMt first causes a reduction of the filler networking energy and then it starts to increase with increase of EOMt content, reaching the maximum value of 4.23 kJ/mol for 16 phr of EOMt and then followed by a slight decrease for 20 phr. This decrease is due to the re-agglomeration of the EOMt which was already concluded by XRD and TEM investigations. The obtained results clearly show that the presence of the EOMt above some critical concentration can strengthen the hybrid-filler networking in NR nanocomposites.

CONCLUSION

The method of ESR can be successfully applied for analysis of the interactions between the MWCNTs and EOMt in NR hybrid filler nanocomposites. Electron spin resonance (ESR) spectra of multi-walled carbon nanotubes (MWCNT) in natural rubber (NR) based nanocomposites filled with MWCNT/EOMt hybrid filler have a symmetrical Lorentzian shape, indicating good dispersion of the MWCNT throughout the NR matrix, regardless of the EOMt concentration. The sharp decrease in the double integral of the resonance spectra, when EOMt quantities higher than 8 phr are used in the matrix, suggested that above a certain amount of EOMt a synergism engenders between the two nanofillers, resulting in a sharp spin concentration decrease. This was for the first time demonstrated by changes in the ESR spectra. Whit these findings it is shown that the synergism between these two nanofillers, which led to their better dispersion in some solvents and polymer matrices, is also manifested by changes in the ESR spectra on the MWCNT in dependence of the concentration of EOMt in nanocomposites. The apparent filler networking energy, assessed by applying the CCA-model to the results from the DMA temperature sweep measurements, suggested that the presence of EOMt strengthens the hybrid-filler networking when its concentration reaches critical value.

Acknowledgement: The authors gratefully acknowledge the COST action CM1302 (SIPs) for financing the Short Term Scientific Mission in Rudjer Bošković Institute in Zagreb during which the ESR measurements were performed. We also thank Prof. Gert Heinrich from the Leibniz Institut for polymer research in Dresden for the realization of the research stay in this Institute during which the samples were prepared. This work was partially supported by the Croatian Science Foundation project 1102 and RISK project from the University of Rijeka.

REFERENCES

[1] S. Bandow, Magnetic properties of nested carbon nanostructures studied by electron spin resonance and magnetic susceptibility measurements, *J. Appl. Phys.*, **80** (1996), pp. 1020–1027. DOI: http://dx.doi.org/10.1063/1.362835

[2] J. N. Coleman, D. F. O'Brien, A. B. Dalton, B. McCarthy, B. Lahr, R. C. Barklie, W. J. Blau, Electron paramagnetic resonance as a quantitative tool for the study of multiwalled carbon nanotubes, *J. Chem. Phys.*, **113** (2000), pp. 9788–9793. DOI: http://dx.doi.org/10.1063/1.1322032

[3] P. Petit, E. Jouguelet, J. E. Fischer, A. G. Rinzler, E. E. Smalley, Electron spin resonance and microwave resistivity of single-wall carbon nanotubes, *Phys. Rev. B.*, **56** (1997), pp. 9275–9278. DOI: http://dx.doi.org/10.1103/PhysRevB.56.9275

[4] L. C. Venema, V. Meunier, Ph. Lambin, C. Dekker, Atomic structure of carbon nanotubes from scanning tunneling microscopy, *Phys. Rev. B*, **61** (2000), pp. 2991–2996. DOI: http://dx.doi.org/10.1103/PhysRevB.61.2991

[5] T. Belin, F. Epron, Characterization methods of carbon nanotubes: a review, *Mat. Sci. Eng. B-Solid.*, **119** (2005), pp, 105–118. DOI: http://dx.doi.org/10.1016/j.mseb.2005.02.046

[6] K. Shen, D. L. Thierney, T. Pietrass, Electron spin resonance of carbon nanotubes under hydrogen adsorption, *Phys. Rev. B*, **68** (2003), pp. 165418.

[7] H. Yokomichi H, Changes in electron spin resonance spectra of carbon nanotubes by thermal annealing, *Vacuum*, **3–4** (2004), pp. 677–681.

[8] M. Chipara, F. Iacomi, J. M. Zaleski, J. B. Bai, Electron spin resonance spectroscopy investigations of carbon nanotubes-epoxy composites, *J. Optoelectron. Adv. M.*, **8** (2006), pp. 820–824.

[9] V. Likodimos, S. Glenis, N. Guskos, C. L. Lin, Magnetic and electronic properties of multiwall carbon nanotubes, *Phys. Rev. B*, **68** (2003), pp. 045417.

[10] S. Garaj, L. Thien-Nga, R. Gaal, L. Forro, K. Takahashi, F. Kokai, M. Yudasaka, S. Iijima, Electronic properties of carbon nanohorns studied by ESR, *Phys. Rev. B*, **62** (2000), pp. 17115.

[11] M. Chipara, J. M. Zaleski, D. Hui, C. Du, N. Pan, Electron spin resonance on carbon nanotubes–polymer composites, *J. Polym. Sci. Polym. Phys.* **43** (2005), pp. 3406–3412.

[12] D. Arcon, A. Zorko, P. Cevc, A. Mrzel, M. Remskar, R. Dominko, M. Gaberscek, D. Mihailovic, Electron spin resonance of dopedchalcogenide nanotubes, *Phys. Rev. B*, **67** (2003), pp. 125423.

[13] A. Ivanoska-Dacikj, G. Bogoeva-Gaceva, S. Valić, S. Wießner, G. Heinrich, Benefits of hybrid nanofiller networking between organically modified montmorillonite and carbon nanotubes in natural rubber: experiments and theoretical interpretations, *Appl. Clay Sci.*, **136** (2017), pp. 192–198.

[14] M. Chipara, K. Lozano, R. Wilkins, E. V. Barrera, M. X. Pulikkathara, L. Penia-Para, M. Chipara, ESR investigations on polyethylene-single wall carbon nanotube composites, *J. Mater. Sci.*, **43** (2008), pp. 1228–1233. DOI 10.1007/s10853-007-2264-8

[15] R. C. Barklie, Characterisation of defects in amorphous carbon by electron paramagnetic resonance. *Diam. Relat. Mater.*, **12** (2003), pp. 1427–1434. DOI: 10.1016/S0925-9635(03)00004-9

[16] Y. F. Lan, J. J. Lin, Observation of carbon nanotube and clay micellelikemicrostructures with dual dispersion property. J. *Phys. Chem. A*, **113** (2009), pp. 8654–8659. DOI: 10.1021/jp9026805

[17] A. Ivanoska-Dacikj, G. Bogoeva-Gaceva, A. Buzarovska, Clay improved dispersion of carbon nanotubes in different solvents, *Contributions, Sec. Nat. Math. Biotech. Sci., MASA*, **36** (2015), pp. 5–10.

[18] A. Ivanoska-Dacikj, G. Bogoeva-Gaceva, S. Rooj, G. Heinrich, S. Wieβner, Fine tuning of the dynamic mechanical properties of natural rubber/carbon nanotube nanocomposites by organically modified montmorillonite: A first step in obtaining high- performance damping material suitable for seismic application, *Appl. Clay Sci.*, **118** (2015), pp. 99–106. DOI: 10.1016/j.clay.2015.09.009

[19] S. Rooj, A. Das, K. W. Stöckelhuber, S. Wieβner, D. Fischer, U. Reuter, G. Heinrich, 'Expanded organoclay' assisted dispersion and simultaneous structural alterations of multiwall carbon nanotube (MWCNT) clusters in natural rubber, *Compos. Sci. Technol.*, **107** (2015) 36–43. DOI: 10.1016/j.compscitech.2014.11.018

[20] M. Klüppel, The role of disorder in filler reinforcement of elastomers on various length scales, *Adv. Polym. Sci.*, **164** (2003), pp. 1–86.

[21] A. Das, K. W. Stöckelhuber, R. Jurk, M. Saphiannikova, J. Fritzsche, H. Lorenz, M. Klüppel, G. Heinrich, Modified and unmodified multi-walledcarbon nanotubes in high performance solution-styrene-butadiene and butadiene rubber blends, *Polymer* **49** (2008), pp. 5276–5283. DOI: http://dx. doi.org/10.1016/j.polymer.2008.09.031

[22] W. D. Rice, R. T. Weber, A. D. Leonard, J. M. Tour, P. Nikolaev, S. Arepalli, V. Berka, A.-L. Tsai, J. Kono, Enhancement of the electron spin resonance of single-walled carbon nanotubes by oxygen removal, *ACS Nano.* **6** (2012), pp. 2165–2173. DOI: 10.1021/nn204094s

[23] C. P. Poole, H. A. Farach, Lineshapes. In: Poole, C. P. and Farach, H. A. (eds.), *Handbook of Electron Spin Resonance*, Volume 2, Springer-Verlag, New York, 1999, pp. 47–67.

[24] K. A. Müller, Spin Resonance in Neutron-Irradiated Graphite. *Phys. Rev.* **123** (1961), pp. 1550–1552. DOI: http://dx.doi.org/10.1103/PhysRev.123.1550

[25] F. Beuneu, C. l'Huillier, Modification of multiwall carbon nanotubes by electron irradiation: An ESR study, *Phys. Rev. B*, **59** (1999), pp. 5945–5949. DOI: http://dx.doi.org/10.1103/PhysRevB.59.5945

[26] G. Heinrich and M. Klüppel, Recent advances in the theory of filler networking in elastomers. In: Lee, K.S. (Ed.), *Filled Elastomers Drug Delivery Systems Series:* Advances in Polymer Science. Springer, Berlin, 2002, pp. 1–44. DOI: 10.1007/3-540-45362-8_1

[27] G. Kraus, Mechanical losses in carbon black filled rubbers. *J. Appl. Polym. Sci. Symp.*, **39** (1984), pp. 75–92.

ЕЛЕКТРОН-СПИНСКА РЕЗОНАНЦИЈА НА ХИБРИДНИ НАНОКОМПОЗИТИ НА БАЗА НА ПРИРОДНА ГУМА

Александра Иваноска-Дациќ[1], Гордана Богоева-Гацева[1,2], Срећко Валиќ[3,4]

[1]Истражувачки центар за животна средина и материјали,
Македонска академија на науките и уметностите, Скопје, Република Македонија
[2]Технолошко-металуршки факултет, Универзитет „Св. Кирил и Методиј“,
Скопје, Република Македонија
[3]Оддел за хемија и биохемија, Медицинско училиштеи центар за нано-науки и технологии,
Универзитет во Риjека, Риjека, Хрватска
[4]Институт „Руѓер Бошковиќ“, Загреб, Хрватска

Методот електрон-спинска резонанција (ЕСР) е применет како нова алатка за анализа на синергијата меѓу две нанополнила различни по природа, форма и ригидност, диспергирани во матрица од природна гума. Испитувани се примероци од природна гума наполнети со хибридно полнило од повеќesидни јаглеродни наноцевки (2 дела на 100 дела еластомер) и експандиран органомодифициран монморилонит (ЕОМт, 4 до 20 дела на 100 дела еластомер). Утврдена е зависност на двојниот интеграл на резонантниот спектар од количината на ЕОМт во природната гума. Неговото намалување со зголемување на концентрацијата на ЕОМт ја потврдува синергијата меѓу двете употребени нанополнила. Паралелно со ЕСРсенаправени и динамичкомеханички мерења при променлива температура, при што е искористен моделот на кластер-кластер агрегација за процена на привидната енергија на вмрежување. Добиените резултати сугерираат дека

ЕОМт употребен во хибридното полнило над одредена критична концентрација придонесува за зајакнати мрежни интеракции меѓу полнилата.

Клучни зборови: електрон-спинска резонанција, јаглеродни наноцевки, органски-монтморилонит, еластомерни нанокомпозити

ПРИЛОЗИ, Одделение за природно-математички и биотехнички науки, МАНУ, том **39**, бр. 1, стр. 31–49 (2018)
CONTRIBUTIONS, Section of Natural, Mathematical and Biotechnical Sciences, MASA, Vol. **39,** No. 1, pp. 31–49 (2018)

Received: September 12, 2017
Accepted: November 3, 2017

ISSN 1857–9027
e-ISSN 1857–9949
UDC: 556.551:504.5(497.775)
DOI: 10.20903/csnmbs.masa.2018.39.1.118

Original scientific paper

DISTRIBUTION OF CHEMICAL ELEMENTS IN SURFACE WATERS FROM THE CRNA RIVER BASIN, REPUBLIC OF MACEDONIA

Dimitri Tomovski[1], Trajče Stafilov[2,3*], Robert Šajn[4], Katerina Bačeva Andonovska[3]

[1]Alkaloid AD, Skopje, Republic of Macedonia
[2]Institute of Chemistry, Faculty of Natural Sciences and Mathematics,
Ss. Cyril and Methodius University, Skopje, Republic of Macedonia
[3]Research Center for Environment and Materials, Macedonian Academy of Sciences and Arts,
1000 Skopje, Republic of Macedonia
[4]Geological Survey of Slovenia, Ljubljana, Slovenia
e-mail: trajcest@pmf.ukim.mk

An investigation of the distribution of 23 chemical elements (Ag, Al, As, B, Ba, Ca, Cd, Co, Cr, Cu, Fe, K, Li, Mg, Mn, Mo, Na, Ni, P, Pb, Sr, V and Zn) in surface water samples from the entire basin of the Crna River, Republic of Macedonia, was carried out. In total 31 water samples were collected, from which 8 samples from the Crna River and 4 samples from four main tributaries of Crna River in the Pelagonia Valley (Blato, Prilepska Reka, Dragor and Jelaška Reka). Also, surface water samples were collected from 3 locations in the Tikveš Lake, 8 locations from the Majdanska River and river of Blašnica before its inflow into the Tikveš Lake and from 7 locations of the lower course of the Crna River after the dam of Tikveš Lake until its inflow into the river of Vardar. Determination of the concentration of the investigated elements was performed by using atomic emission spectrometry with inductively coupled plasma (ICP-AES). All data obtained for the analyzed samples were statistically processed using software Stat Soft 11.0 where the descriptive statistical analysis of the value for the concentration of the elements was performed. The maps of spatial distribution of the concentration for each element and a histograms for the representation of elements with mean values of the concentrations by regions, were also prepared. The obtained results show that the concentration of investigated element are mainly followed the lithology of the region. However, higher concentrations of arsenic were found in the water samples from the river of Blašnica which is a result of anthropogenic influence from the abounded Allchar mine on the Kožuf Mountain. Also, the increased concentrations of nickel were found in the samples from the lower couse of the Crna River after the dam of Tikveš Lake due to the anthropogenic influence from the ferronickel smelter plant Feni Industry, which can influence the quality parameters of surface waters.

Key words: Crna River, Republic of Macedonia, river basin, water, heavy metals, distribution

INTRODUCTION

Water is one of the most important and most prevalent components on the Earth as well as a source of the life on the planet. Its quality and integrity is of equal and essential importance to all living systems. The required daily quantities of drinking water are increasing every day, even though the aquatic reserves on the Earth are still high. Human activities are broad and complex and lead to irreversible processes and permanent pollution of waters. Heavy metals, in addition to being natural constituents of the Earth's crust, regardless of their origin from natural or anthropogenic sources, are environmental pollutants [1].

Rivers and streams can be defined as dynamic systems that constantly adjust to natural and human-caused changes. Generally, water resources have a direct influence on the quality of life of the people, their health and overall productivity [2, 3]. The increase of the world's population, the rapid development of the industry, the needs for increased crops in agriculture and food technology, as well as the urbanization require increasing quantities of water. In such conditions of increased anthropogenic activities and consumption, the degree of water pollution increases sharply. If the change in the quality and integrity of naturally occurring water, whether it comes from a natural source or from anthropogenic sources, contributes to the unsuitability or danger of use for humans, animals and plants, such water is considered contaminated [4].

About 2% of the territory of the Republic of Macedonia is under water. There are about 35 rivers and 53 natural and artificial lakes. According to the quantities of water resources, Macedonia is an area with satisfactory water resources, but with their uneven distribution. The water pollution in the Republic of Macedonia is connected with the developing industry, agriculture activities, creation of illegal landfills, uncontrolled discharge of sewage waters into rivers contributed to creating contaminated water ecosystems [5, 6]. As a central water ecosystem, river of Vardar's basin which represents the most important and humanly influenced water resource in R. Macedonia, was studied previously [7–11], as well as its tributary the river of Bregalnica [12, 13].

The aim of this work is to shown the status of Crna River which is the largest tributary of the river of Vardar, the main river in the Republic of Macedonia, and the primary objective of this investigation is to present data about the spatial distribution of 23 chemical elements (Ag, Al, As, B, Ba, Ca, Cd, Co, Cr, Cu, Fe, K, Li, Mg, Mn, Mo, Na, Ni, P, Pb, Sr, V и Zn) in samples of surface water collected from different locations in the Crna River basin, Republic of Macedonia, and to interpret and correlate there concentrations with the lithogenic occurrence and possible anthropogenic impact.

EXPERIMENTAL

Investigated area

The spring of the river of Crna Reka is located in the district of the town of Demir Hisar, and it consists of two rivers: Ilinska and Cerska. Before village of Železnec they merge and continue to flow under the common name Crna River (Crna Reka). However, the location of Crna Hole, close to village of Železnec with an altitude of 760 m, is considered as the true spring of Crna River. In its lower stream, the Crna River flows into the artificial Tikveš Lake, and after it flows into the river of Vardar, near the village of Gradsko at an altitude of 129 m (Figure 1). The total length of the river course is 207 km, with a mean slope of 3.1 ‰. The average flow at the stream is 37 m^3/s.

The area of the Crna River basin is an area that extends into two states in the south-western part of the Republic of Macedonia and the northern part of the Republic of Greece. On the territory of the Republic of Macedonia, the Crna River basin extends between 40°51'56" and 41°36'20" north latitude and 20°56'45" and 22°4'58" eastern longitude. Its total length is 207 km with the total area of the catchment area in both countries of 5775 km^2, of which to the Republic of Macedonia belongs the largest part of 4870 km^2, while the catchment area in the Republic of Greece is 905 km^2.

In the river basin of Crna River the influences of the Mediterranean, Mediterranean-altered, temperate-continental and mountainous climate are present. The mean annual air temperature ranges from 8.4 ºC to 13.5 ºC over a period of 23 years. The average absolute maximum air temperatures in the Crna River are within the limits of 32 ºC. The absolute minimum air temperature for the same period is within the limits of –15ºC. The amplitudes of the extreme temperatures are quite large and they range from 51.5 ºC to 66.6 ºC [14]. The warmest months for all meteorological stations in the Crna River basin are July and August and the coldest month is January. According to the regions of this basin, in Tikveš Valley the influence of the sub-Mediterranean climate is generally present, in the central part of the basin (Pelagonia Valley) the continental climate is represented, while the influence of the moderate continental climate appears in the upper part of the basin [14, 15].

The Crna River basin belongs to three geotectonic structural units: the upper western part lies in the area of the West-Macedonian zone, the middle part is on the Pelagonian zone and the lower part to the Vardar zone [16]. The upper western part which lies in the area of the West-Macedonian zone is built mainly from Paleozoic and Triassic formations, primarily from crystalline schists and limestones (marbles and dolomites), as well as from granites. The middle part which belongs to the Pelagonian geotectonic zone is dominated by Precambrian rocks, such as: micas and marbles, as well as Neogene deluvial and alluvial formations. In the lower part of the flow of Crna River, which belongs to the Vardar zone, covering the areas of the eastern part of Mariovo and part of the Tikveš Valley, the most present are the crystalline schists, granites and granodiorites, flysch sediments, volcanic breccias, limestones, marble dolomites etc. [15, 16].

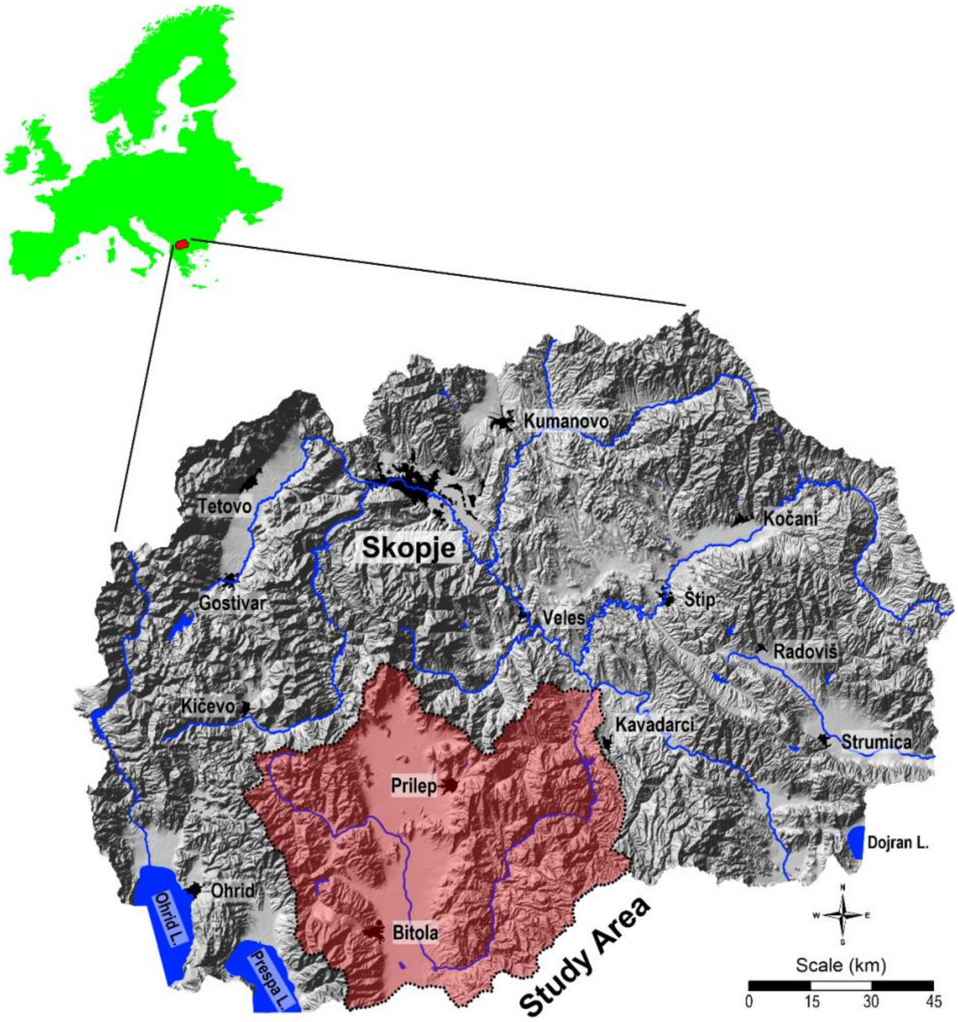

Figure 1. Map of the Republic of Macedonia indicating the Crna River Basin

Sampling

In the period from June to September 2016 year, 31 water samples were collected, from which 13 water samples are collected from the source of Crna River to the estuary in Tikveš Lake, including 8 from the Crna River and 4 from four main tributaries of Crna River in the Pelagonia Valley (Blato, Prilepska Reka, Dragor and Jelaška Reka). Also, surface water samples were collected from 4 locations in the Tikveš Lake, 8 locations of the river Blašnica and its tributary Majdanska River before its inflow into the Tikveš Lake and 7 locations of the lower course of the Crna River after the dam of Tikveš Lake (Figure 2).

Depending on location conditions and availability, samples were collected in the near vicinity of the previously specified locations. When collecting samples, the geographical coordinates were recorded using a global positioning system and each sample was inscribed with the sample mark, sample type and date of sampling. From each location, one sample of water was taken in a purely sterile plastic bottle with a plastic closure. Surface water samples (1 liter each) are prepared immediately upon arrival in the laboratory, filtered through a Whatman membrane filter with a pore sizes < 0.45 μm using vacuum pump (Merck) and acidified with 1 ml of concentrated nitric acid (HNO_3, 69 %, ultra pure). The preserved samples were stored in the refrigerator until analysis. The reagent blank was prepared by filtering MilliQ water through the filter and acidified the sample.

All data for the concentration of the tested elements were statistically processed using the software Stat Soft, 11.0. For 31 water samples the basic descriptive statistical analysis of the values for the concentration of the elements was performed. By using bivariate statistics with a level of significance $p < 0.05$; $p > 0.01$ the degree of correlation of the values of the concentrations of the chemical elements in the samples is estimated, and the coefficients of correlation are presented in the correlation matrix.

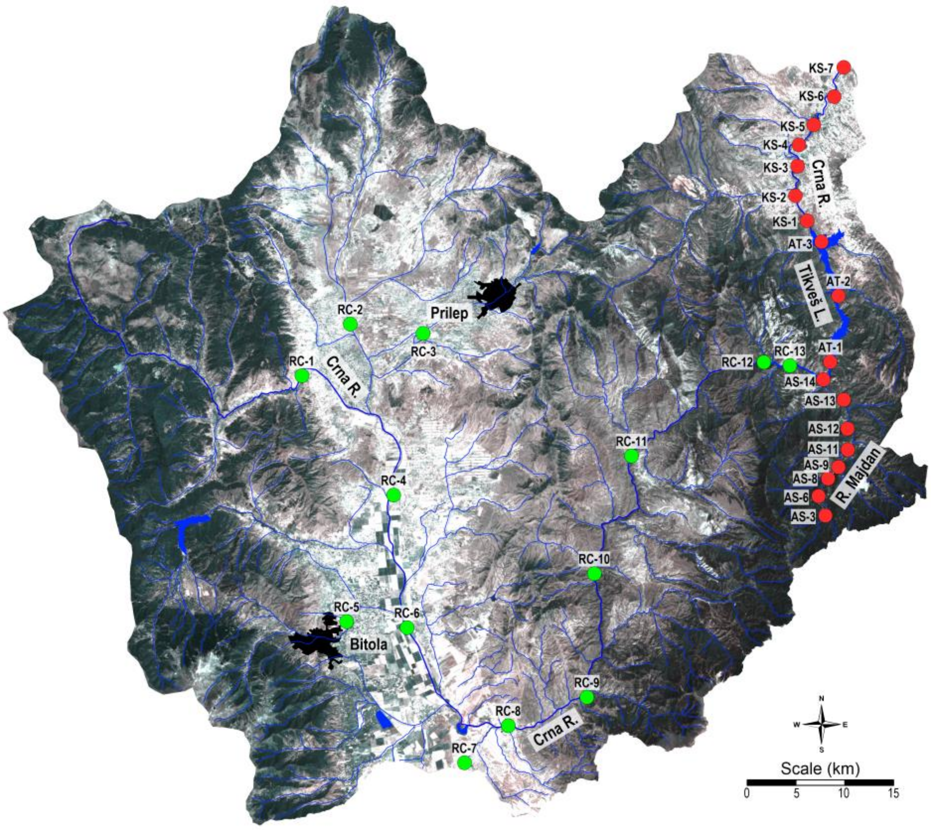

Figure 2. Map of the investigated basin with the locations of water samples

The analysis of water samples was performed using an atomic emission spectrometry with the inductively coupled plasma – atomic emission spectrometry, ICP-AES (Varian, 715ES). For better adjusting of the sensitivity for the most of the analyzed elements in the moss digests, an ultrasonic nebulizer CETAC (ICP/U-5000AT) was used. In all samples, a total of 23 chemical elements were analyzed: Ag, Al, As, B, Ba, Ca, Cd, Co, Cr, Cu, Fe, K, Li, Mg, Mn, Mo, Na, Ni, P, Pb, Sr, V и Zn. Standard solutions of elements were prepared by dilution of 1000 mg/l solutions (11355-ICP multi-element standard solution). The method of standard additions was applied, and it was found that the recovery of the investigated elements ranged between 98 and 101 % for ICP-AES. The optimal instrumental parameters for these techniques are given in our previously published paper [17].

RESULTS AND DISCUSSION

The obtained data for the concentration of the analyzed elements determined in surface water samples from 13 locations from the source of Crna River to the estuary in Tikveš Lake, including 8 from the Crna River, and 4 from four main tributaries of Crna River in the Pelagonia Valley (Blato, Prilepska Reka, Dragor and Jelaška Reka), as well as 7 locations of the lower course of the Crna River after the dam of Tikveš Lake. They were statistically processed. Their descriptive statistics are presented in Table 1. Due to the specificity of the lithology and mining activities in the Kožuf Mountain region, the descriptive statistics of the concentrations of the same elements in the surface water samples collected from 8 locations of the Majdanska and Blašnica rivers (the right tributary of Crna River) before its inflow into the Tikveš Lake, are given in a separate table (Table 2). The following statistical parameters are given in Tables 1 and 2: X – arithmetic mean, Md – median, Min – minimum, Max – maximum, P_{10} – 10 percentiles, P_{90} – 90 percentiles, S – standard deviation, S_x - standard deviation (standard error), CV – coefficient of variation, A – asymmetry and E – distribution.

Tables 1 and 2 give data on concentrations of only 14 elements because the concentration of the other elements are below the detection limit of 0.001 mg/l for Ag, B, Cd, Co, Cr and V, 0.005 mg/l for Mo and Ni and 0.01 mg/l for P and Pb.

Table 1. Descriptive statistics of the concentrations of the analyzed elements in surface water samples collected from the Pelagonia Valley, Mariovo region, Tikveš Lake and from the part of the Crna River after the dam of the Tikveš Lake (in mg/l)

Element	X	Md	Min	Max	P_{10}	P_{90}	S	S_x	CV	A	E
Al	0.076	0.052	0.021	0.45	0.027	0.12	0.09	0.018	115	3.86	16.50
As	< 0.010	< 0.010	< 0.010	< 0.010							
Ba	0.031	0.028	0.015	0.051	0.022	0.045	0.01	0.002	31	0.80	-0.19
Ca	42	39	10	74	32	59	14	2.9	34	0.11	0.84
Cu	0.017	0.015	0.002	0.063	0.003	0.027	0.01	0.003	77	1.97	6.00
Fe	0.16	0.11	0.021	0.85	0.032	0.28	0.18	0.037	114	2.88	10.39
K	4.8	4.8	2.4	10	3.0	6.7	1.6	0.33	33	1.50	4.11
Li	0.029	0.033	0.001	0.051	0.004	0.047	0.02	0.004	59	-0.59	-1.26
Mg	11	11	2.6	18	5.0	17	4.1	0.86	36	-0.42	-0.28
Mn	0.064	0.040	0.006	0.31	0.009	0.15	0.07	0.014	107	2.44	7.19
Na	11	13	0.005	37	0.005	19	9.3	1.9	85	0.65	1.01
Ni	0.033	0.019	0.005	0.11	0.007	0.071	0.03	0.006	84	1.17	0.92
Sr	0.19	0.19	0.050	0.28	0.11	0.28	0.06	0.012	31	-0.42	0.38
Zn	0.023	0.021	0.005	0.088	0.011	0.029	0.02	0.004	77	2.67	7.96

X – arithmetic mean, Md – median, Min – minimum, Max – maximum, P_{10} – 10 percentiles, P_{90} – 90 percentiles, S – standard deviation, S_x – standard deviation (standard error), CV – coefficient of variation, A – asymmetry, E – distribution

Table 2. Descriptive statistics of the concentrations of 8 surface water samples collected from the Majdanska and Blašnica rivers (in mg/l)

Element	X	Md	Min	Max	P_{10}	P_{90}	S	S_x	CV	A	E
Al	0.081	0.075	0.015	0.145	0.015	0.145	0.002	0.042	0.039	0.044	-0.357
As	0.082	0.052	0.010	0.199	0.010	0.199	0.005	0.071	0.066	0.938	-0.714
Ba	0.047	0.042	0.032	0.084	0.032	0.084	0.000	0.017	0.016	1.71	3.182
Ca	51	52	24	74	24	74	327	18.09	16.92	-0.17	-1.40
Cu	0.017	0.012	0.004	0.053	0.004	0.053	-	0.016	0.015	1.982	4.266
Fe	0.107	0.076	0.013	0.327	0.013	0.327	0.010	0.100	0.094	1.769	3.469
K	2.7	2.3	1.6	4.1	1.6	4.1	1.2	1.1	1.04	0.431	-2.121
Li	0.008	0.003	0.001	0.019	0.001	0.019	0.000	0.009	0.008	0.637	-2.206
Mg	15	13	5.3	22	5.26	22.4	42.2	6.50	6.1	0.021	-1.482
Mn	0.060	0.017	0.012	0.35	0.012	0.352	0.014	0.12	0.111	2.811	7.926
Na	3.99	2.77	2.48	6.50	2.48	6.50	3.62	1.90	1.78	0.642	-2.186
Ni	< 0.005	< 0.010	< 0.010	< 0.010							
Sr	0.24	0.21	0.14	0.35	0.14	0.35	0.007	0.083	0.077	0.426	-1.934
Zn	0.06	0.041	0.021	0.161	0.021	0.161	0.003	0.051	0.048	1.274	0.492

X – arithmetic mean, Md – median, Min – minimum, Max – maximum, P_{10} – 10 percentiles, P_{90} – 90 percentiles, S – standard deviation, S_x – standard deviation (standard error), CV – coefficient of variation, A – asymmetry, E – distribution

To determine the degree of correlation between the analyzed elements in the samples of surface water in the investigated area the bivariate statistics was used to obtain the correlation coefficients between the analyzed elements. If the absolute value of the correlation coefficient ranges between 0.50 and 0.72, it is considered that we have good correlation between the individual elements and a strong correlation between the analyzed elements exists if the correlation coefficient ranges from 0.72 and 1. Table 3 provides the correlation coefficient matrix for 31 surface water samples in all zones of the investigated area. It could be seen that a strong correlation was obtained between the concentrations of the earth-alkaline elements: Mg-Sr (0.98), Ca-Sr (0.88), Ca-Mg (0.88), Ba-Sr (0,80), Ba-Mg (0.77) and Ba-Ca (0.79) and between Fe-Al (0.87), while a good correlation exists between the concentrations of the following elements: Mn-Al (0.69), Mn-Ba (0.56), Zn-Cu (0.54), Na-K (0.54) and for the Blašnica river between As and Zn (0.50). All of these data are in agreement with the distribution of these elements in soil from the Crna River Basin [16].

Table 3. Matrix of correlation coefficients for the analyzed elements in the samples of surface and waters from the Crna River Basin

Element	Al	As	Ba	Ca	Cu	Fe	K	Li	Mg	Mn	Na	Ni	Sr	Zn
Al	1.00													
As	0.12	1.00												
Ba	0.22	0.40	1.00											
Ca	-0.07	0.22	**0.79**	1.00										
Cu	0.35	0.20	-0.18	-0.17	1.00									
Fe	**0.87**	-0.01	0.14	-0.14	0.13	1.00								
K	-0.04	-0.42	0.08	0.30	-0.15	0.13	1.00							
Li	-0.25	-0.40	-0.16	0.03	-0.19	-0.10	0.47	1.00						
Mg	-0.03	0.21	**0.77**	**0.88**	-0.19	-0.13	0.29	0.30	1.00					
Mn	0.69	0.05	0.58	0.32	0.08	**0.73**	0.28	-0.09	0.28	1.00				
Na	0.11	-0.27	-0.20	-0.18	0.00	0.44	0.54	0.09	-0.25	0.25	1.00			
Ni	-0.01	-0.31	0.13	0.27	-0.02	-0.15	0.26	0.41	0.27	0.09	-0.42	1.00		
Sr	-0.01	0.15	**0.80**	**0.88**	-0.19	-0.09	0.29	0.29	**0.98**	0.33	-0.24	0.26	1.00	
Zn	0.16	0.50	0.21	0.16	0.54	-0.08	-0.30	-0.32	0.15	-0.04	-0.30	-0.13	0.16	1.00

According to the national Decree on the categorization of water courses, lakes, accumulations and ground water [18] the water quality of the Crna River and its tributaries are defined as follow:

– Second class: water from Crna River at sampling locations close to the spring (RC-1), all locations after the dam of Tikveš Lake (KS-1 to KS-7), water from the tributary Eleška River – RC-7 (which is the only tributary that covers the catchment area in Greece), sampling locations of Majdanska River (AS-3, AS-6 and AS-8) and water from Tikveš Lake (AT-1, AT-2 and AT-3).

– Third class: water from the tributaries Blato (RC-12), Prilepska River (RC-3), Dragor (RC-5) and water from the Crna River from the town of Bitola to the inflow into Tikveš Lake (RC-8 to RC-13).

Such a classification of waters, in fact, defines the quality of surface waters in the Republic of Macedonia, since for each class there are maximum permissible concentrations of individual parameters and pollutants given in the national Decree on classification of waters [19]. The maximum permitted concentrations of the analyzed elements are given in Table 4. According to this Decree there are no limits for the concentrations of Ca, K, Li, Mg, Na and Sr.

Table 4. Maximum permissible concentration of the analyzed elements according to the Decree on Classification of Waters [19]

Element	Maximum permissible concentration, mg/l	
	Class II	Class III
Al	1.5	1.5
As	0.03	0.05
Ba	1.0	4.0
Cu	0.01	0.05
Fe	0.3	1.0
Mn	0.05	1.0
Ni	0.05	0.1
Zn	0.1	0.2

Table 5. Mean, median, minimal and maximal concentration of the analyzed elements for the whole river basin and for the zones (in mg/l)

Element/region		Al	As	Ba	Ca	Cu	Fe	K	Li	Mg	Mn	Na	Ni	Sr	Zn
Whole area	Mean	0.078	0.029	0.035	44.0	0.017	0.144	4.30	0.024	12.2	0.053	12.5	0.025	0.200	0.034
	Median	0.054	0.010	0.031	39.3	0.015	0.099	4.21	0.030	11.8	0.034	13.2	0.013	0.190	0.022
	Min	0.015	0.010	0.015	10.4	0.002	0.013	1.63	0.001	2.6	0.006	2.5	0.003	0.050	0.005
	Max	0.451	0.199	0.084	74.2	0.063	0.855	10.0	0.051	22.4	0.310	36.8	0.115	0.346	0.161
Pelagonia	Mean	0.121	0.010	0.030	37.0	0.020	0.268	4.71	0.010	7.8	0.101	15.2	0.020	0.144	0.021
	Median	0.083	0.010	0.028	37.0	0.020	0.185	4.42	0.006	6.9	0.089	14.5	0.019	0.144	0.021
	Min	0.036	0.010	0.015	10.4	0.006	0.074	2.42	0.001	2.6	0.022	5.1	0.007	0.050	0.014
	Max	0.451	0.010	0.049	74.2	0.035	0.855	10.0	0.047	14.4	0.310	36.8	0.038	0.231	0.028
Mariovo	Mean	0.054	0.010	0.026	35.4	0.016	0.209	4.95	0.045	11.2	0.053	17.6	0.019	0.188	0.019
	Median	0.054	0.010	0.025	34.7	0.015	0.190	4.21	0.047	10.9	0.043	18.0	0.013	0.190	0.023
	Min	0.031	0.010	0.023	31.9	0.009	0.146	3.63	0.037	10.2	0.023	15.5	0.003	0.167	0.005
	Max	0.069	0.010	0.028	39.2	0.027	0.284	7.27	0.051	12.1	0.098	18.9	0.050	0.202	0.029
Tikveš Lake	Mean	0.045	0.010	0.026	34.8	0.019	0.046	4.28	0.032	10.5	0.008	13.8	0.012	0.162	0.018
	Median	0.053	0.010	0.025	35.0	0.017	0.146	4.52	0.041	10.8	0.030	16.5	0.015	0.177	0.020
	Min	0.041	0.010	0.024	34.2	0.015	0.032	3.79	0.030	10.5	0.006	13.2	0.007	0.159	0.015
	Max	0.052	0.010	0.028	35.0	0.025	0.068	4.81	0.033	10.7	0.009	14.2	0.015	0.167	0.022
Lower flow of Crna River	Mean	0.055	0.010	0.038	54.0	0.014	0.041	5.18	0.038	15.8	0.053	14.7	0.007	0.246	0.032
	Median	0.051	0.010	0.041	50.7	0.004	0.034	5.26	0.040	15.2	0.034	15.9	0.007	0.225	0.016
	Min	0.021	0.010	0.025	49.7	0.002	0.021	4.94	0.031	14.4	0.015	12.3	0.005	0.221	0.008
	Max	0.118	0.010	0.051	60.8	0.063	0.099	5.36	0.042	17.7	0.152	17.2	0.011	0.279	0.088
Majdanska and Blašnica rivers	Mean	0.081	0.082	0.047	51.3	0.017	0.107	2.74	0.008	14.8	0.020	4.0	0.063	0.235	0.063
	Median	0.075	0.052	0.042	51.6	0.012	0.075	2.34	0.003	13.1	0.017	2.80	0.050	0.207	0.041
	Min	0.015	0.010	0.032	24.4	0.004	0.013	1.63	0.001	5.3	0.012	2.50	0.047	0.141	0.021
	Max	0.145	0.199	0.084	73.9	0.053	0.327	4.16	0.019	22.4	0.035	6.50	0.115	0.346	0.161

In order to easily notice the differences that would arise between the concentrations of the analyzed elements, the investigated region is divided into five zones, as follows:

– Crna River and its tributaries in the Pelagonia Valley (8 samples),

– the part of Crna River in Mariovo (3 samples),

–Tikveš Lake (3 samples),

– lower flow of Crna River after the dam of Tikveš Lake (8 samples), and

– rivers Majdanska and Blašnica in the Kožuf Mt. area (8 samples).

The mean, median, minimal and maximal concentrations of the analyzed elements for the whole river basin and for the zones are presented in Table 5. The results for each individual element together with the maps for their spatial distribution and histograms with the mean values for each river basin zone are given and interpreted in the text below.

Aluminum is the third most abundant largest element in the Earth's crust just after oxygen and silicon with the content of 8%. Aluminum is a light, non-ferrous, odorless, silver-white metal. Aluminum is a highly reactive metal and is not present in a free form in nature. Aluminium is commonly present in silicates in clay, soil, various minerals, rocks and precious stones. Higher concentrations of aluminum can have a negative impact on plants and animals in different ways. Spatial distribution of Al in surface water samples from the investigated river basin is shown in Figure 3.

The concentration of Al in water samples from the whole Crna River basin ranges from 0.015 to 0.451 mg/l with the mean concentration of 0.078 mg/l and median value of 0.054 mg/l (Tables 1, 2 and 5, Figure 4). The determined concentrations of Al in all water samples are below the maximum allowable concentration of Al for the second and third class of water (1.5 mg/l) according to the Decree for Classification of Waters of the Republic of Macedonia [19] in which the waters from the investigated region are classified [18].

The highest concentration of Al was found in the sample of surface water from the river Blato, a tributary of Crna River near the village of Vrbjani, municipality of Krivogaštani (0.45 mg/l) in the Pelagonia Valley. Probably the reason for such high concentration is the water treatment plant in the near vicinity of the sampling location (about 1 km upstream) using usually aluminum salts for the water purification. Considering the values obtained for Al concentrations by the zones in the river basin the highest concentration are found in the water samples from the Pelagonia Valley (mean concentration of 0.121 mg/l) and the courses of Majdanska and Blašnica rivers with a mean value of 0.081 mg/l (Table 5, Figures. 3 and 4) which is in agreement with the lithology of the river basin with the highest content of Al in these two zones [16].

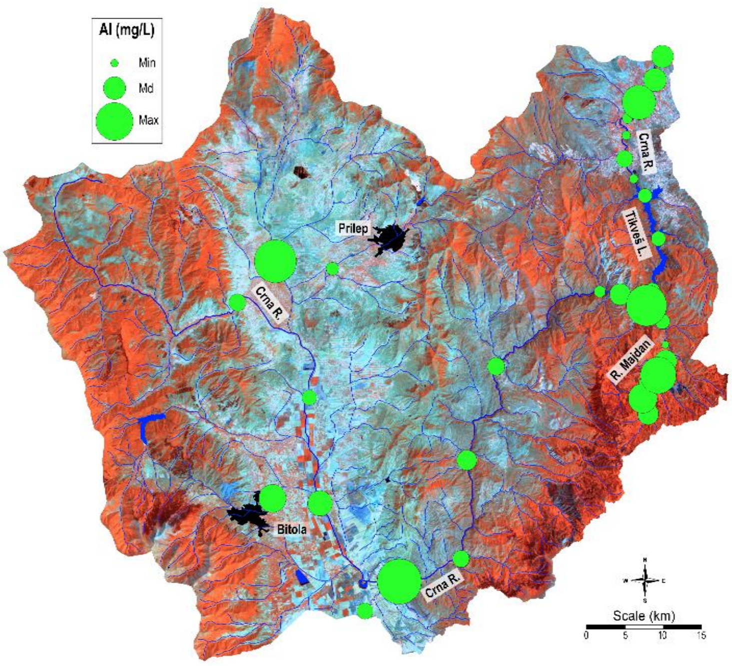

Figure 3. Spatial distribution of the concentrations of Al

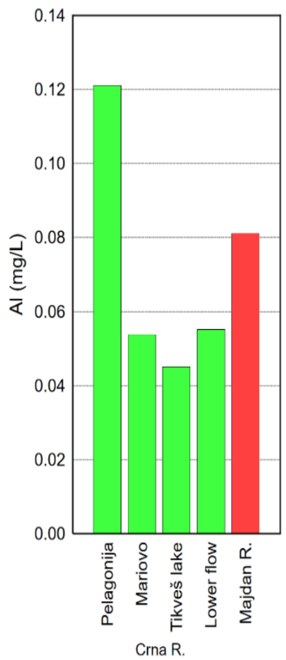

Figure 4. Mean concentrations of Al by zones

Arsenic is metalloid metal and it is usually present in the nature in the form of sulfides. By the content it is 40th element in the Earth's crust. The average presence of arsenic in soils in the world is 5 mg/kg [20]. This element is found in various allotropic modifications but only the gray form is significant from an industrial point of view. Arsenic and its compounds, especially trioxide, are widely used in the production of pesticides, herbicides and insecticides. The toxicity of arsenic is associated with its solubility, which is directly affected by the pH of the environment.

Certain regions in the Republic of Macedonia are rich in arsenic, among which is the Kožuf Mountain. Arsenic has a significant impact on the environment, especially in the region around the abandoned mine of arsenic, antimony and thallium "Allchar" [21–24]. As it can be seen from data presented in Tables 1, 2 and 5, and Figures 5 and 6, the concentration of arsenic is bellow the detection limit (< 10 mg/l) in all of the samples except for the samples from the Majdanska and Blašnica rivers after Allchar locality, where its concentration ranges from 0.010 to 0.199 mg/l, with a mean concentration of 0.082 mg/l and median of 0.052 mg/l, which is higher than the maximum permissible concentration (Table 4) for the second (0.03 mg/l) and the third class (0.05 mg/l). This very high concentration of As in waters from Majdanska and Blašnica rivers originated from the former mining activities at the former As-Sb-Tl mine "Allchar" [25–27], as well as high content of As in the soil from this locality [16, 23].

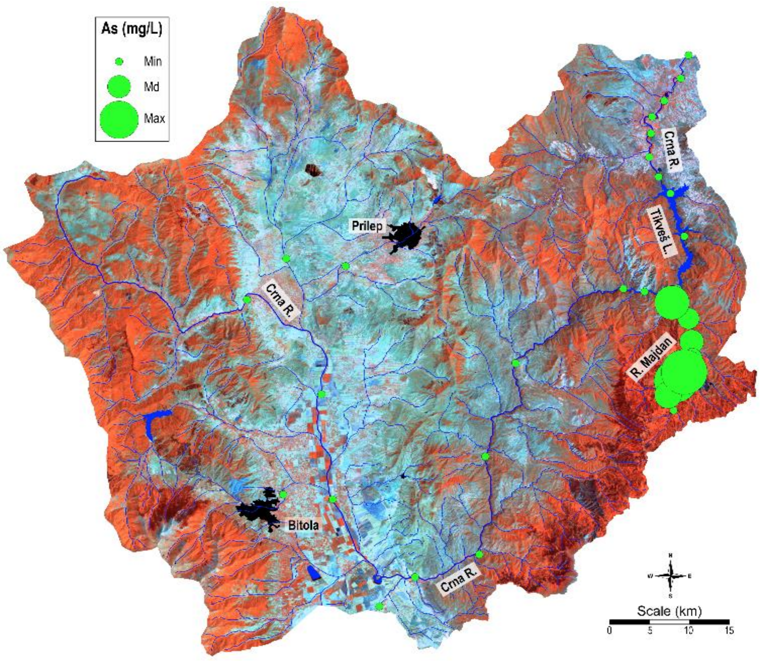

Figure 5. Spatial distribution of the concentrations of As

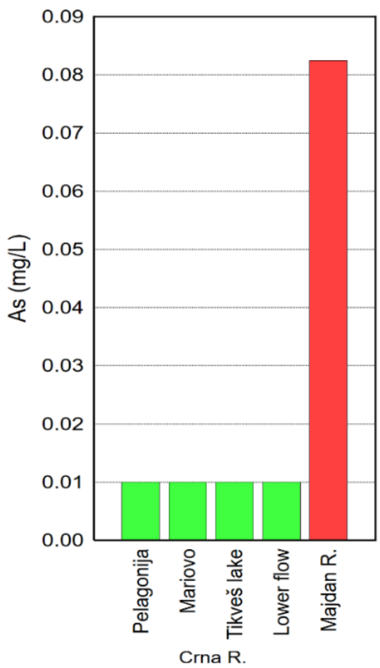

Figure 6. Mean concentrations of As by zones

Barium is found to be 14th most abounded element in the Earth's crust. Its compounds whether they are water soluble or acidic, are toxic. The most present Ba mineral is barite, but Ba is present in various silicate minerals. The spatial distribution of the concentrations of Ba in all water samples in the river basin is presented in Figure 7 while the histogram with the mean values for the zones in the basin is presented on Figure 8. The concentration of Ba ranges from 0.015 to 0.084 mg/l with the mean value of 0.035 mg/l and median of 0.031 mg/l, which is a much lower than the maximum permissible concentration for the second (1.0 mg/l) and third class (4.0 mg/l) of waters. The lowest Ba concentration was obtained in the water sample from the Crna River and the tributaries in the middle and lower flow of the Crna River in the Pelagonia Valley as well as in the Mariovo area, while the highest concentration of Ba was found in the waters from Majdanska and Blašnica rivers with the mean concentration of 0.081 mg/l. These differences are in agreement with a very high content of barium in soil and rocks from the Kožuf Mt. (over 800 mg/kg) [16].

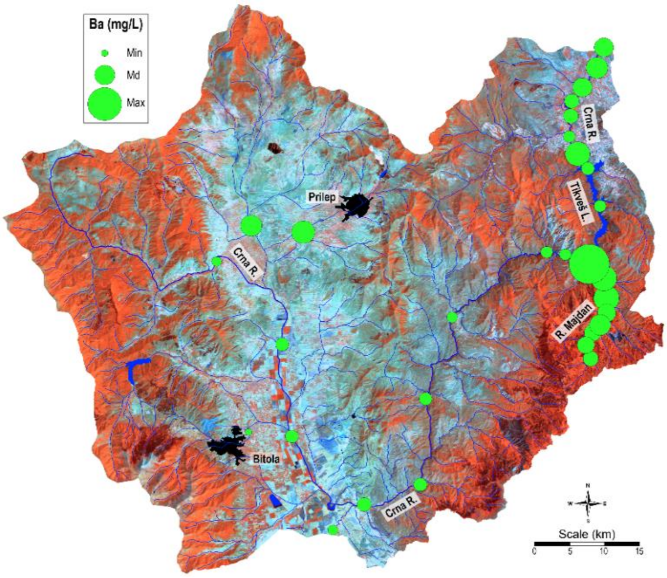

Figure 7. Spatial distribution of the concentrations of Ba

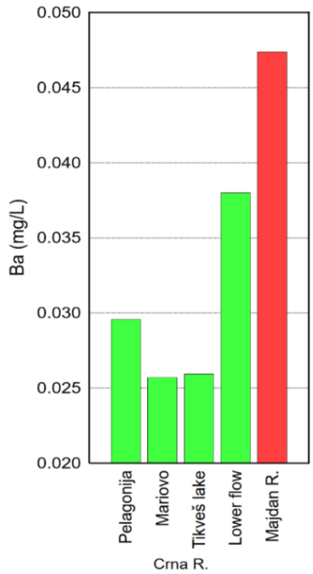

Figure 8. Mean concentrations of Ba by zones

Calcium is the fifth most abounded element in the Earth's crust. It is reactive, weak-yellow metal that exposes the air to form a dark oxide or nitride layer. It belongs to the group of alkaline earth metals. Calcium carbonate is the calcium compound that is most common on Earth. Calcium is an essential element for plants, animals and humans. Due to the high solubility of calcium compound in water its concentration in surface waters is usually high. The concentration of Ca in the waters from the Crna River basin is similar almost in the whole area (Figures 9 and 10) ranges from 10.4 to 74.2 mg/l with a mean value of 44.0 mg/l and median of 39.3 mg/l (Tables 1, 2 and 5). The highest Ca concentration of 74 mg/l is determined in the samples from the river Prilepska Reka (village of Kadino, Prilep) coming from the area rich in calcite and dolomite mineralization [16], while the lowest concentration (10 mg/l) was found in the sample from the Dragor river, a tributary of Crna River passing through the city of Bitola collecting all waste waters from the urban area. The increased concentrations of Ca in the waters of the Kožuf massif (mean concentration of 51.3 mg/l) and those from the lower flows of Crna River (mean concentration of 54 mg/l) are due to the increased contents of Ca in the rocks and soils in the tectonic Vardar zone to which this areas belongs [16].

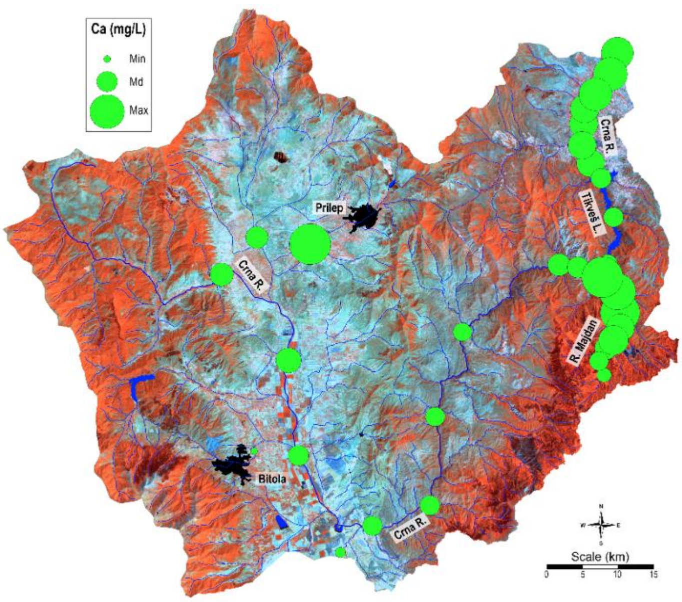

Figure 9. Spatial distribution of the concentrations of Ca

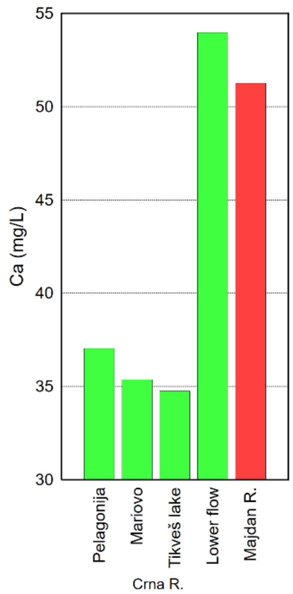

Figure 10. Mean concentrations of Ca by zones

Copper is known for its high thermal and electrical conductivity and therefore it is the most commonly used metal as a heat and electricity conductor in the industry. The spatial distribution of the concentrations of copper in water samples from the Crna River basin and the mean concentration of the waters from the zones are shown in Figures 11 and 12. The concentrations of Cu for the whole area range from 0.002 to 0.063 mg/l with a mean value of 0.017 mg/l and median value of 0.015 mg/l (Table 5). The highest value for the concentration of Cu (0.063 mg/l) was obtained from a sample of water of the lower flow of Crna River (Table 5), and the lowest value was obtained in the sample collected from Crna River after the dam of Tikveš Lake (0.002 mg/l). Sources of copper in surface waters are wastewater from industry, agricultural drainage waters that are partially or not completely purified and as such flow into the rivers. From the Figures 11 and 12 it could be seen that higher concentration of Cu was found in water from the river Dragor (0.035 mg/l) as a result of urban pollution from the city of Bitola. In general most of the obtained concentrations for Cu are bellow the maximal permitted concentrations for surface waters of II and III class.

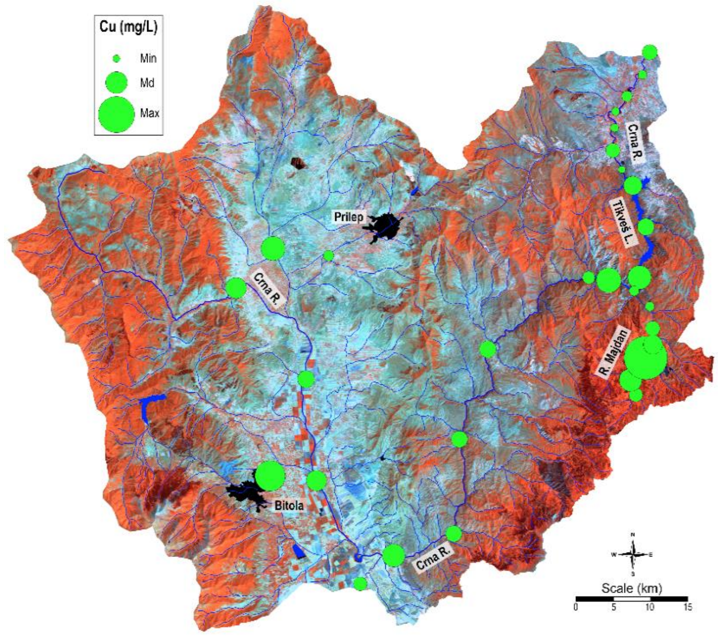

Figure 11. Spatial distribution of the concentrations of Cu

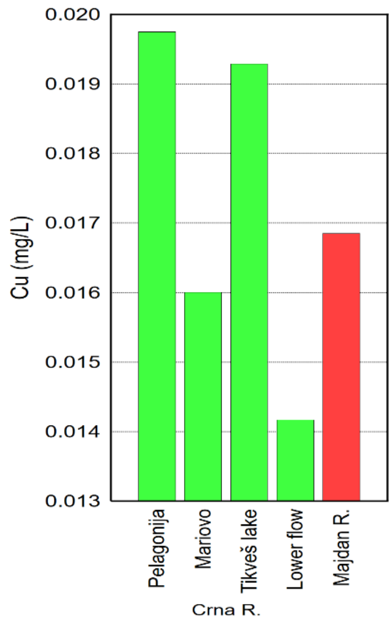

Figure 12. Mean concentrations of Cu by zones

The concentration of **iron** in the water samples from the investigated area ranges from 0.013 to 0.855 mg/l with a mean value of 0.144 mg/l and median of 0.099 mg/l (Table 5). Higher concentration of Fe was found in waters from the upper stream of Crna River, Pelagonia Valley and Mariovo ranges of 0.021 mg/l to 0.85 mg/l (Table 1 and 5) and mean value of 0.16 mg/l and median value of 0.11 mg/l. According to the zones (Figures 13 and 14) the highest average concentration of Fe was determined in water samples from the Pelagonia Valley (0.268 mg/l) and Mariovo zone (0.209 mg/l). This is probably as a result of the increased content of Fe in south-western part of the Pelagonia Valley [16], usage of iron salts as a fertilizer in agriculture, as well as a results of the pollution from industrial wastewater from the coal mines located in the Pelagonia Valley with high content of Fe_2O_3 (from 4.65% to 7.60%) [28].

The spatial distribution of **potassium** in the samples of water in the Crna River basin, as well as the histogram for the mean values of the obtained potassium concentrations in the surface water samples by zones are given in Figures 15 and 16, respectively. The concentration of potassium in the water from the Crna River basin ranges from 1.63 to 10.0 mg/l with a mean value of 4.30 g/l and median value of 4.21 mg/l (Tables 1, 2 and 5, Figures. 15 and 16). The lowest concentrations of K were found in the water samples from the Majdanska and Blašnica rivers (mean value of 2.74 mg/l) which is in accordance with the low content of K in the rocks and soils of the Kožuf Mountain region [16]. The mean concentrations of K in waters from the other zones are similar and range from 4.28 mg/l for waters from Tikveš Lake to 5.18 mg/l for waters from the lower flow of the Crna River (Tables 1, 2 and 5).

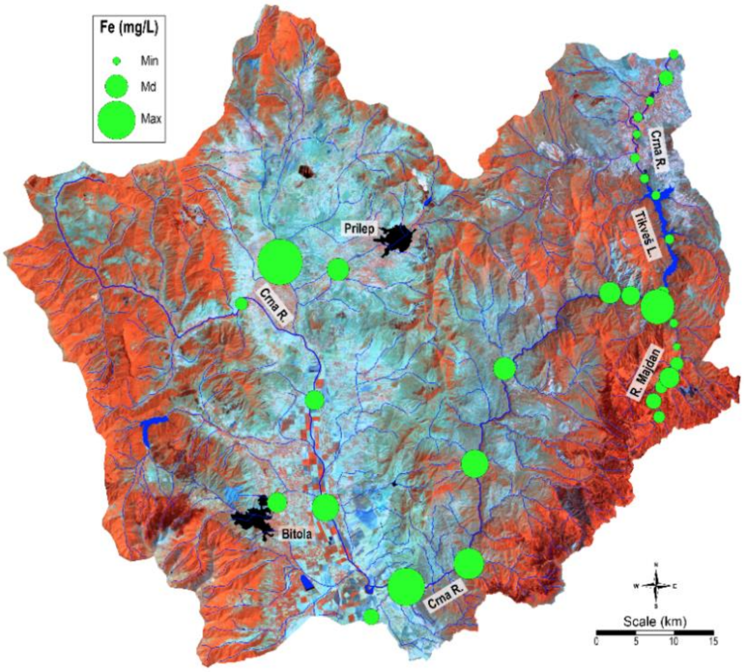

Figure 13. Spatial distribution of the concentrations of Fe

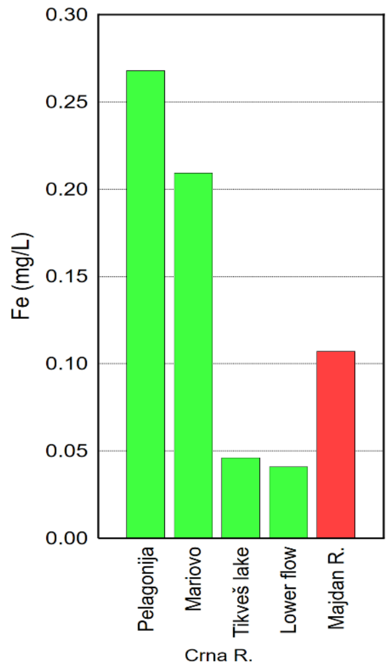

Figure 14. Mean concentrations of Fe by zones

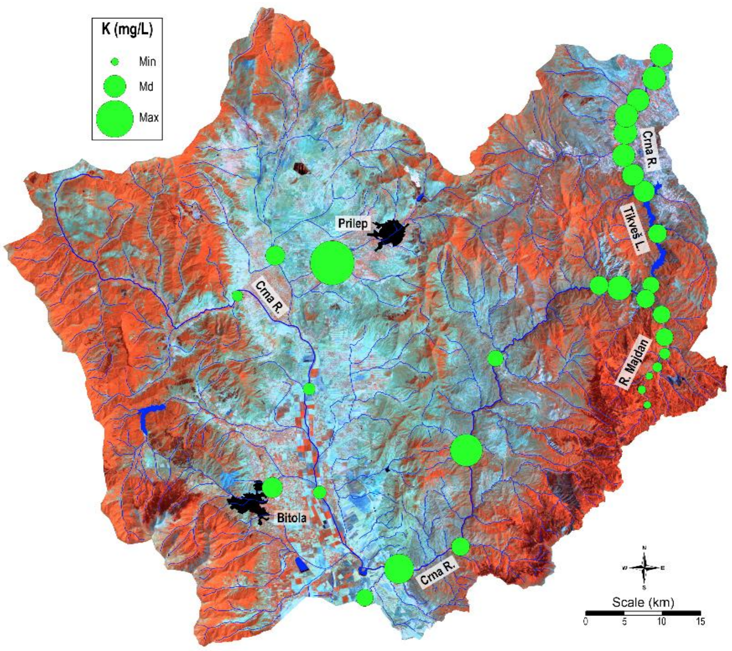

Figure 15. Spatial distribution of the concentrations of K

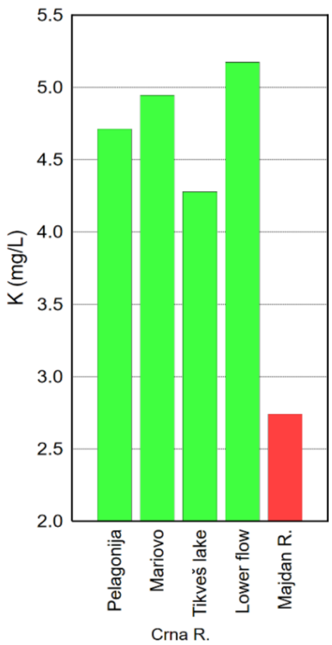

Figure 16. Mean concentrations of K by zones

The concentrations of **lithium** in the water samples from the Crna River basin are very low range from 0.001 mg/l to 0.051 mg/l with a mean concentration of 0.24 mg/l and median of 0.030 mg/l (Table 5). A maximal concentration was found in water sample collected from the river Crna River near the village of Skočivir (Figure 17). In general, according to zones, the concentration of Li is the highest in the samples from the Crna River in the Mariovo region with a mean value of 0.045 mg/l (Figure 18), which is in accordance with the high Li content in rocks and soils in this region, in particular the area of the Nidže Mountain located south of Mariovo [16]. This influence on the increase in the concentration of Li continues (with a certain decrease) in the water from the lower course of the Crna River (mean value of 0.038 mg/l), as well as in the water of Tikveš Lake (mean value 0.032 mg/l) (Figure 18).

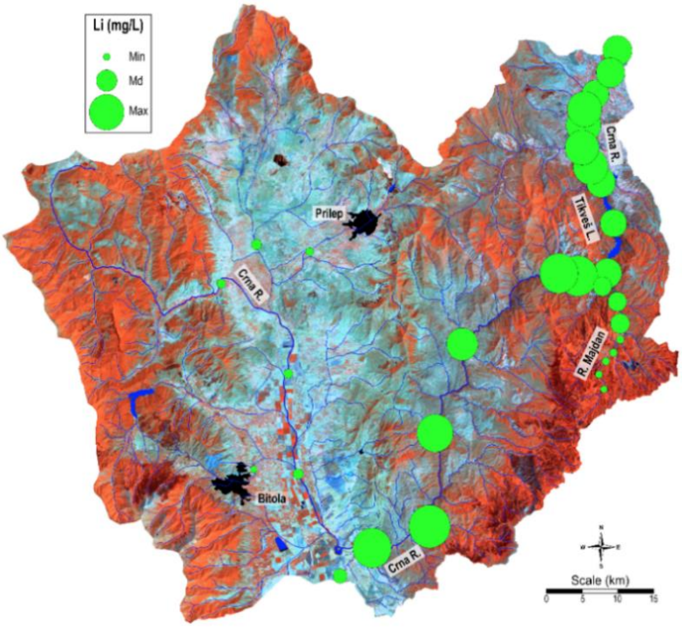

Figure 17. Spatial distribution of the concentrations of Li

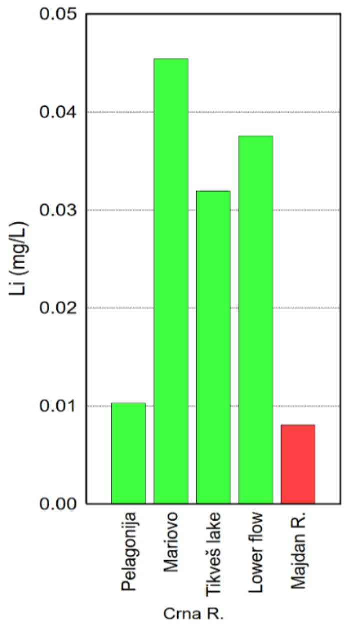

Figure 18. Mean concentrations of Li by zones

Magnesium is an alkaline earth metal found in dolomite, magnesite, epsomite, and other minerals. The spatial distribution of the concentrations of magnesium in water samples from the Crna River basin is given in Figure 19. Its concentration for the whole basin ranges from 2.6 mg/l to 22.4 mg/l, with a mean concentration of 12.2 mg/L and medina of 11.8 mg/l (Tables 1, 2 and 5). The highest concentrations of Mg are determined in the water from the lower course of the river Blašnica (mean concentration of 14.8 mg/l and its basin in Tikveš Lake, and the waters from the lower course of the Crna River (mean value of 15.8 mg/l) (Figure 20). This increased concentration of Mg in waters from these areas is due to its increased content in rocks and soils in the region of Kožuf Mountain and Tikveš Field, where the Neogene magmatic rocks and Neogene clastitic sediments are predominant [16]. On the other hand, the lowest concentrations of Mg are recorded in the waters from the region of Pelagonia (mean value of 7.8 mg/l), a region where the poorest rocks and soils with magnesium in Macedonia are present. Namely, the average content of Mg in soils in Macedonia is 0.92%, while in the region of Pelagonia its content is 0.67% [16].

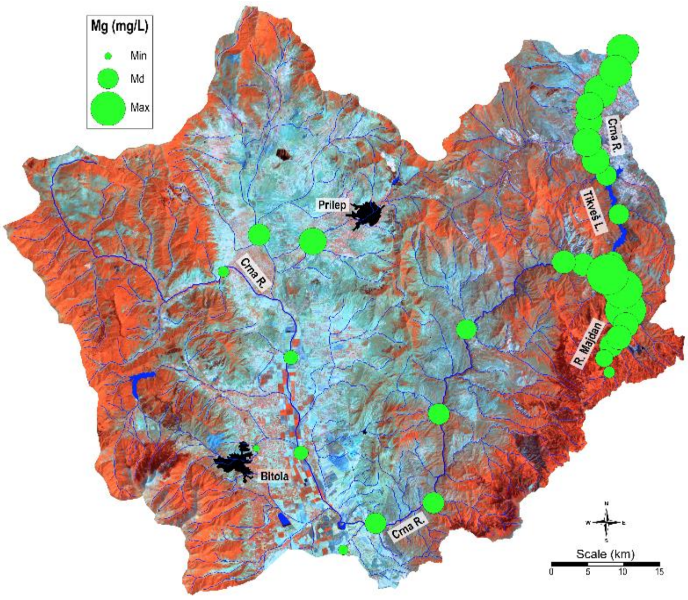

Figure 19. Spatial distribution of the concentrations of Mg

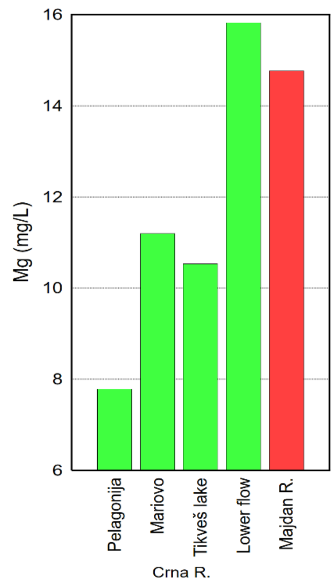

Figure 20. Mean concentrations of Mg by zones

Manganese is the 25th most abounded element in the Earth's crust, with an average content of 774 mg/kg, while its content in the Macedonian soils is 880 mg/kg [16]. Manganese is widely distributed in wildlife, and is a microelement of exceptional and essential importance. The spatial distribution of manganese in surface water samples is shown in Figure 21. The highest Mn concentration of 0.31 mg/l is determined in the water sample from the rivers Blato and Prilepska Reka, a tributaries of Crna River in the upper flow of Crna River and exceeds the maximum allowable concentration for water from the II class probably due to some anthropogenic influence (Figures 21 and 22) The concentration of Mn in almost all other samples does not exceed the maximum permissible concentration of Mn for the corresponding II class (0.05 mg/l) or III class (1.0 mg/l).

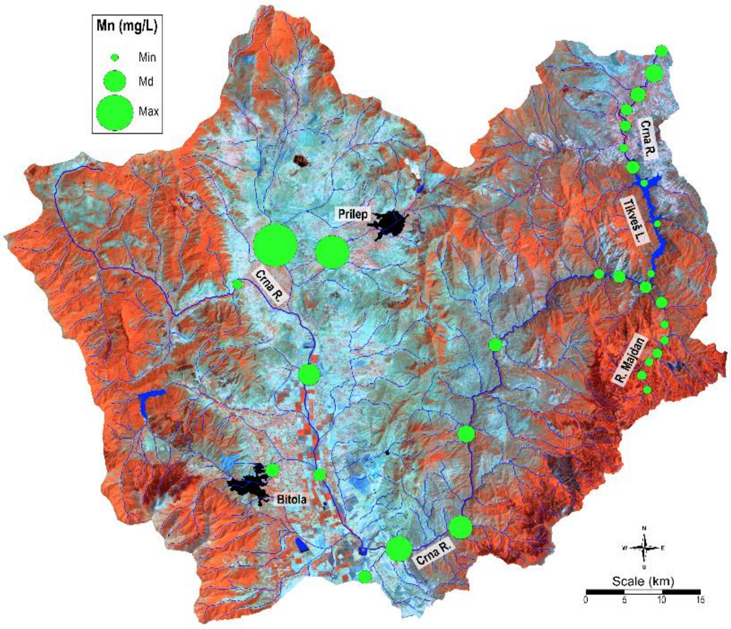

Figure 21. Spatial distribution of the concentrations of Mn

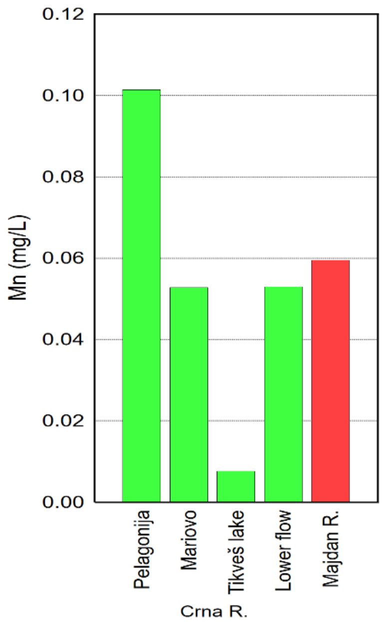

Figure 22. Mean concentrations of Mn by zones

Sodium is an alkali metal which is the sixth most abounded element in the Earth's crust. The spatial distribution of sodium in the water samples from the investigated area is shown in Figure 23. Its concentration ranges from 2.5 mg/l to 36.8 mg/l with a mean concentration of 12.5 mg/l and median of 13.2 mg/l (Table 5). The highest concentration of sodium is found in the sample of water from the tributary of Prilepska River (37 mg/l), which can be interpreted as a result of the increased content of Na in soils from the region of the city of Prilep (over 2.3% versus 1.2% content of Na in Macedonian soils) [16]. When comparing the Na concentrations by zones (Table 5, Figure 24), higher mean concentrations were found in the waters of the Mariovo region (17.6 mg/l) and Pelagonia (15.2 mg/l), while the lowest concentrations were found in the waters from lower flow (1.23 mg/l).

Nickel with atomic number 28 and chemical symbol Ni is placed as 28th the most abounded element in the Earth's crust with an average content of 34 mg/kg. It is a shiny, strong and elastic metal with a silvery tint. It is used in many industries. Similar to copper, it is used for preparing special alloys. Its main use is in the production of stainless steels and stainless steel cast iron. The spatial distribution of nickel concentrations in surface water samples and the histogram with mean values for nickel concentrations divided by regions are shown in Figures 25 and 26, respectively. It is obvious that the concentrations of Ni in the water samples from all of the region (beside lower flow of the Crna River) are very low, bellow 0.020 mg/L (Table 5, Figure 26), which is much lower than the maximal allowed concentration for the waters of II and III class of 0.05 mg/l and 0.1 mg/l, respectively. Higher concentration of Ni in waters from the lower flow of Crna River can be explained as being the result of waste water contamination from the ferro-nickel smelter plant "Feni industry" located near the Crna River close to the village of Vozarci [29–33].

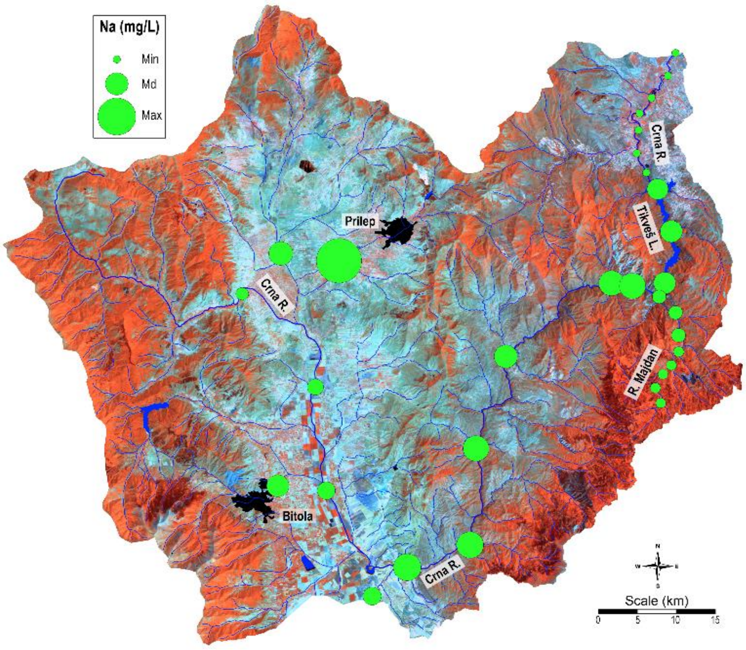

Figure 23. Spatial distribution of the concentrations of Na

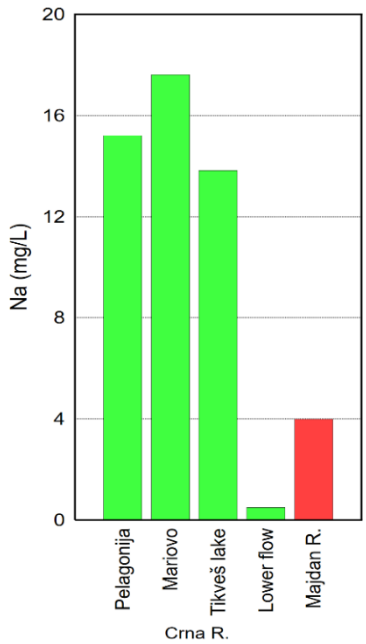

Figure 24. Mean concentrations of Na by zones

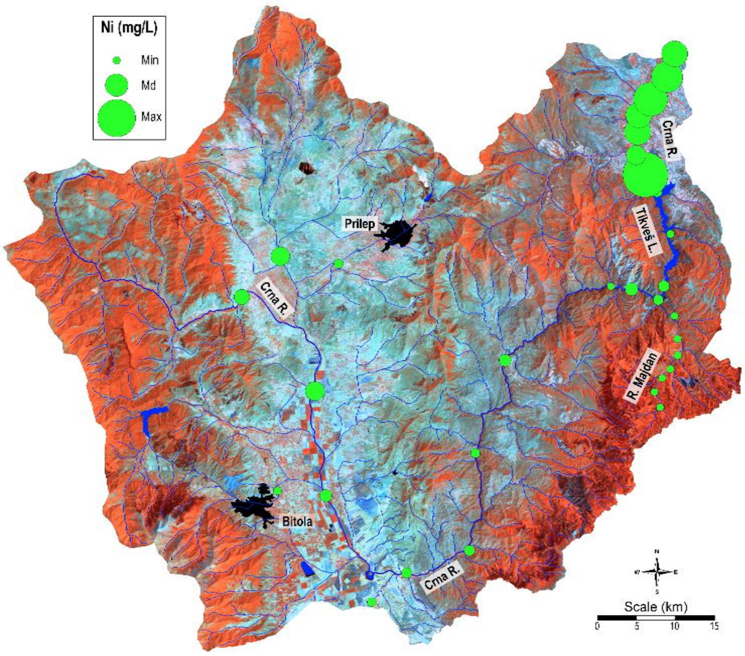

Figure 25. Spatial distribution of the concentrations of Ni

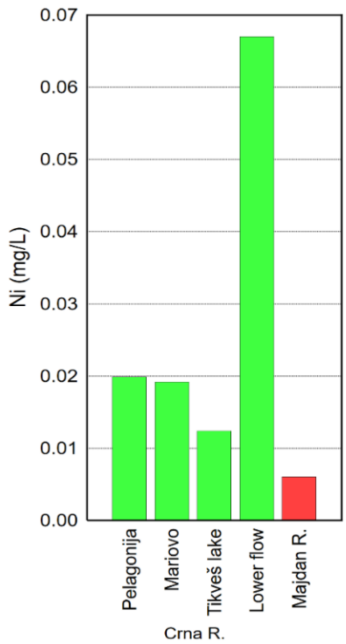

Figure 26. Mean concentrations of Ni by zones

Spatial distribution of **strontium** concentrations in surface water samples is shown in Figure 27. The highest concentration of Sr is found in samples from the lower flow of the Blašnica River of 0.35 mg/l as well as in the samples from the water from the lower stream of Crna River after the dam of the Tikveš Lake (Table 5, Figures 27 and 28). The higher concentration of Sr in the samples in these areas is due to the high content of Sr in rocks and soils in the region of Kožuf Mountain and Tikveš Field, where the Neogene magmatic rocks and Neogene clastitic sediments are dominant with the contents of Sr over 300 mg/kg compared to its average content in the Macedonian soils of 140 mg/kg [16].

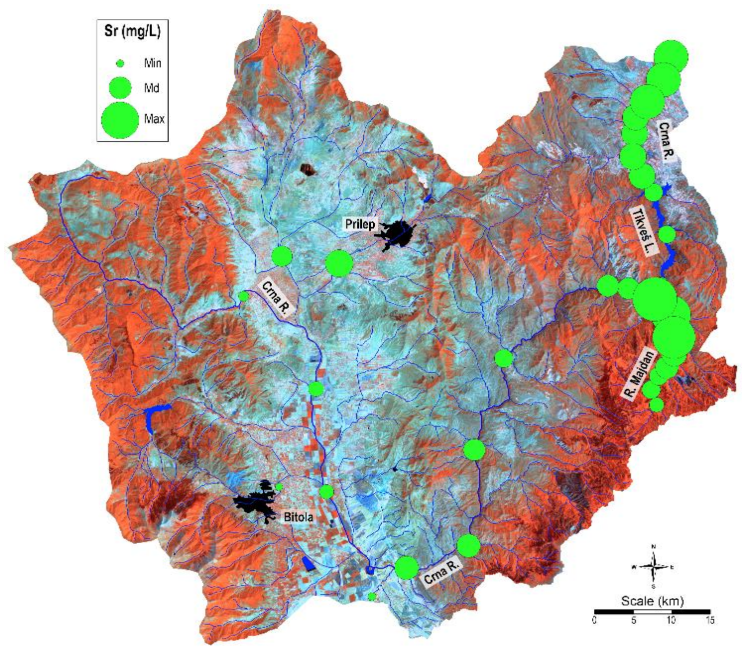

Figure 27. Spatial distribution of the concentrations of Sr

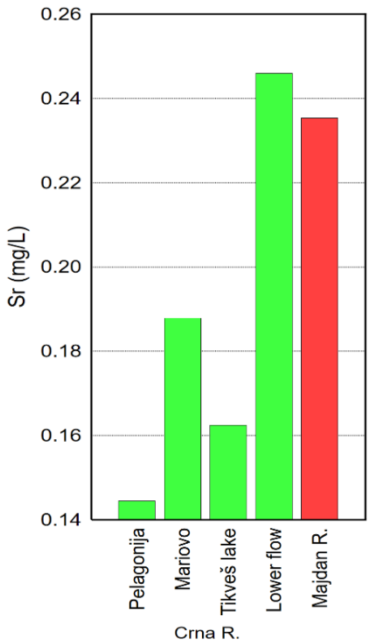

Figure 28. Mean concentrations of Sr by zones

Spatial distribution of **zinc** concentrations in water samples from the whole basin is shown in Figure 29 and the histogram with a mean concentration of Zn by region is shown in Figure 30. The concentrations of Zn in all of the samples from the regions of Pelagonia, Mariovo, Tikveš Lake and lower flow of Crna River are about 10 times lower (mean concentration ranges from 0.018 to 0.034 mg/l) from the maximal allowed concentration for the waters from II and III class (0.1 mg/l and 0.2 mg/l, respectively). The exception is only the water from the Majdanska and Blašnica rivers where the concentration of Zn is increased (0.063 mg/l), although it is still lower than the maximum permissible concentration, which is probably due to the anthropogenic influence of the activities of the nickel mine "Ržanovo" [23].

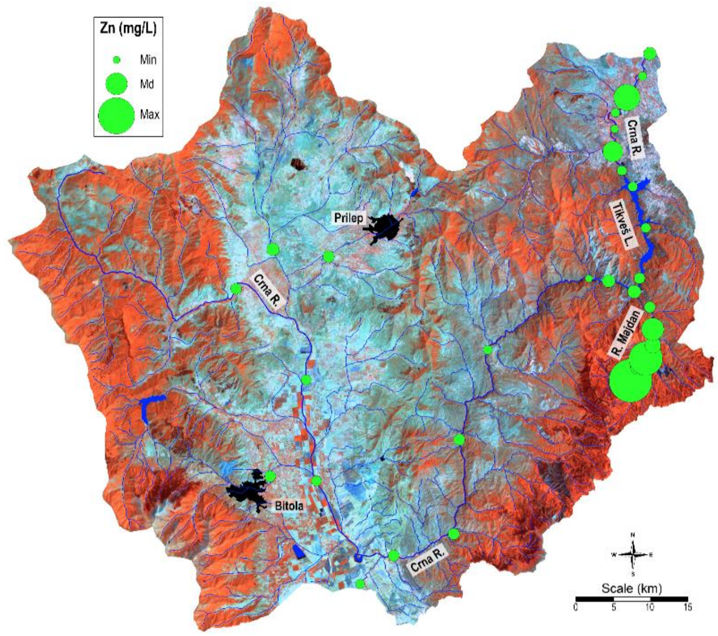

Figure 29. Spatial distribution of the concentrations of Zn

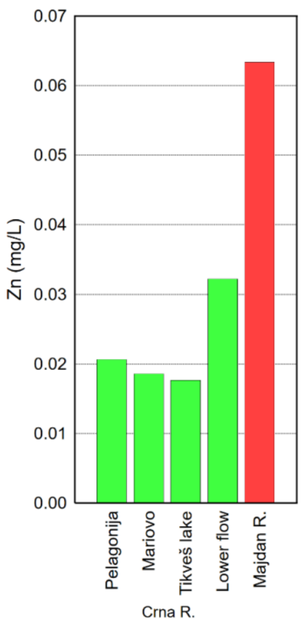

Figure 30. Mean concentrations of Zn by zones

CONCLUSION

In this study the results of the concentration of 23 elements (Ag, Al, As, B, Ba, Ca, Cd, Co, Cr, Cu, Fe, K, Li, Mg, Mn, Mo, Na, Ni, P, Pb, Sr, V, Zn) in samples of surface water from the Crna River basin are presented. All data obtained were statistically processed using software Stat Soft, 11.0 and a descriptive statistical analysis of the value for the concentration of the elements was performed. The maps of spatial distribution of elements and histograms with the mean concentrations of the elements analyzed by regions were also prepared. The obtained results show that the concentration of investigated elements follow the lithology of the region. However, higher concentration of As were found in the water samples from the river Blašnica which is a result of anthropogenic former mining activities at the abounded Allchar mine. Increased concentrations of Ni were found in the samples from the lower couse of the river Crna River after the dam of Tikveš Lake due to the anthropogenic influence from the ferronickel smelter plant Feni Industry.

REFERENCES

[1] A. Kabata-Pendias, A. B. Mukherjee, *Trace Elements Form Soil to Human*, Springer, Berlin, 2007.

[2] R. Naiman, R. E. Bilby, *River Ecology and Management*, Wayerhaevser Company, Tacoma, USA, 2008.

[3] R. M. Bhardwaj, J. Chilton, J. van der Gun, Y. Dieng, S. Diop, C. Gaye, A. Hansen, S. Mtetwe, O. Natale, H. Neikerk, K. Neilsen, W. Rast, B. Toguebaye, *Water Quality for Ecosystem and Human Helath*, GEMS Water Programme, Ontario, Canada, 2008.

[4] J. I. Drever, *Surface and Ground Water, Weathering and Soils*, Elsevier, Amsterdam, 2005.

[5] O. Dimitrovska, B. Markoski, B. Apostolovska Toshevska, I. Milevski, S. Gorin, Surface water pollution of major rivers in the Republic of Macedonia. *Procedia Environ. Sci*., **14** (2012), pp. 32–40.

[6] T. Stafilov, Environmental pollution with heavy metals in the Republic of Macedonia, *Contrib. Sect. Nat. Math. Biotech. Sci. MASA*, **35** (2014), pp. 81–119.

[7] S. Krstić, L. Melovski, Z. Levkov, P. Stojanovski, Complex investigations the river Vardar. II. The most polluted sites in the first three months, *Ecol. Protect. Environ*., **2** (1994), pp. 13–29.

[8] Z. Levkov, S. Krstic, Use of algae for monitoring of heavy metals in the River Vardar, Macedonia, *Mediterr. Mar. Sci*., **3** (2002), pp. 99–112.

[9] T. Stafilov, Z. Levkov, *Summary of Vardar River Basin Field Survey*, European Agency for Reconstruction and Ministry of Environment & Physical Planning of the Republic of Macedonia, Skopje, Macedonia, 2007.

[10] J. M. Serafimovska, S. Arpadjan, T. Stafilov, S. Ilik Popov, Dissolved inorganic antimony, selenium and tin species in water samples from various sampling sites of river Vardar (Macedonia/Greece), *Maced. J. Chem. Chem. Eng.*, **30** (2011), pp. 181–188.

[11] S. Ilić Popov, T. Stafilov, R. Šajn, C. Tánáselia, K. Bačeva, Applying of factor analyses for determination of trace elements distribution in water from river Vardar and its tributaries, Macedonia/Greece, *Sci. World J.*, **2014** (2014), Article ID 809253, pp. 1–11.

[12] B. Balabanova, T. Stafilov, R. Šajn, C. Tănăselia, Multivariate factor assessment for lithogenic and anthropogenic distribution of trace and macro elements in river water from Bregalnica River basin, R. Macedonia, *Maced. J. Chem. Chem. Eng*, **34** (2016), pp. 235–250.

[13] S. Krstić, T. Stafilov, Z. Zdravkovski, M. Kostadinovski, V. Slavevska-Stamenković, V. Kostov, Problems asocciated with not properly conducted wfd based monitoring during preparation of river basin management plans – Bregalnica river case study, *Water Resour. Manage.*, **6** (2016), pp. 35–43 .

[14] A. Lazarevski, *Climate in Macedonia*, Kultura, Skopje, 1993 (in Macedonian).

[15] C. P. Koteski, *Crna River Basin – Geographic-Cartographic Modeling, Differentiation and Functional Development of Selected Regional Parts*, PhD thesis, Faculty of Natural Sciences and Mathematics, Ss. Cyril and Methodius University, Skopje, 2009 (in Macedonian).

[16] T. Stafilov, R. Šajn, *Geochemical Atlas of the Republic of Macedonia*, Faculty of Natural Sciences and Mathematics, SS. Cyril and Methodius University, Skopje, 2016.

[17] B. Balabanova, T. Stafilov, K., Bačeva, R. Šajn, Biomonitoring of atmospheric pollution with heavy metals in the copper mine vicinity located near Radoviš, Republic of Macedonia. *J. Environ. Sci. Health A*, **45** (2010) 1504–1518.

[18] Decree on the categorization of watercourses, lakes, accumulations and groundwater, *Official Gazette of the Republic of Macedonia*, No. 18, March 31, p. 1173, 1999.

[19] Decree on classification of waters, *Official Gazette of the Republic of Macedonia*, No. 18, March 31, p. 1165, 1999.

[20] H. J. Rösler, H. Lange, *Geochemical Tables*, Elsevier, Amsterdam, 1972.

[21] K. Bačeva, T. Stafilov, R. Šajn, C. Tănăselia, Air dispersion of heavy metals in vicinity of the As-Sb-Tl abounded mine and responsiveness of moss as a biomonitoring media in small scale investigations, *Environ. Sci. Pollut. Res.*, **20** (2013), pp. 8763–8779.

[22] K. Bačeva, T. Stafilov, V. Matevski, Bioaccumulation of heavy metals by endemic *Viola* species from the soil in the vicinity of the As-Sb-Tl mine "Allchar", Republic of Macedonia, *Int. J. Phytoremediation,* **16** (2014), pp. 347–365.

[23] K. Bačeva, T. Stafilov, R. Šajn, C. Tănăselia, P. Makreski, Distribution of chemical elements in soils and stream sediments in the area of abandoned Sb–As–Tl Allchar mine, Republic of Macedonia, *Environ. Res.*, **133** (2014), pp. 77–89.

[24] K. Bačeva, T. Stafilov, V. Matevski, Distribution and mobility of toxic metals in *Thymus alsarensis* Ronniger in the Allchar As-Sb-Tl mine, Republic of Macedonia, *Plant Biosyst.,* **149** (2015), pp. 884–893.

[25] S. Janković, B. Boev, T. Serafimovski, *Magmatism and Tertiary Mineralization of the Kožuf Metalogenetic District, the Republic of Macedonia, with Particular Reference to the Allchar Deposit*, Faculty of Mining and Geology, Štip, Special Issue No. 5, pp. 1–262, 1997.

[26] B. Boev, V. Bermanec, T. Serafimovski, S. Lepitkova, S. Mikulcic, M. Soufek, G. Jovanovski, T. Stafilov, M. Najdoski, Allchar mineral assemblage, *Geol. Macedonica*, **15/16** (2001–2002) 1–23.

[27] B. Boev, S. Jelenković, Allchar deposit in Republic of Macedonia – Petrology and Age Determination, in: A. I. Juboury. (ed.), *Petrology - New Perspectives and Applications,* InTech, Rijeka, 131−168, 2012.

[28] M. Stojanovski, *Technology for selective exploitation of coal and interlayer tailings in a complex geotechnical conditions in PC "Brod Gneotino"*, MSc Thesis, University "Goce Delcev", Štip, 2012 (In Macedonian).

[29] K. Bačeva, T. Stafilov, R. Šajn, Biomonitoring of nickel air pollution near the city of Kavadarci, Republic of Macedonia, *Ecol. Protect. Environ.*, **12** (2009) 57–69.

[30] K. Bačeva, T. Stafilov, R. Šajn, C. Tănăselia, S. Ilić Popov, Distribution of chemical elements in attic dust in the vicinity of ferronickel smelter plant, *Fresenius Environ. Bull.*, **20** (2011) 2306–2314.

[31] K. Bačeva, T. Stafilov, R. Šajn, C. Tănăselia, Moss biomonitoring of air pollution with heavy metals in the vicinity of a ferronickel smelter plant, *J. Environ. Sci. Health A*, **47** (2012) 645–656.

[32] K. Bačeva, T. Stafilov, R. Šajn, Monitoring of air pollution with heavy metals in the vicinity of ferronickel smelter plant by deposited dust, *Maced. J. Ecol. Environ.*, **1** (2012) 47–57.

[33] B. Boev, T. Stafilov, K. Bačeva, A. Šorša, I. Boev, The nickel smelter plant influence on the mineralogical composition of attic dust in Tikveš Valley, Republic of Macedonia, *Environ. Sci. Pollut. Res.*, **20** (2013) 3781–3788.

ДИСТРИБУЦИЈА НА ХЕМИСКИ ЕЛЕМЕНТИ ВО ПОВРШИНСКИТЕ ВОДИ ОД СЛИВОТ НА ЦРНА РЕКА, РЕПУБЛИКА МАКЕДОНИЈА

Димитри Томовски[1], Трајче Стафилов[2,3], Robert Šajn[4], Катерина Бачева Андоновска[3]

[1]Алкалоид АД, Скопје, Република Македонија
[2]Институт за хемија, Природно-математички факултет, Универзитет „Св. Кирил и Методиј“, Скопје, Република Македонија
[3]Истражувачки центар за животна средина и просторно планирање, Македонска академија на науките и уметностите, Скопје, Република Македонија
[4]Geological Survey of Slovenia, Ljubljana, Slovenia

Извршено е истражување на дистрибуцијата на 23 хемиски елементи (Ag, Al, As, B, Ba, Ca, Cd, Co, Cr, Cu, Fe, K, Li, Mg, Mn, Mo, Na, Ni, P, Pb, Sr, V и Zn) во површинските води од сливот на Црна Река, Република Македонија. Вкупно се земени 31 примерок од вода, од кои 13 примероци се земени во делот од изворот на Црна Река до нејзиниот влив во Тиквешкото Езеро, вклучувајќи 8 примероци од Црна Река и 4 примероци од нејзините главни притоки од Пелагониската Котлина (Блато, Прилепска Река, Драгор и Јелашка Река). Исто така, се земени примероци вода од 3 локации од Тиквешко Езеро, од 8 локации од Мајданска Река и реката Блашница пред нејзиниот влив во Тиквешко Езеро како и од 7 локации од долниот тек на Црна Река по браната на Тиквешкото Езеро до нејзиниот влив во реката Вардар. Определувањето на концентрацијата на испитуваните елементи е извршено со примена на атомската емисиона спектрометрија со индуктивно спрегната плазма (АЕС-ИСП). Сите податоци од анализираните примероци статистички се обработени со примена на софтверот Stat Soft, 11.0, со што е извршена дескриптивна статистичка анализа на вредностите на концентрациите на сите испитувани елементи. Изработени се и карти на просторната дистрибуција на елементите, како и хистограми на застапеноста на елементи со средните концентрации по региони од сливот на Црна Река. Добиените резултати покажуваат дека концентрациите на испитуваните елементи главно ја следат литологијата на речниот слив. Меѓутоа, повисоките концентрации на арсен кои беа најдени во водите од реката Блашница покажуваат антропогено влијание од поранешните рударски активности на рудникот Алшар кој се наоѓа на планината Кожуф. Беа најдени зголемени концентрации на никел во водите од долниот тек на Црна Река, по браната на Тиквешкото Езеро, што исто така е резултат на антропогено загадување од отпадните води од топилницата за фероникел „Фени индустри“, коешто може да влијае на параметрите на квалитетот на површинските води.

Клучни зборови: Црна Река; Република Македонија; речен слив; води; тешки метали; дистрибуција

ПРИЛОЗИ, Одделение за природно-математички и биотехнички науки, МАНУ, том **39**, бр. 1, стр. 51–68 (2018)
CONTRIBUTIONS, Section of Natural, Mathematical and Biotechnical Sciences, MASA, Vol. **39,** No. 1, pp. 51–68 (2018)

Received: October 31, 2017
Accepted: May 31, 2018

ISSN 1857–9027
e-ISSN 1857–9949
UDC: 551.7.02:550.4.02(497.72/.74)
DOI: 10.20903/csnmbs.masa.2018.39.1.119

Original scientific paper

EAST VARDAR OPHIOLITES REVISITED: A BRIEF SYNTHESIS OF GEOLOGY AND GEOCHEMICAL DATA

Blažo Boev[1*], Vladica Cvetković[2], Dejan Prelević[2], Kristina Šarić[2], Ivan Boev[1]

[1]Goce Delčev University, Štip, Republic of Macedonia
[2]Faculty of Mining and Geology, University of Belgrade, Belgrade, Serbia

e-mail: blazo.boev@ugd.edu.mk

The study reports and synthesizes the available geological and geochemical data on the East Vardar ophiolites comprising most known occurrences from the South Apuseni Mountains in Romania to the tip of the Chalkidiki Peninsula in Greece. The summarized geological data suggest that the East Vardar ophiolites are mostly composed of the magmatic sequences, whereas the mantle rocks are very subordinate. The members of the magmatic sequences are characterized by the presence of abundant acid and intermediate volcanic and intrusive rocks. The age of these ophiolites is paleontologically and radiometrically constrained and these data suggest that the East Vardar ophiolite formed as a short-lived oceanic realm that was emplaced before the uppermost Kimmeridgian. A relatively weak adakitic affinity is shown by intra-ophiolitic acid and intermediate rocks in many East Vardar provinces. It can be taken as evidence that the subduction of the young and hot slab, most likely along the earlier spreading ridge has occurred. A paleo-tectonic reconstruction consisting of four stages is proposed. It involves: a) an early/mid-Jurassic north-northeastward subduction of the West Vardar oceanic plate; b) the formation of a mid-Jurassic volcanic arc and a narrow back-arc oceanic stripe of East Vardar behind it; c) the mid-/Upper Jurassic initiation of East Vardar subduction along the ridge axis, and d) complex and heterogeneous emplacement of the East Vardar ophiolites. So far available data allow for having relatively clear ideas about the origin and evolution of the East Vardar ophiolites. However, in order to provide better understanding of all aspects of its evolution we need to answer additional questions related to the true structural position of the East Vardar ophiolites slices in Serbia, the exact nature of subduction that caused back-arc spreading (intraoceanic vs subduction under continent?) and the full significance of the adakitic signature shown by rocks in the East Vardar provinces other than Demir Kapija.

Key words: ophiolites; subduction; back-arc; Tethys; Balkan Peninsula

INTRODUCTION

It is generally accepted that geological framework of the central part of the Balkan Peninsula formed in response to the long-lasting convergence between Africa and Europe [1]. This convergence induced around 3000 km of shortening via consummation of vast oceanic areas and formation of many accretionary wedges and stacked nappes [2]. When studying such convergent zones it is always important to distinguish between accretionary wedges that commonly represent upper crustal levels and fundamental boundaries between underthrusting and overriding plates [3–5]. A first-order prerequisite for this distinguishing is to understand the true nature of the present ophiolite belts in sufficient details, at first place to elucidate their geodynamic affinity and the mode of emplacement. The central Balkans host three ophiolite belts that belong to a huge and complex ophiolite mega-zone stretching from the Western Mediterranean to the Himalayas, which resulted from the closure of the Mesozoic Tethys [1, 6, 7]. According to the most simplistic division (from west to east), they are: Dinaridic ophiolites (i.e., Albanian ophiolites or Pindos Zone in Albania and Greece, respectively), West Vardar ophiolites (also known as Almopias

Zone in Greece) and East Vardar ophiolites (Peonias Zone in Greece).

The present-day understanding of the geodynamic implications of these ophiolite belts can be explained by underlying the two most important interpretations, namely the single- and the multi-ocean hypothesis. The single-ocean hypothesis proposed by Smith and Spray [8] (see also: [9–11], and more recently [5]), considers all ophiolite belts in the Balkan Peninsula as having originated from a single ocean – Vardar Tethys (or Neotethys). According to this view, the Vardar Tethys is directly correlated to the Meliata Ocean in the Eastern Alps and Carpathians, i.e. [12]. The advocates of the single-ocean hypothesis locate the main Neotethyan suture along the main axis of the Balkan Peninsula, along the westernmost margin of the East Vardar [5]. Simultaneously, they regard the ophiolites on both sides of this suture as having resulted from westward (Dinaridic and West Vardar) and eastward (East Vardar) obduction, respectively. Accordingly, the authors adopting the single ocean hypothesis believe that Paleozoic units that geographically separate the ophiolite belts represent progressively more distal margins of Adria, which acted as the African promontory. On the other hand, a number of other authors ([13–19], among others) argue that the ophiolite belts in the Balkan Peninsula represent remnants of distinctive oceanic domains, all of them separated by individual Paleozoic to early Mesozoic microcontinents, i.e. terranes.

These two hypotheses are principally contrasting about the nature and the origin of the western ophiolite belts and pre/early Mesozoic continental geotectonic units situated in between, whereas both groups of authors agree that the East Vardar ophiolites represent a particular ophiolite belt in many respects.

In this study, we aim to report a brief synthesis of the existing data on the East Vardar ophiolites with special emphasis on their geology and geochemical affinity. The synthesis is based on the available data on the largest and best-studied occurrences of the East Vardar ophiolites, from the South Apuseni Mountains in Romania to the very tip of the Sithonia Peninsula in Greece (see references below). The results of this synthesis confirm some of the important conclusions about the East Vardar ophiolites, suggesting a slightly refined geodynamic model and eventually argue that several aspects of the origin of these ophiolites still remain to be answered.

GEOTECTONIC POSITION OF THE EAST VARDAR

The position of the East Vardar Zone is given in a simplified geological sketch map shown in Figure 1 (modified from [20]). The most striking geotectonic feature of the East Vardar is that it structurally belongs to the westernmost margin of the predominantly eastward-facing geological units of the European plate (present coordinates), i.e. to the upper plate in the context of the final closure of the Neotethys [2]. In contrast to the westwardly situated Dinaridic and West Vardar ophiolites that appear either passively obducted over the African margin (sensu [5]; note, however, that for these two ophiolite belts they use a single name – West Vardar) or incorporated into a complex nappe stacking formed by accretion of microcontinents (*sensu* [19]), the East Vardar forms a narrow, several tens of kilometers wide zone that completely follows the European-derived geotectonic units of the Dacia microplate. In this context, the East Vardar has the same geotectonic position as the Circum Rhodope Belt, which is known to possess mixed Africa-Europe geotectonic affinities [21–23].

The East Vardar Zone stretches throughout the main part of the Balkan Peninsula and its rock series are exposed as a N-S line of mostly also N-S elongated outcrops that are found in Serbia, Macedonia and northern Greece and continue further south-east underneath the Aegean Sea. In the north, the East Vardar ophiolites do not follow the general trend of the Dinaridic ophiolites but are traced north-eastwards in the South Apuseni Mountains in the Mureş Valley in Romania, where they were displaced by South-Transylvanian fault [24–27].

EAST VARDAR OPHIOLITES: A BRIEF SUMMARY

In the following subsections the available data on geological and geochemical characteristics of the East Vardar ophiolites in Romania [10, 29–31], Serbia [32–36], Macedonia [33–37] and Greece [33, 38–40], are summarized. The locations of the ophiolite massifs/outcrops addressed in this study are shown in Figure 1. From north to south they are: South Apuseni and Transylvanian ophiolites (Romania), Ždraljica and Kuršumlija (Serbia), Guevgeli (southernmost Macedonia/northernmost Greece) and Circum Rhodope ophiolites that comprise several relatively small massifs between north from the Gulf of Thessaloniki (e.g., Oraeokastro and Thessaloniki ophiolites) and the tips of the Chalkidiki Peninsula (e.g., Kassandra and Sithonia). The ophiolites occurring more to the south in the Aegean Sea are not addressed here. In the following two subsections will be reported the main geological and geochemical features of the magmatic rocks from the above ophiolite provinces, using the division and naming given above.

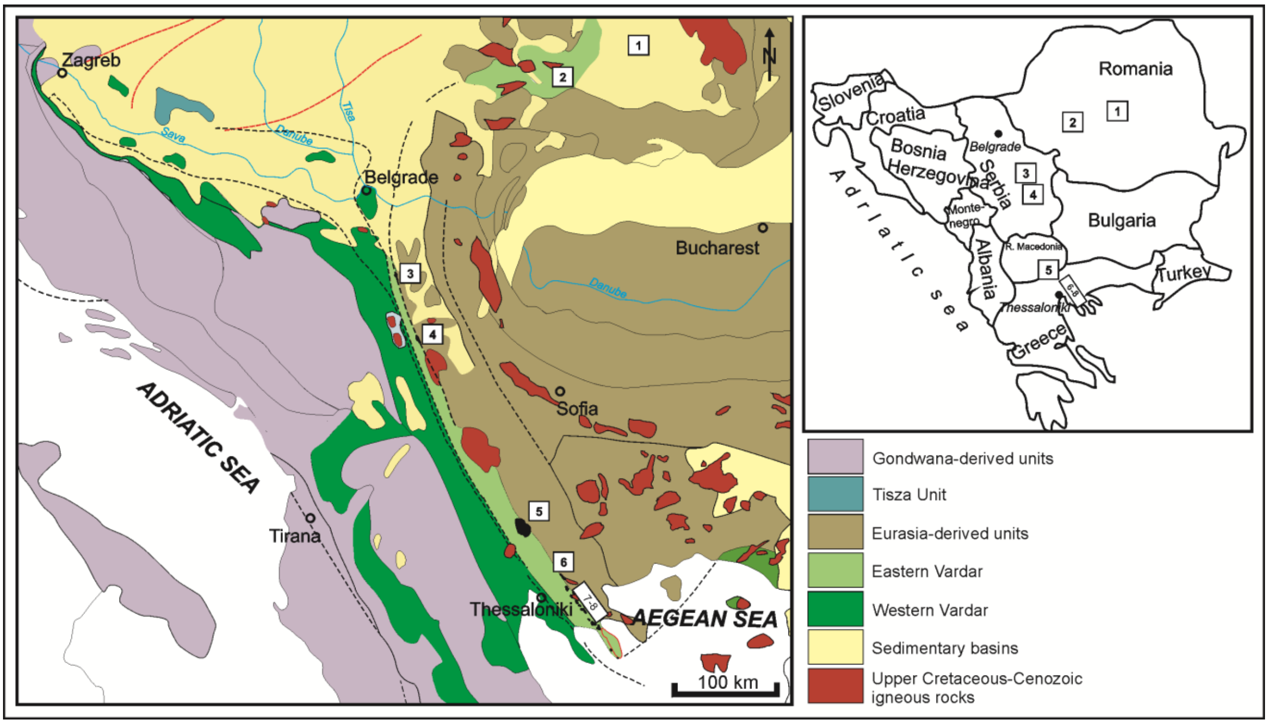

Figure 1. The geological sketch showing positions of the East Vardar provinces comprised by this study. The sketch is a simplified version of the geological sketch of South-East Europe [20] and represents a compilation of the Geological Atlas of Serbia 1:2,000,000 [28] and of the tectonic map 1:5,000,000 [5]; 1 – Transylvanian ophiolites (drill holes), 2– South Apuseni ophiolites, 3 – Ždraljica ophiolites, 4 – Kuršumlija ophiolites, 5 – Guevgeli ophiolites, 6 – Oraeokastro ophiolites, 7–8 – Thessaloniki-Chalkidiki ophiolites).

Geology

The northernmost occurrences of the East Vardar ophiolites are located in the **South Apuseni Mountains** (for details see: [27, 29, 31]). It is a pile of nappes composed of the Biharia basement that represents counterparts of the Supragetic unit (i.e., Serbo-Macedonian Massif sensu [5]). The basement is overlain by Late Cretaceous clastic sediments and the entire section is tectonically overlain by the Mureş nappe that includes the East Vardar Middle Jurassic ophiolites. The ophiolites consist of a gabbroic complex overlain by a sheeted dyke and volcanic sequence that includes massive lava flows and pillow-lavas. The latter are spatially associated to Callovian - Oxfordian radiolarians. The mafic ophiolite members are intruded by calc-alkaline granitoids and covered by a calc-alkaline volcanic series composed of basalts, basaltic andesites, andesites, dacites and rhyolites. The overstep sequence is on the top and is represented by Late Jurassic shallow-water limestones showing the transition to Cretaceous carbonate deposits. The U–Pb ages of mafic ophiolites members and accompanying intra-ophiolite granitoids revealed similar ages 158.9–155.9 Ma and 158.6–152.9 Ma, respectively [31].

The presence of analogous ophiolitic rocks is indirectly revealed by deep wells in the **Transylvanian Depression** [30]. A few of the wells drilled the Middle/Upper Jurassic volcanic rocks ranging in composition from basalts to andesite are interpreted to represent counterparts of the calc-alkaline series that overlies the South Apuseni Mountains ophiolites. The presence of underlying ophiolites is only inferred by geophysical data [30].

The East Vardar ophiolites in Serbia are represented by two relatively small and elongated massifs of **Ždraljica** and **Kuršumlija** [32, 41, 42]. They occur as up to 20 km long and only several km wide NNW-SSE aligned outcrops that are in tectonic contacts with the mid- to Upper Jurassic mélange and high/medium-grade meta-igneous and metasedimentary rocks of the Serbo-Macedonian

Massif. The contacts between the ophiolites and the Serbo-Macedonian Massif are at places sealed by Neogene sediments [43]. In [35], 2D modelling of gravity and magnetic data and pseudo-3D modelling on the East Vardar ophiolites in Serbia were reported and it was suggested that they are dipping to the east beneath the Serbo-Macedonian Massif. The age of these ophiolites is mostly geologically constrained by the age of the overstep sequence represented by Tithonian reef limestone and/or flysch-like Lower Cretaceous sedimentary rocks [44–46]. The Serbian East Vardar ophiolites are predominantly composed of series of basic igneous rocks, whereas ultramafic members are almost absent. The **Ždraljica** complex is represented by cummulitic gabbros in the form of irregularly shaped bodies. The gabbro bodies are cut by isolated shallow intrusive dolerites, which at some places appear as relicts of sheeted-dyke series. Pillow basalts are substantially rare. The **Kuršumlija** complex contains more abundant dolerite dykes and 5-10 m thick series of pillow lavas. It is worth noting that in both ophiolite complexes occur numerous shallow intrusive and subordinate volcanic rocks of acid to intermediate compositions.

The largest exposure of the East Vardar ophiolites is the **Guevgeli complex**. In the east, the Guevgeli complex is in tectonic contacts with the Serbo-Macedonian Massif forming a narrow mylonitic-phyllitic zone. In the west, it is in contact with the metamorphic rocks of the Paikon unit that consists of Triassic marbles, clastic sediments, micaschists and various Upper Jurassic volcanic rocks that range in composition from rhyolite to basalt [47–49]. The northern part of the Guevgeli complex is the **Demir Kapija ophiolites** [33, 34, 37]. It is situated in southernmost Macedonia as an NNW-SSE elongated, 50 km long and 25 m wide and partially dismembered belt. It is transgressively covered by conglomerates overlain by Upper Tithonian reef limestones [50] that are themselves covered by Palaeogene-Neogene sediments. The structural position of the Demir Kapija ophiolites is also inferred by 2D and pseudo-3D geophysical modelling, which suggests that they have a very steep contact that dips towards the east-southeast under the Serbo-Macedonian Massif [36]. The Demir Kapija ophiolite is predominantly built of volcanic rocks, although small serpentinite blocks occur within tectonic mélange near Rabrovo [51]. The volcanic-intrusive series of Demir Kapija is represented by pillow lavas, diabase dyke swarms and gabbros of variable grain-size. Small serpentinized chromite-bearing dunite, wehrlite and lherzolite are very subordinate. The complex also contains numerous small-scale (< 5 m thick) shallow intrusions of acid to intermediate compositions. In the both northern and southern part of the complex, however, occur much larger granitoid intrusive bodies, such as Štip, Konče, Gradeške Mts. and Plauš-Furka-Fanos, some of them covering more than 70 km^2. These granitoids cut the basement and are, therefore, considered as post-ophiolite intrusions [52]. Božović et al. [37] reported U/Pb zircon age for gabbros of Demir Kapija at 166 ± 1.8 Ma constraining the age of the oceanic crust, which agrees well with Bathonian–Callovian radiolarian [53]. It is also obtained only a slightly lower age of 164 ± 0.5 Ma for presumably younger subduction-related rocks by Ar/Ar analyses of feldspars [37].

These ophiolites continue southwards across the Macedonian-Greek border and form two branches. The western one is known as the **Skra ophiolite** which is composed of cummulitic olivine- and isotropic normal gabbros as well as of an extrusive sequence consisted of massive lavas and dykes accompanied by felsic shallow intrusives; ultramafic rocks are extremely rare [54]. Spray et al. [55] reported ^{40}Ar/^{39}K ages on biotite and kaersutite mineral separates from gabbros and diorites between 149 ± 3 Ma and 163 ± 3 Ma. Danelian et al. [56] studied radiolarians from the overstep sequence and determined Oxfordian age (161.2–155.7 Ma). Zachariadis [38] studied zircons from plagiogranite found in gabbros of the Skra complex and reported an intrusion age of 166.6 ± 1.8 Ma. The **Evzonoi ophiolites** occur in the east and are entirely composed of massive and pillow lavas and dolerite dyke swarms. The sheeted dyke sequence is frequently cut by rocks of rhyolite composition that make sharp contacts towards the adjacent mafic rocks and sometimes even enclose them as xenoliths. Apart of these small-scale felsic intrusions, the Skra and Evzonoi ophiolites are intruded by a much larger (~65 km^2) granitoid intrusion of Fanos, presumably representing the continuation of the Plauš-Fourka granitoid in the southernmost Macedonia [33]. Anders et al. [49] reported an U/Pb age of the Fanos granitoid of 158 ± 1 Ma. Zachariadis [38] argued that the Fanos granitoid intruded the Guevgeli ophiolites after their emplacement and reported the presence of, albeit rare, occurrences of mafic dykes that intrude the Fanos granite.

Further to the south the East Vardar ophiolites occur as a lineament of more than ten isolated ophiolite slices hereafter collectively named the **Circum Rhodope ophiolites**. The first is **Oraeokastro ophiolite** that crops out as an NW-SE elongated (2.5 × 12 km) slice situated ~5 km northern of Thessaloniki. In the east, the Oraeokastro ophiolite is in contact with phyllites and Triassic limestones, whereas the latter tectonically overlie the ophiolite. According to Zachariadis [38], the phyllite represents ophiolitic material that was milonitized during overthrusting of the limestone. In the west, the ophiolite is transgressively covered by Tithonian fossiliferous conglomerate in which pebbles of ophiolitic origin occur [22, 47]. Ultramafic rocks appear as a small body of 2–3 km north-east from the main ophiolite slice and is represented by harsburgite tectonite. The margins of this isolated body are sheared. Mafic shallow intrusives are found cutting gabbros and as relicts of sheeted dykes. Extrusive ophiolite rocks are rare and mainly occur along the western border. They are composed of massive and/or pillow lavas and accompanied hyaloclastite deposits. Felsic rocks are common and are found as dykes and irregular lenses inside the series of mafic rocks.

The **Thessaloniki ophiolite** is represented by a volcanic ophiolite sequence that was excavated during the civil engineering activities along the north-eastern periphery of the city. Gabbros that occur in a wider area were poorly known and were not even considered as a part of an ophiolite [21, 22, 57–59]. The Thessaloniki ophiolite predominantly consists of dolerite dykes and subordinate lavas, mostly massive and rarely as pillows as well. Hornblende gabbro from Thessaloniki ophiolite was dated by K/Ar method at 174 ± 4.8 Ma [60] (details are lacking). Zachariadis [38] reported a zircon (one crystal) age on a diorite (outskirts of the city of Thessaloniki) as a concordia of 169 ± 1 Ma, and interpreted as the crystallization age of the diorite. He also dated a diorite from the Chortiatis magmatic suite and obtained an age of 159 ± 4 Ma, which demonstrated that the Chortiatis magmatic suite is younger than Thessaloniki ophiolite for around 10 Ma.

The southernmost outcrops of the East Vardar ophiolites of the Greek shoreline are represented by the **Chalkidiki ophiolites**. They crop out as several dismembered slices. The largest are along the southernmost edges of the Kassandra and Sithonia peninsulas. The Kassandra ophiolites are in contact with younger rocks exclusively, i.e. they are covered by an overstep sequence of Cretaceous/Upper Jurassic limestones and by a thick series of Cenozoic sediments. The ophiolites are represented by mafic extrusive rocks ([61], and references therein), mainly as variably vesicular massive lavas and rarely pillows. The Sithonia ophiolites outcrop as elongated slices that have tectonic contacts with the Eocene Sithonia granite [62, 63] and the Triassic to Middle Jurassic Svoula flysch [64]. In the south, the ophiolites are covered by Upper Jurassic reef limestones. The Sithonia ophiolite is represented by series of mafic magmatic rocks that appear as thin stripes along the south and south-west shoreline as well as offshore on small islands (e.g. Kelyfos). It is an extrusive sequence with extremely well-preserved pillow lavas at some places, and sometimes associated with feeding dykes or rarely with dyke swarms. More to the south, including the very tip of the peninsula (e.g. Cape Laemos) deeper ophiolite members represented by coarse- to medium-grained gabbro, at some places cut by hornblendite veins, occur. Zachariadis [38] reported U/Pb zircon ages for gabbro-diorite/diorite rocks from two places of the Chalkidiki ophiolites: namely from the Metamorphosis area and from Sithonia. Zircons from the Metamorphosis yielded a concordia age of 165.3 ± 2.2 Ma whereas those from Sithonia gave an average age of 160 ± 1.2 Ma.

Rock geochemistry

Geochemical characteristics of the magmatic member of the East Vardar ophiolite provinces are summarized and illustrated in Figures 2–5. The synthesis was restricted to volcanic and subvolcanic basic (SiO_2 < 55%) as well as intrusive (±volcanic) acid/intermediate rocks (SiO_2 > 55%), which compose the above described ophiolites (the references are listed above and in caption for Figure 2). The analyses of peridotite rocks and cummulitic gabbros are omitted from further consideration.

The Nb/Y vs TiO_2/Zr diagram commonly used for classification of magmatic rocks occurring in ophiolitic sequences is shown in Figure 2 [65]. It reveals that most East Vardar basic rocks (dotted symbols) stretch across the fields of subalkaline basalts and basaltic andesites, and that they mostly compositionally overlap with the field occupied by the basic rocks of West Vardar ophiolites (pink area). However, in all the studied East Vardar provinces occur abundant acid to intermediate rocks represented by calc-alkaline volcanic, subvolcanic or typical intrusive rocks (open symbols). This is different from the West Vardar ophiolites in which acid to intermediate rocks are substantially rare (see also the inset that shows the total alkali vs silica diagram [66]). The Upper Jurassic granitoids occurring in southernmost Macedonia (e.g. Štip, Dolane, Konče, etc.) and northernmost Greece (Fanos) are spatially associated to the Guevgeli ophiolite complex but are plotted with separate symbols (red dots). They have so far been interpreted as intrusions into both the East Vardar ophiolites and the basement rocks, and, therefore, we intended to distinguish them from other typically intra-ophiolitic acid to intermediate rocks of the Guevgeli complex.

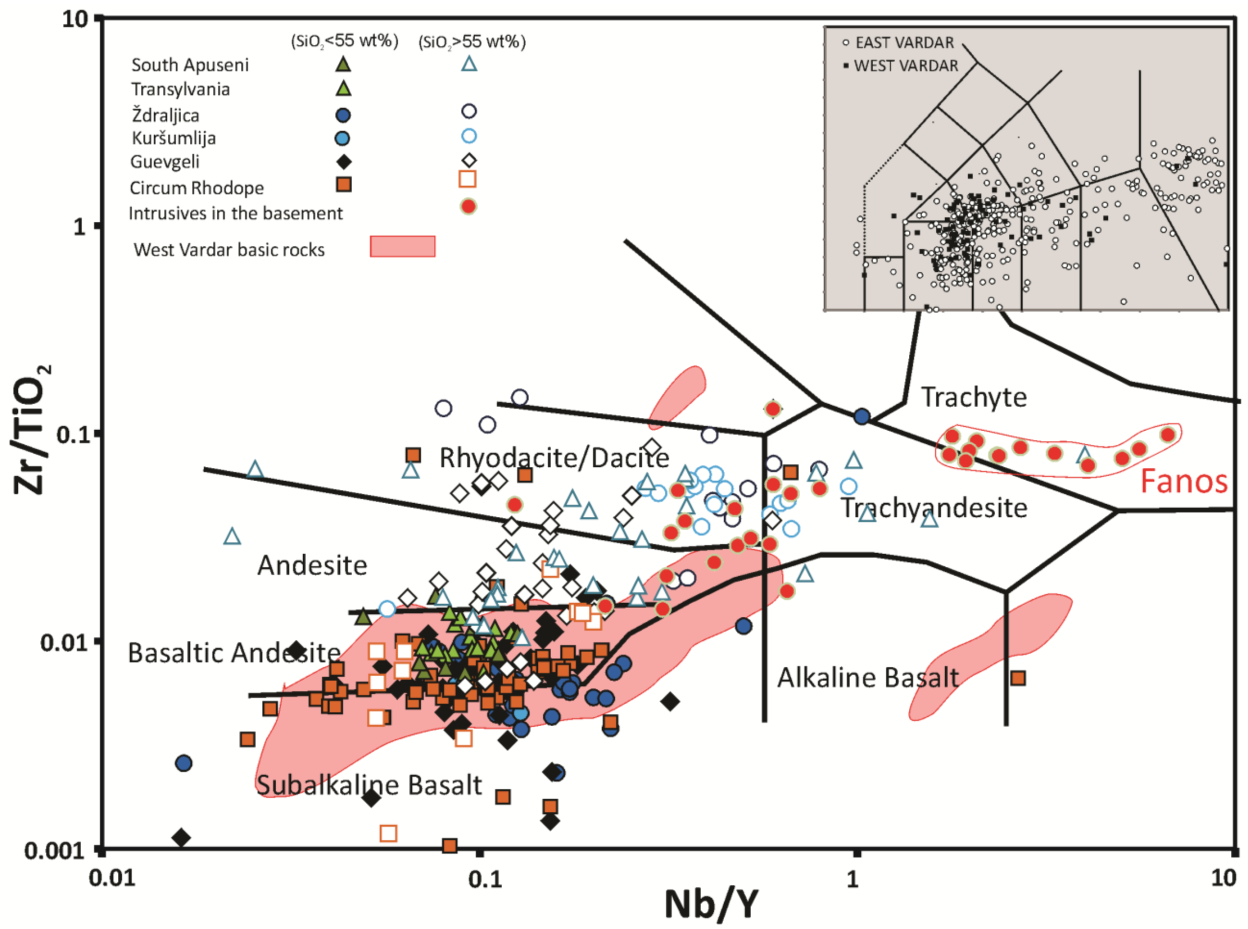

Figure 2. Nb/Y vs Zr/TiO_2 classification diagram [65]; the inset shows the distribution of all the bulk rock analyses comprised by this study on the total alkali vs silica (TAS) diagram [66]. Data sources: South Apuseni – [10], [31]; Transylvania – [30]; Ždraljica and Kuršumlija – [32–34]; Guevgeli – [37–39]; Circum Rhodope – [38, 40]; Intrusives in the basement – [33]; West Vardar basic rocks – [17, 34, 67, 68].

It is evident, however, that these granitoids believed to cut the metamorphic basement also form two different subgroups. For instance, the Fanos samples are plotted towards high Nb/Y values (>1) (Figure 2).

Primitive mantle-normalized multielement and chondrite-normalized rare earth elements (REE) diagrams are shown in Figures 3 and 4, respectively. The rocks from all the studied ophiolite provinces are also subdivided into basic (SiO_2 < 55%; diagrams in the left) and acid/intermediate (SiO_2 > 55%; diagrams in the right) rocks. The basic rocks range from light-rare earth elements (LREE) enriched through relatively flat REE patterns to LREE depleted chondrite-normalized patterns and almost ubiquitously show troughs on Nb-Ta and often, but less pronounced on Ti as well as peaks on U-Th on primitive mantle-normalized diagrams. These characteristics are different from those shown by the basic rocks of the West Vardar ophiolites, which exhibit much smoother primitive mantle-normalized patterns.

In keeping with their more evolved character, the intermediate/acid rocks of the East Vardar display more pronounced crustal geochemical signature. This is evident from LREE-enriched chondrite-normalized pattern often with negative Eu-anomaly as well as from large ion lithophile elements (LILE)-enriched and Nb-Ta-Ti-depleted spiked patterns on primitive mantle-normalized diagrams. It is noteworthy that these acid/inter–mediate rocks display a relatively wide range of heavy REE (HREE) concentrations, ranging from < 2 × chondrite to around 10 × chondrite values. Božović et al. [37] reported the presence of Y- and HREE-depleted acid/intermediate rocks from the Demir Kapija ophiolites and interpreted them as having adakitic affinity using this as an important argument for suggesting a refined geodynamic interpretation. The occurrence of rocks of similar adakitic-like geochemical affinity has been reported in Serbia by Šarić et al. [33], but these rocks have not been given a strong geodynamic significance.

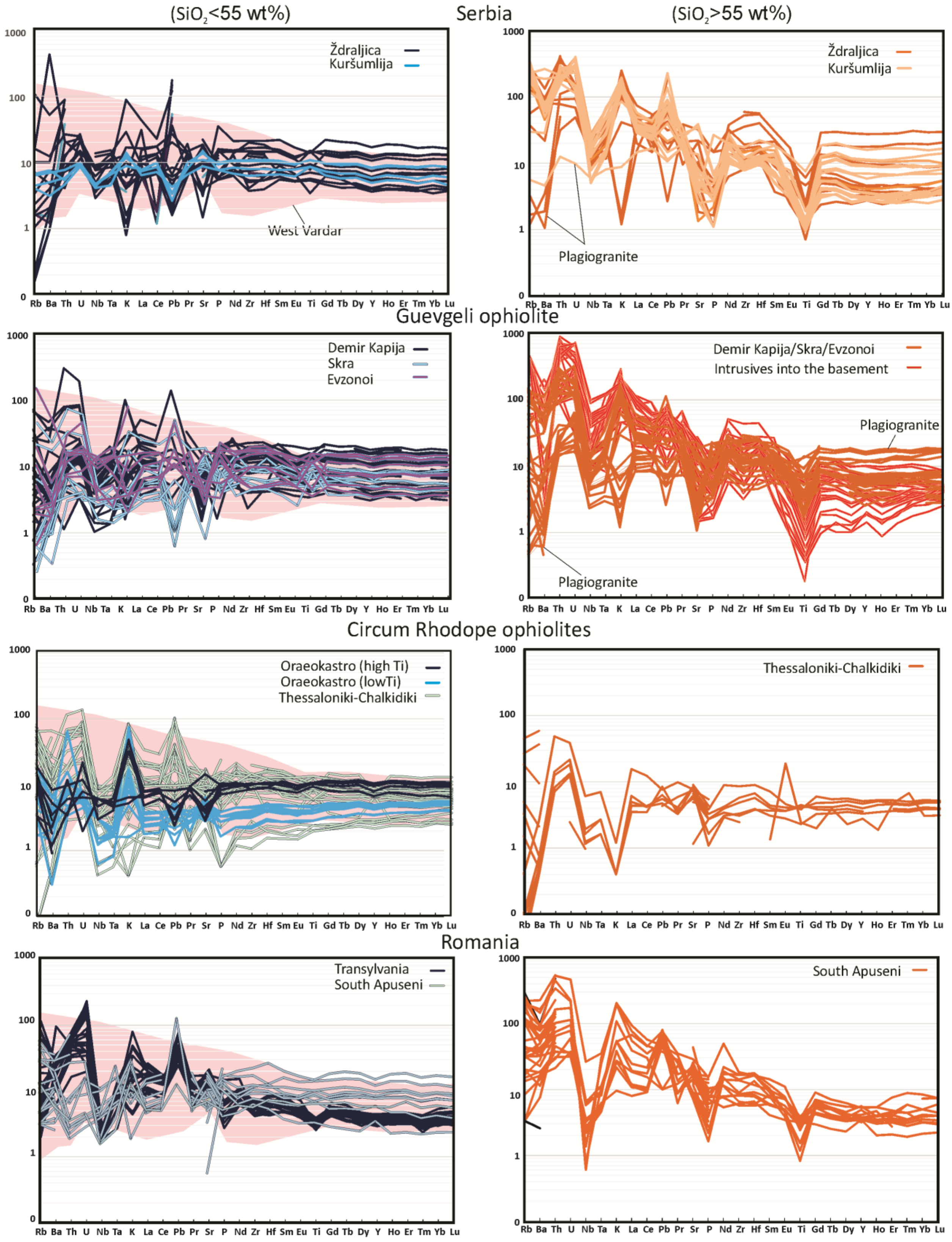

Figure 3. Primitive mantle-normalized multielement diagrams for the East Vardar magmatic rocks; the normalization coefficients after [69]. See capture in Figure 2 for data sources.

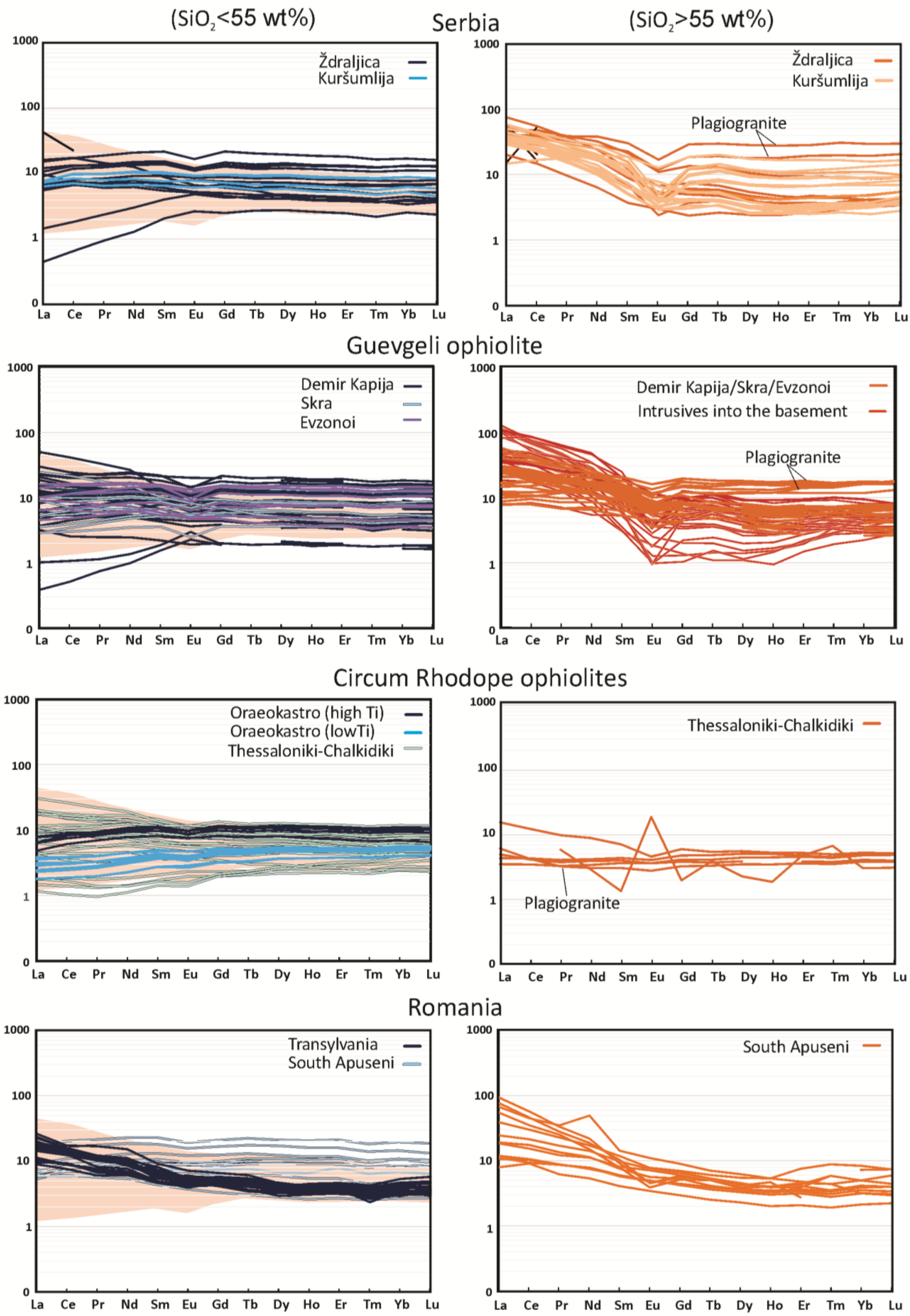

Figure 4. Chondrite-normalized REE diagrams for the East Vardar magmatic rocks; the normalization coefficients after [69]. See capture in Figure 2 for data sources.

Note also that a few silica-rich samples are characterized by relatively flat REE patterns as well as by high absolute heavy REE concentrations and low LILE concentrations, and they most probably represent oceanic plagiogranites. These acid rocks are not considered in the further discussion.

Sr-Nd compositions of the studied rocks are shown in Figure 5. It can be seen that the basic rocks of most provinces the East Vardar overlap in Sr-Nd isotopic composition and display somewhat higher $^{87}Sr/^{86}Sr$ and lower $^{143}Nd/^{144}Nd$ isotopes in comparison to the basic rocks of the West Vardar ophiolites. In terms of Sr-Nd isotopes, among the ophiolite-related acid/intermediate rocks of the East Vardar, at least two groups can be distinguished. The first group (rectangle in Figure 5) partly overlaps with or is only slightly enriched in Sr and depleted in Nd isotopes than the accompanying basic rocks. The second group of acid/intermediate rocks plots towards the enriched quadrant of the diagrams and is characterized by a relatively continuous and steady increase in $^{87}Sr/^{86}Sr$. Although the strong increase in Sr isotope ratios can be partly explained by seawater alteration processes (see also [34]), there is less pronounced but also a continuous increase in $^{143}Nd/^{144}Nd$ isotope ratios shown by these rocks, suggesting that these variations must be related to the input of crustal material in the mantle-derived melts. These isotopically crustal-like granitoids form two subgroups, initially recognized in [33] as low Sr*i* ($^{87}Sr/^{86}Sr_{initial}$ ~0.7033–0.7076) and high Sr*i* ($^{87}Sr/^{86}Sr_{initial}$ > 0.7095). To the low Sr*i* belong all intra-ophiolitic granitoids of Ždraljica, part of the Kuršumlija intrusives and the samples of the Fanos granitoids, whereas the rest of the Kuršumija samples and all the granitoids from Macedonia that intrude the basement belong to the high Sr*i* group.

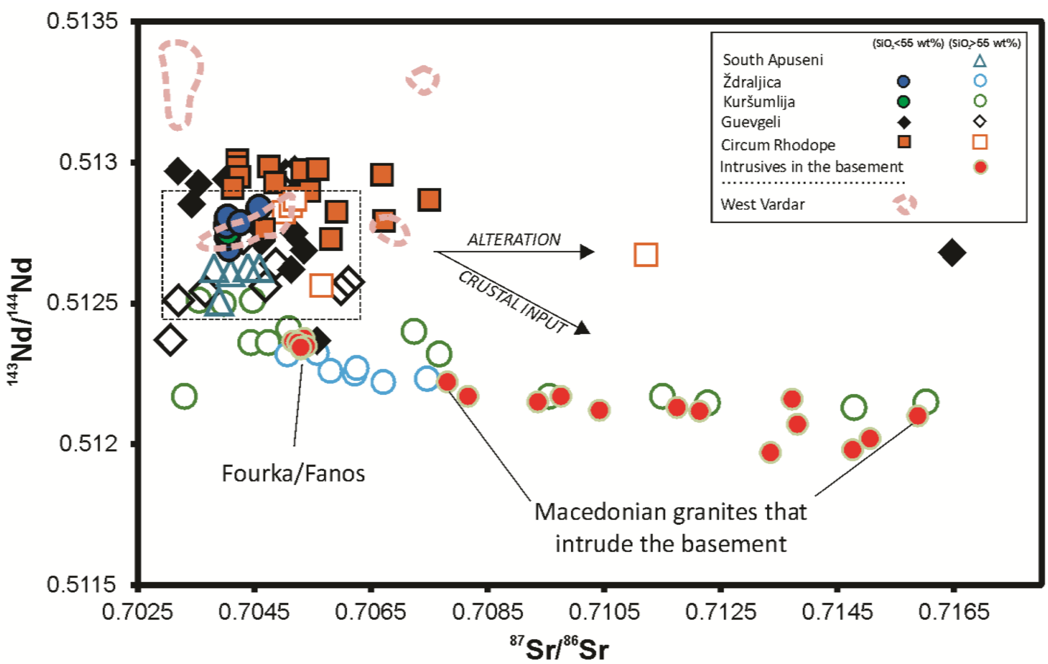

Figure 5. The $^{87}Sr/^{86}Sr$ vs $^{143}Nd/^{144}Nd$ plot for the East Vardar magmatic rocks; the rectangle encloses the field of the East Vardar acid/intermediate rocks that overlap in Sr-Nd isotopic composition with the majority of the accompanying basic rocks. See capture in Figure 2 for data sources.

DISCUSSION

The above presented overview of the most important geological and geochemical characteristics exhibited by the magmatic rocks of the East Vardar Zone ophiolites allows for recognition of several mutual features that can be underlined. They are related to the structural and stratigraphic position, age, rock facies, and the rocks' geochemical affinity. In the following sections, we summarize this information again in order to underline those issues that are most important and provide the first order geodynamic implications.

Tectonostratigraphy and age

Most here addressed East Vardar ophiolite slices are elongated in N-S direction (present coordinates) and are in tectonic contacts with metamorphic rocks of the Serbo-Macedonian Massif. The only exceptions are the South Apuseni ophiolites that presently stretch E-W due to substantial (~90°) clockwise rotations in the Cenozoic [70, 71]. The South Apuseni ophiolites lay upon the Biharia basement, which is considered part of the westernmost margin of Dacia, i.e. the Supragetic unit or the counterpart of the Serbo-Macedonian Massif [5]. The contacts between the East Vardar ophiolites and the Serbo-Macedonian Massif change towards the south. Recent geophysical modelling suggests that the contacts between the East Vardar ophiolites in Serbia and Macedonia and the Serbo- Macedonian Massif are steeply dipping and that at least some parts of the East Vardar ophiolites dip eastwards beneath the Serbo-Macedonian Massif [35, 36]. In this area, the contact between the East Vardar and Serbo-Macedonian unit is usually marked by the presence of narrow stripes of strongly deformed phyllites that sometimes contain serpentinite blocks [51]. This structural position is in agreement with the observations that the East Vardar ophiolites are thrust westwards onto the metamorphic rocks of the Paikon block or its counterparts [38, 39, 72]. Further to the south, the East Vardar ophiolites are strongly dismembered and appear as individual blocks within highly heterogeneous Circum Rhodope Belt.

The geologically and radiometrically constrained ages of the East Vardar ophiolites are recently comprehensively summarized by Gallhofer et al. [31]. They concluded that the maximal emplacement (obduction) age of the East Vardar ophiolites is the uppermost Kimmeridgian (<152 Ma), which is in agreement with the geological evidence, i.e. by the fact that the ophiolites are commonly covered by Tithonian limestones or Lower Cretaceous clastic sediments (e.g., [50]). It is worth noting that the presumed crystallization ages of mafic members of these ophiolites are mostly younger than 165 Ma and that there is no substantial age difference between the mafic and acid/intermediate members, which suggests that this oceanic realm was rather short-lived, i.e. it underwent a relatively fast evolution from ocean floor spreading to subduction and obduction processes [31, 37, 38, 40].

Subduction geochemical affinity shown by the basic rocks

The East Vardar ophiolites, in general, share two striking petrological characteristics: i) they are predominantly composed of volcano-intrusive sequences, whereas serpentinized peridotites are very scarce, and ii) in most of the East Vardar ophiolite provinces occur abundant acid to intermediate volcanic and/or intrusive rocks. The basic volcanic and shallow intrusive rocks of the East Vardar are generally similar to those of other Balkan ophiolites (see Figures 2–7), but the magmatic rocks of the East Vardar ophiolites are consistently more LREE- and sometimes LILE-enriched and plot towards enriched isotopic composition in the Sr-Nd space, which suggests that subduction processes have likely been involved in their origin.

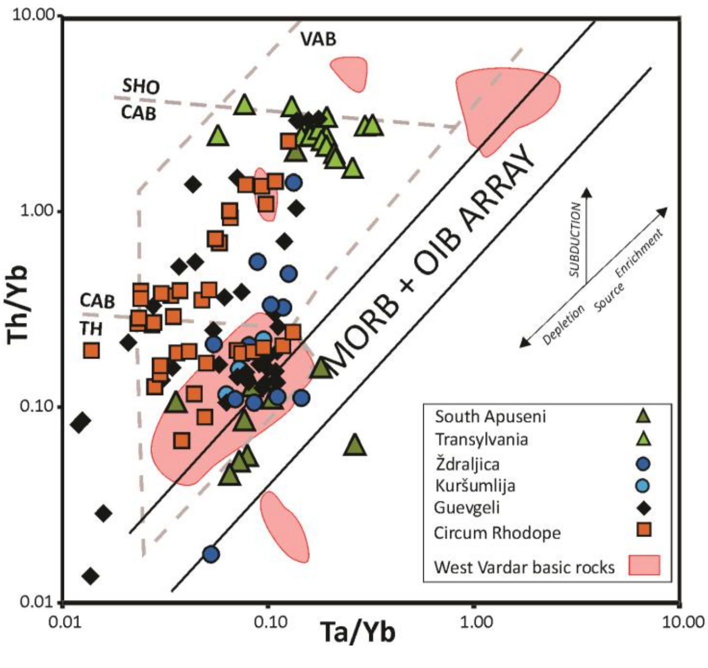

Figure 6. The Ta/Yb vs Th/Yb plot for distinguishing primitive basaltic magmas formed by subduction processes [73]. See capture in Figure 2 for data sources.

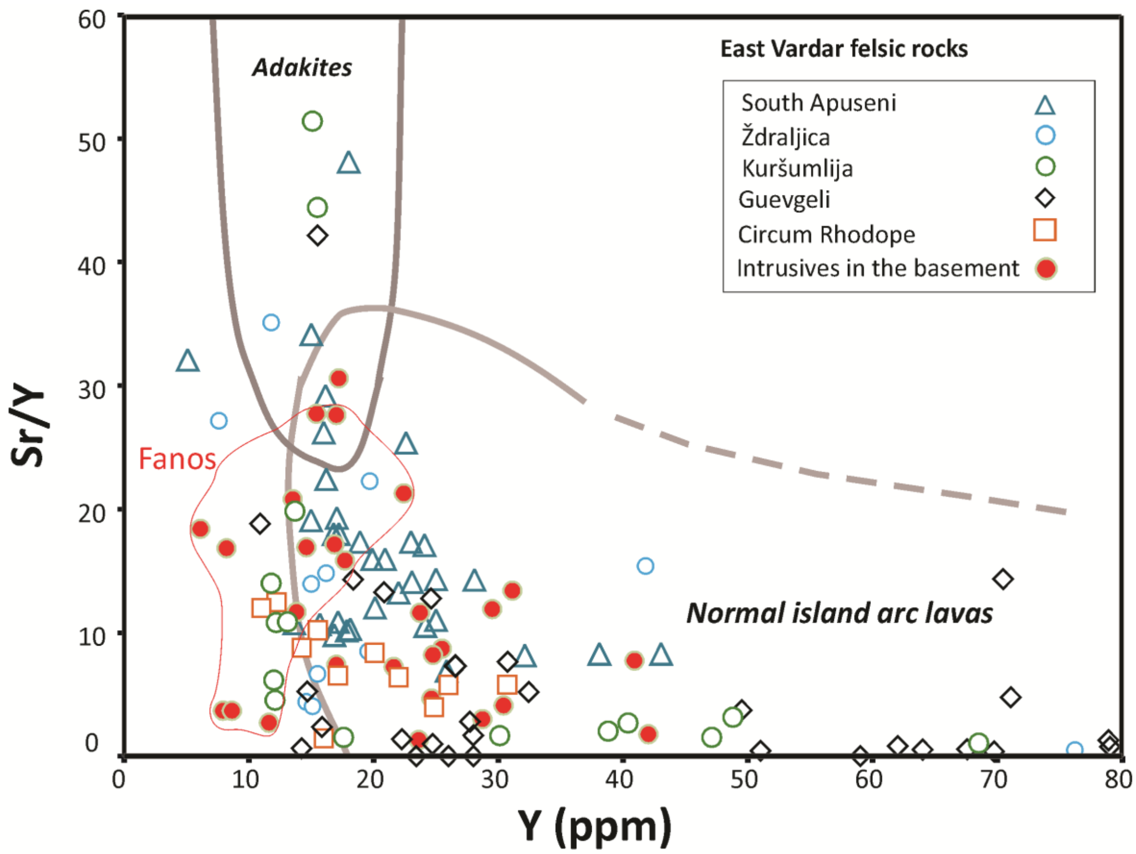

Figure 7. The Y vs Sr/Y plot for distinguishing between normal arc magmas and those having adakitic geochemical signature [75]. See capture in Figure 2 for data sources.

The subduction-related affinity (island arc or back-arc) of the rocks from many East Vardar occurrences have so far suggested by many authors (e.g., [31, 33, 37, 39], among others). Here we illustrate this affinity by using the Ta/Yb vs Th/Yb diagram [73] that is commonly applied for distinguishing the involvement of subduction-related enrichments from the source enrichments unrelated to active margin processes. From the diagram shown in Figure 6 it is evident that most ophiolite-related basic rocks of the East Vardar depart from the mid-ocean ridge – ocean island basalts array and plot towards the area characterized by increased Th/Yb ratios. This can be explained by involvement of subduction fluids plus a certain amount of sediments in melting regions from which these primary melts originated (e.g. [74]).

The message provided by the composition of felsic rocks

The above discussed subduction affinity is further corroborated by the fact that in almost all East Vardar provinces the basic rocks are accompanied with ubiquitously present and in some provinces very abundant felsic rocks. These felsic rocks (excluding oceanic plagiogranites), as it can be expected, display even more pronounced geochemical signature of subduction. However, the message taken from their characteristics is by no means clear, because certain issues regarding their origin and evolution still wait to be adequately constrained.

It is clear that the felsic rocks related to the East Vardar ophiolites are heterogeneous both compositionally and in terms of relative age of emplacement. For instance, most of the felsic rocks comprised by this study represent true intra-ophiolitic intrusives that appear as relatively small bodies always spatially enclosed by other ophiolites rock members. These, commonly collectively named intra-ophiolitic granitoids were regarded by many authors as representing felsic melts that originated during the evolution of this oceanic domain, which further means that these bodies have already been part of the ophiolite slices upon the ophiolite emplacement [31, 33]. By contrast, larger masses of granitoids occurring mainly in southern Macedonia clearly cut the basement of the Serbo-Macedonian Massif [33]. Most of these granitoids contain crustal xenoliths and exhibit distinctive crustal-like incompatible trace element patterns and Sr-Nd isotopic signature. The granitoid of Fanos departs from this. It intrudes into the southern part of the Guevgeli complex and is interpreted as also post-dating the emplacement of ophiolites (e.g. [38]), but it has distinctively less crustal-like isotopic characteristics, which are similar to the majority of intra-ophiolitic granitoid bodies [33, 37].

A weak adakitic affinity of some East Vardar intra-ophiolitic felsic rocks was mentioned in [33] for the occurrences in Serbia, but the authors did not give any geodynamic connotation to this observation. This issue has been given full attention in [37], who reported the presence of rocks of adakitic-like geochemical affinity in the Demir Kapija ophiolites. Božović et al. [37] argued that the adakitic-like magmas formed simultaneously with normal arc melts, and they used that as evidence for proposing a scenario of slab plus sediment melting in an unusually hot subduction zone (i.e. subduction of young oceanic crust). The authors went a step further and stated that this magmatism was associated with a progressive change in melting depth, suggesting that there was a relatively abrupt increase in temperature within the subducted slab soon after subduction initiation. They eventually concluded that the Demir Kapija ophiolites formed in a short-lived (intra-oceanic) back-arc basin. However, Zachariadis [38] and Saccani et al. [39] did not recognize a significant adakitic geochemical signature in the rocks occurring in the Greek part of the Guevgeli complex.

In order to contribute to this issue, here we plot all the felsic rocks comprised by this synthesis on the classical Y vs Sr/Y diagram for distinguishing between the normal arc and adakitic magmas [75]. We limited the vertical axis to only slightly elevated Sr/Y values (< 60) in order to see the samples distribution better. It can be seen that the felsic rocks from most of the East Vardar provinces indeed show weak adakitic characteristics, with maybe the exception of the Circum Rhodope ophiolites, which can be due to sample bias. Note, for instance, that some samples from the South Apuseni and the Serbian East Vardar ophiolites exhibit distinctively higher Sr/Y values than do most rocks from Demir Kapija. In addition, the group of the granites that presumably intrude both the East Vardar ophiolites and the basement is dividied into two subgroups. The Fanos rocks (red dots circled by a red line) plot towards the elevated Sr/Y values, whereas the granitoids from southern Macedonia (the rest of the red dots) have typical normal arc (i.e. crustal-like) geochemical characteristics.

Summary of geological and geochemical information: What does it say about geodynamics?

Numerous authors offered their geodynamic interpretations of the East Vardar ophiolites usually including appropriate geotectonic sketches and drawings (e.g. [31, 37–39], among others). The majority of these geotectonic interpretations are based on at least three common points: 1) the East Vardar ophiolites originated in a relatively narrow oceanic basin, 2) the basin was short-lived, namely, it formed, evolved and closed in a relatively short time-span between early/middle to uppermost Jurassic, 3) this oceanic realm originated in a back-arc position of the eastward (present coordinates) subducting oceanic plate of the much wider Neotethys/West Vardar or Meliata ocean. However, there are also significant differences in the suggested geodynamic views. Ionescu et al. [30] proposed westward subduction for the origin of South Apuseni and Transylvania ophiolites in order to explain the clear evidence that these ophiolites slices were obducted onto the European plate. For the southern East Vardar provinces, disagreements are related to the immediate setting in which spreading of the narrow oceanic realm occurred. Zachariadis [38] and Božović et al. [37] regard the East Vardar ocean as having developed within the already existing ocean floor of Neotethys, i.e. in an intraoceanic environment. Consequently, they understand the Paikon block as an immature island arc behind which back-arc spreading of East Vardar has occurred. Other authors (e.g. [39, 40, 72, 76],) argued that the Paikon block was founded by the Paleozoic basement and that it was a continental ribbon split-off the westernmost European margin. In such a scenario, the East Vardar oceanic segment formed in response to ensialic backarc rifting.

As the result of this synthesis, we propose a paleotectonic reconstruction graphically presented in Figure 8. It consists of four stages and comprises the period from early- to uppermost Jurassic. The orientation of major structures (mostly E-W) is different from those of the present day (N-S), which are the result of later rotations. The first stage (Figure 8A; early/mid-Jurassic) involves north-northeastward subduction of the West Vardar oceanic plate, which is the main cause for the formation of the East Vardar ocean. The subduction front is intra-oceanic in the east, whereas in the west it is much closer to the European continent. Note that there is another subduction within the Neotethys, it has the same orientation, but is situated more to the south. During the second stage (Figure 8B; mid-Jurassic) a complex volcanic arc is formed along the ocean-continental transition corridor of the European margin. In the north, it represents an intra-oceanic immature arc, whereas in the south it develops on the continental lithosphere (the future Paikon block). Immediately following is the phase of back-arc spreading and the formation of the narrow oceanic stripe of East Vardar. The third stage (Figure 8C; mid-/Upper Jurassic) is characterized by the termination of the northward subduction of the West Vardar oceanic lithosphere and by the initiation of another subduction, this time along the very East Vardar ridge. This is the onset of the closure of the East Vardar Ocean, which will be completed when the previously mentioned volcanic arcs are docked to the European margin. The situation immediately following the closure of the East Vardar ocean is shown in the last sketch (Figure 8D; uppermost Jurassic). It shows that the uppermost Jurassic remnants of both West and East Vardar ocean floor have been emplaced as ophiolites. However, in contrast to the West Vardar ophiolites that have been rather homogeneously obducted onto the African margin, the emplacement of the East Vardar ophiolites was much more heterogeneous. In the north (South Apuseni and Transylvania), they have been obducted northwards onto the European plate, in the far south (Macedonia and Greece) they emplaced towards the south onto the Paikon block, whereas in the central part (Serbia) they likely accreted as steeply dipping ophiolites slices.

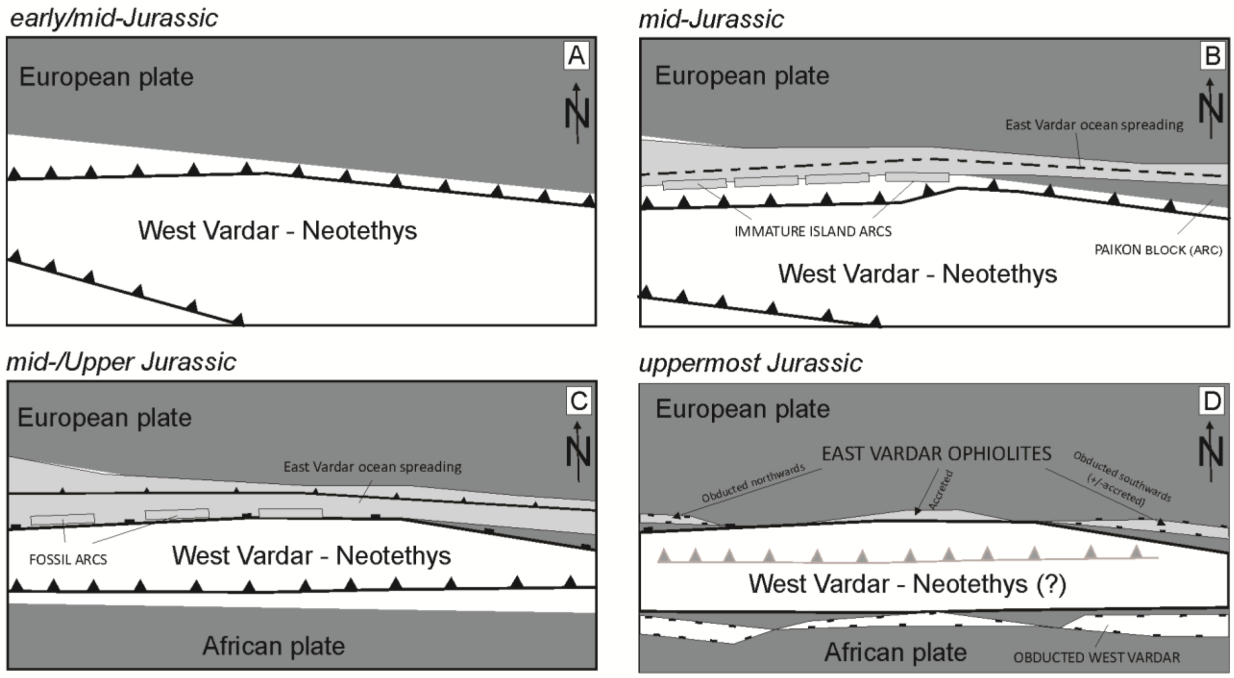

Figure 8. A sketch illustrating the paleotectonic reconstruction of the origin and evolution of East Vardar; the orientation of major structures is roughly E-W, i.e. different from their present day directions because of Cenozoic rotations; **A)** the first stage (early/mid Jurassic) involves north-northeastward subduction of the West Vardar oceanic plate; it is intraoceanic in character in the north and subduction under continent in the south; note that there is another intraoceanic subduction towards the south-southwest. **B)** The formation of a volcanic arc (mid Jurassic); it is an intraoceanic immature arc in the east, whereas in the west it forms onto the continental lithosphere (Paikon block); a narrow oceanic stripe of East Vardar's ocean floor is also formed. **C)** The termination of subduction of the West Vardar oceanic lithosphere and the initiation of subduction along the East Vardar ridge (mid/Upper Jurassic). **D)** The closure of the East Vardar ocean (uppermost Jurassic) and emplacement of both West and East Vardar ophiolites; note that the West Vardar ophiolites are found homogeneously obducted onto the African margin, whereas the East Vardar ophiolites are obducted northwards (onto European plate) in the east (in the north in present coordinates), southwards (onto the Paikon block) in the west (in the south in present coordinates) and simply accreted as steeply dipping ophiolites slices in the central parts.

In summary, the available data allow for having relatively clear ideas about the origin and evolution of the East Vardar ophiolites and in particular to recognize striking differences between these ophiolites and the much more widespread ophiolites of the West Vardar. However, in order to make a new step forward in our knowledge of the evolution of the East Vardar Ocean as well as in order to be able to refine the existing geodynamic models significantly, we need more information with regards to almost all aspects of these ophiolite rocks. We emphasize the three, albeit not exhaustive questions: i) what is the true structural position of the East Vardar ophiolites slices in Serbia, ii) were the East Vardar ophiolites in Serbia formed via intra-oceanic subduction, and iii) what is the real significance of the adakitic signature shown by rocks in East Vardar provinces other than Demir Kapija.

CONCLUSIONS

The synthesis of the available geological and geochemical data for the East Vardar ophiolites occurring in Romania, Serbia, Macedonia and Greece enable us to derive the following conclusions:

1) The East Vardar ophiolites display the most pronounced supra-subduction signature of all the Balkan ophiolite belts. These geochemical characteristics are evident in all the East Vardar provinces comprised by this study and are shown by both basic and accompanied acid- to intermediate rocks.

2) The structural position of the East Vardar ophiolitic slices is different. The northern occurrences in Romania clearly overlie the Supragetic-Serbo-Macedonian unit, suggesting that they have emplaced onto the European plate. Towards the south, the contacts between the East Vardar ophiolites and adjacent units become steeper, whereas in the southernmost occurrences (Macedonia and Greece) they are west-vergent and lay upon the Paikon block.

3) The East Vardar was a narrow and short-lived oceanic realm that most likely closed via subduction initiated along the ridge axis. The adakitic-like geochemical signature is taken as evidence that this subduction involved slab (plus sediments) melting. A four-stage paleotectonic reconstruction is proposed.

4) In order to improve the existing geodynamic models there is a great need for more information about the true structural position of the East Vardar ophiolites slices in Serbia, about the possible continuation of the Paikon block towards the north and about the true significance of the adakitic signature that is shown by felsic rocks in many, if not all, East Vardar provinces.

Acknowledgements: This study is carried out in the frame of bilateral collaboration between the Macedonian Academy of Sciences and Arts and the Serbian Academy of Sciences and Arts. The authors thank to BSc student Jovan Resimić for help in preparing the excel data base as well as to an anonymous reviewer for useful corrections of the originally submitted manuscript.

REFERENCES

[1] G. M. Stampfli, G. Borel, The TRANSMED transects in space and time: constraints on the paleotectonic evolution of the Mediterranean domain, in: *The TRANSMED Atlas: the Mediterranean Region from Crust to Mantle*, W. Cavazza, F. M. Roure, W. Spakman et al. (eds.), Springer, Heidelberg, 2004, pp. 53–80.

[2] D. J. J. van Hinsbergen, E. Hafkenscheid, W. Spakman, J. E. Meulenkamp, W. Wortel, Nappe stacking from subduction of oceanic and continental lithosphere below Greece, *Geology*, **33** (2004), pp. 325–328.

[3] C. Faccenna C. L. Jolivet, C. Piromallo et al., Subduction and the depth of convection in the Mediterranean mantle, *J. Geophys. Res.*, **108** (2003), p. 2099.

[4] S. M. Schmid, E. Kissling, The arc of the Western Alps in the light of geophysical data on deep crustal structure, *Tectonics*, **19** (2000), pp. 62–85.

[5] M. S. Schmid, D. Bernoulli, B. Fügenschuh, L. Matenco, S. Schefer, R. Schuster, M. Tischler, K. Ustaszewski, The Alps-Carpathians-Dinarides connection: a correlation of tectonic units, *Swiss J. Geosci.*, **101** (2008), pp. 139–183.

[6] M. Săndulescu, Cenozoic tectonic history of the Carpathians, in: *The Pannonian Basin. A Study in Basin Evolution*, L. H. Royden, F. Horvath (eds), AAPG Mem **35,** 1988, pp. 17–25.

[7] J. Haas, S. Pero, Mesozoic evolution of the Tisza Mega-unit, *Int. J. Earth Sci.*, **93** (2004), pp. 297–313.

[8] J-P. Rampnoux, Regards sur les Dinarides internes yougoslaves (Serbie-Monténégro oriental): stratigraphie, évolution paléogéographique, magmatisme, *Bull. Soc. géolog. France*, **12,** 6 (1970), pp. 948–966.

[9] A. G. Smith, J. G. Spray, A half-ridge transform model for the Hellenic-Dinaric ophiolites, in: *The Geological Evolution of the Eastern Mediterranean*, J. E. Dixon et al. (eds.), Geol. Soc. London Spec. Publ., **17,** (1984), pp. 589–603.

[10] V. Bortolotti, M. Marroni, I. Nicolae, L. Pandolfi, G. Principi, E. Saccani, An update of the Jurassic ophiolites and associated calc-alkaline rocks in the south Apuseni Mountains (western Romania), *Ofioliti*, **29**, 1 (2004), pp. 5–18.

[11] V. Bortolotti, G. Principi, Tethyan ophiolites and Pangea break-up, *Island Arc*, **14** (2005), pp. 442–470.

[12] J. E. T. Channell, H. W. Kozur, How many oceans? Meliata, Vardar, and Pindos oceans in

Mesozoic Alpine paleogeography, *Geology,* **25** (1997), pp. 183–186.

[13] D. Mountrakis, Structural evolution of the Pelagonian Zone in northwestern Macedonia, in: *Geological Evolution of the Eastern Mediterranean*, J. E. Dixon, A. H. F. Robertson (eds.), Geol. Soc. London Spec. Publ., **17,** (1984), pp. 581–590.

[14] A. H. F. Robertson, P. D. Clift, P. J. Degnan, G. Jones, Palaeogeographic and palaeotectonic evolution of the Eastern Mediterranean Neotethys, *Palaeogeography, Palaeoclimatology, Palaeoecology,* **87** (1991), pp. 289–343.

[15] J. Dercourt, M. Gaetani, B. Vrielynck, E. Barrier, B. Biju-Duval, M. F. Brunet, J. P. Cadet, S. Crasquin, M. Sandulescu, (eds.), *Peri-Tethys Palaeogeographical Maps Atlas*. CCMGCGMW, Paris, (2000).

[16] G. Stampfli, J. Moser, P. Favre, A. Pillevuit, J. C. Vannay, Permo–Mesozoic evolution of the western Tethys region: the Neotethys–East Mediterranean basin connection, in: *Peri-Tethys Memoir* 6, P. Ziegler, W. Cavazza, A. H. F. Robertson, S. Crasquin-Solea (eds.), Mem. Natn. Hist., Paris, Natural History Museum, Paris, **186**, (2001), pp. 51–108.

[17] A. H. F. Robertson, S. Karamata, The role of subduction–accretion processes in the tectonic evolution of the Mesozoic Tethys in Serbia, *Tectonophysics*, **234** (1994), pp. 73–94.

[18] S. Karamata, The geological framework of the Balkan Peninsula: its origin due to the approach, collision and compression of Gondwanian and Eurasian units, in: *Tectonic Development of the Eastern Mediterranean Region,* A.H.F. Robertson, D. Mountrakis (eds), Geol. Soc. Lond. Spec. Publ., **260** (2006) pp. 155–178.

[19] A. H. F. Robertson, S. Karamata, K. Šarić, Overview of ophiolites and related units in the Late Palaeozoic–Early Cenozoic magmatic and tectonic development of Tethys in the northern part of the Balkan region, *Lithos,* **108** (2009), pp. 1–36.

[20] V. Cvetković, D. Prelević, S. Schmid, Geology of South-Eastern Europe, in: *Mineral and Thermal Waters of Southeastern Europe*, P. Papić (ed.), 2015, pp. 1–29.

[21] F. Kockel, H. Mollat, H. W. Walther, Geologie des Serbo-Mazedonischen Massivs und seines mesozoischen Rahmens (Nordgriechenland), *Geol. Jahrb.*, **89** (1971), pp. 529–551.

[22] F. Kockel, H. Mollat, H. W. Walther, *Erlauterungen zur geologischen karte der Chalkidiki und angrenzender Gebiete 1 : 100000* (Nord Griechenland), *Bundesanstalt fur* Geowissenschaften und Rohstoffe, Hannover, (1977),.

[23] A. Michard, B. Goffé, A. Liathi et al., Découverte du facies schiste bleu dans les nappes du Circum-Rhodope; un element d'une ceinture HP-BT éohéllenique en Grèce septentrionale, *Compte Rendu Académie des Sciences,* **318,** 2 (1994), pp. 1535–1542.

[24] B. C. Burchfiel, *Geology of Romania*, Geol. Soc. Am. Spec. Papers, **158,** (1976), 82 pp.

[25] M. Bleahu, S. Bordea, M. Lupu, A. Ştefan, D. Patrulius, S. Panin, The structure of the Apuseni Mts. B3 Field trip guide, *XII Congress of the Carpathian-Balkan Geological Association, Bucharest 1981*. Institutul de Geologie şi Geofizică, 1981, 107 pp.

[26] I. Nicolae, Tectonic setting of the ophiolites from the South Apuseni Mountains: magmatic arc and marginal basin, *Roman. J. Tect. Reg. Geol.,* **76** (1995), pp. 27–39.

[27] V. Bortolotti, M. Marroni, I. Nicolae, L. Pandolfi, G. Principi, E. Saccani. Geodynamic implications of Jurassic ophiolites associated with island-arc volcanics, South Apuseni Mountains, Western Romania, *Int. Geol. Rev*., **44** (2002), pp. 938–955.

[28] M. D. Dimitrijević, Geological Atlas of Serbia 1, 1:2.000.000, Republical Foundation for Geological Investigations and Geological Institute GEMINI, Grafimex, Belgrade, 1992.

[29] I. Nicolae, E. Saccani, Petrology and geochemistry of the Late Jurassic calcalkaline series associated to Middle Jurassic ophiolites in the South Apuseni Mountains (Romania), *Schweizerische Mineralogische Petrographische Mitteilungen,* **83** (2003), pp. 81–96.

[30] C. Ionescu, V. Hoeck, C. Tomek, F. Koller, I. Balintoni, L. Beşuţiu, New insights into the basement of the Transylvanian Depression (Romania), *Lithos,* **108** (2009), pp. 172–191.

[31] D. Gallhofer, A. von Quadt, S. M. Schmid, M. Guillong, I. Peytcheva, I. Seghedi, Magmatic and tectonic history of Jurassic ophiolites and associated granitoids from the South Apuseni Mountains (Romania), *Swiss J. Geosci.*, **10**, 2 (2017), pp. 699–719.

[32] K. Resimić, *Petrology of igneous rocks of diabase-chert formation near Kragujevac*, Master Thesis, Faculty of Mining and Geology, University of Belgrade, (2000) 169 pp.

[33] K. Šarić, V. Cvetković, R. L. Romer, G. Christofides, A. Koroneos, Granitoids associated with East Vardar ophiolites (Serbia, F.Y.R. of Macedonia and northern Greece): Origin, evolution and geodynamic significance inferred from major and trace element data and Sr-Nd-Pb isotopes, *Lithos,* **108** (2009), pp. 131–150.

[34] M. Božović, *Petrology and Geochemistry of the Balkan Ophiolites*, Johannes Gutenberg University Mainz, PhD thesis, 2013, 254 pp.

[35] D. Petrović, V. Cvetkov, I. Vasiljević, V. Cvetković, A new geophysical model of the Serbian part of the East Vardar ophiolite: Implications

for its geodynamic evolution, *J. Geodyn*., **90** (2015), pp.1–13.

[36] D. Petrović, V. Cvetkov, V. Cvetković, Spatial distribution of the Demir Kapija (Macedonia) ophiolite based on geomagnetic data, *Tehnika*, **2** (2016), pp. 215–220.

[37] M. Božović, D. Prelević, R. L. Romer, M. Barth, P. Den Bogaard, B. Boev, The Demir Kapija ophiolite, Macedonia (FYROM): a snapshot of subduction initiation within a back-arc, *J. Petrol.*, **54**, 7 (2013), pp. 1427–1453.

[38] P. Zachariadis, *Ophiolites of the Eastern Vardar Zone, N. Greece*, PhD dissertation, Johannes Gutenberg-Universität, Mainz, 2007, pp. 1–131.

[39] E. Saccani, V. Bortolotti, M. Marroni, L. Pandolfi, A. Photiadis, G. Principi, The Jurassic association of backarc basin ophiolites and calc-alkaline volcanics in the Guevgueli complex (Northern Greece): implications for the evolution of the Vardar zone, *Ofioliti*, **33** (2008), pp. 209–227.

[40] N. Bonev, P. Marchev, R. Moritz et al., Jurassic subduction zone tectonics of the Rhodope Massif in the Thrace region (NE Greece) as revealed by new U-Pb and ^{40}Ar/^{39}Ar geochronology of the Evros ophiolite and high-grade basement rocks, *Gondwana Res.*, **27** (2015), pp. 760–775.

[41] K. Resimić-Šarić, S. Karamata, A. Popević, K. Balogh, The eastern branch of the Vardar zone – the scar of the main Vardar ocean, in: *Geology and Metallogeny of the Dinarides and the Vardar zone*, S. Karamata, S. Janković (eds.), Zvornik, 2000, pp. 81–85.

[42] K. Resimić-Šarić, V. Cvetković, K. Balogh, Radiometric K/Ar data as evidence of the geodynamic evolution of the Zdraljica Ophiolitic Complex (central Serbia). *Ann. Géol. Pénin*. *Balk*., **66**, (2005), pp. 73–79.

[43] M. Malešević, M. Vukanović, T. Brković, J. Obradović, L. Karajičić, M. D. Dimitrtijević, R. Stanislavijević, *Basic Geologcal Map SFRY, 1:100.000, Sheet Kuršumlija and Explanations*, 1978.

[44] M. N. Dimitrijević, M. D. Dimitrijevic, *The Turbiditic Basins of Serbia*, Serbian Academy of Sciences and Arts, Department of Natural and Mathematical Sciences, 1987.

[45] M. D. Dimitrijević, *Geology of Yugoslavia*, Geological Institute GEMINI spec. publ., Belgrade, (1997).

[46] M. D. Dimitrijević, Dinarides and the Vardar Zone: a short review of the geology, *Acta Vulcan.*, **13** (2001), pp. 1–8.

[47] J. Mercier, Mouvements orogéniques et magmatisme d'age Jurassique Supérieur–É ocrétacé dans les Zones Internes des Hellénides (Macédoine, Grèce), *Revue de Géographie Physique et de Géologie Dynamique*, **2**, VIII (4) (1966), pp. 265–278.

[48] S. A. M. Brown, A. H. F. Robertson, Sedimentary geology as a key to understanding the tectonic evolution of the Mesozoic-Early Tertiary Paikon Massif, Vardar suture zone, N Greece, *Sedim. Geol*., **160** (2003), pp. 179–212.

[49] B. Anders, T. Reischmann, U. Poller, D. Kostopoulos, Age and origin of granitic rocks of the eastern Vardar Zone, Greece: new constraints on the evolution of the Internal Hellenides, *J. Geol. Soc.*, **162** (2005), pp. 857–870.

[50] B. Boev, S. Lepitkova, The age of the ophiolite rocks on the territory of the Republic of Macedonia. *XVII Congress of the Carpathian-Balkan Geological association*, 2002, Bratislava.

[51] B. Boev, D. Prelević, M. Božović, S. Erić, V. Cvetković, Olivine websterite veins cutting the rabrovo serpentinites (south Macedonia): new evidence of the arc setting of the East Vardar Ophiolites?, *Contributions*, *MASA*, *Sec. Nat. Math. Biotech. Sci.*, **34** (1–2), (2013), pp. 69–81.

[52] K. Šarić, V. Cvetković, R. L. Romer, I. Peytcheva, A. von Quadt, Petrogenesis of intraophiolitic calc-alkaline and tholeiitic granitoids of Eastern realm of the Vardar zone in Serbia, in: *Proceedings of the 15th Congress of Geologists of Serbia with International Participation*, N. Banjac (ed.), Belgrade, (2010), p. 43.

[53] D. Kukoč, Š. Goričan, A. Košir et al., Middle Jurassic age of basalts and the post-obduction sedimentary sequence in the Guevgueli Ophiolite Complex (Republic of Macedonia), *Int. J. Earth Sci.*, **104** (2), (2015), pp. 435–447.

[54] J. Bébien, L'association igne´e de Gue´vgue´li (Mace´doine grecque), *Expressiond'un magmatisme ophiolitique dans une de´chirure continentale*. DSc thesis, Universite´ de Nancy I. (1982).

[55] J. G. Spray, J. Babien, D. C. Rex, J. C. Roddick, *Age constraints on the igneous and metamorphic evolution of the Hellenic-Dinaric ophiolites*, Geol. Soc. London, Sp. Publ., **17** (1984) pp. 619–627.

[56] T. Danelian, A. H. F. Robertson, S. Dimitriadis, Age and significance of radiolarian sediments within basic extrusives of the marginal basin Guevgueli Ophiolite (northern Greece), *Geol. Mag.*, **133** (1996), pp. 127–136.

[57] E. Sapountzis, The Thessaloniki gabbros, *Petrology*, **20** (1979), pp. 37–70.

[58] S. Dimitriadis, Discussion of 'The Thessaloniki Gabbros' by E. Sapountzis, *J. Petrol.*, **21** (1980), pp. 437–440.

[59] J. Mercier, P. Vergély, J. Bébien, Les ophiolites helléniques »obductées« au Jurassique supérieur sont-elles les vestiges d'un Océan téthysien ou d'une mer marginale péri-européene? *Comptes Rendes Sommaires de la Soc. Géol. France*, **17** (1975), pp. 108–111.

[60] K. Mussallam, D. Jung, Petrology and geotectonic significance of salic rocks preceding ophiolites in the eastern Vardar Zone, Greece. TMPM *Tschermaks Mineralogische und Petrographische Mitteilungen*, **35** (1986) pp. 217–42.

[61] A. H. F. Robertson, Overview of the genesis and emplacement of Mesozoic ophiolites in the Eastern Mediterranean Tethyan region, *Lithos*, **65** (2002), pp. 1–67.

[62] G. Christofides, T. Soldatos, A. Koroneos, Geochemistry and evolution of the Fanos granite, N. Greece, *Miner. Petrol.*, **43** (1990), pp. 49–63.

[63] G. Christofides, A. Koroneos, T. Soldatos, G. Eleftheriadis, A. Kilias, Eocene magmatism (Sithonia and Elatia plutons) in the Internal Hellenides and implications for Eocene–Miocene geological evolution of the Rhodope massif (Northern Greece), in: *Tertiary Magmatism in the Dinarides, Acta Vulcanologica*, H. Downes, V. Orlando (eds.), **13** (2001), pp. 73–89.

[64] G. Kauffmann, F. Kockel, H. Mollat, Notes on the stratigraphic and paleogeographic position of the Svoula formation in the Innermost Zone of the Hellenides (Northern Greece), *Bull. Soc. Géol. France*, **18** (1976), pp. 225–230

[65] J. A. Winchester, P. A. Floyd, Geochemical Discrimination of Different Magma Series and Their Differentiation Products Using Immobile Elements, *Chem. Geol.*, **20** (1977), pp. 325–343.

[66] M. J. Le Bas, R. W. Le Maitre, A. Streckeisen, B. A. Zanettin, Chemical classification of volcanic rocks based on the total alkali silica diagram. *J. Petrol.*, **27** (1986), pp. 745–750.

[67] B. Lugović, R. Altherr, I. Raczek, A. W. Hofmann, V. Majer, Geochemistry of peridotites and mafic igneous rocks from the Central Dinaric Ophiolite Belt, Yugoslavia, *Contrib. Miner. Petrol.*, **106** (1991), pp. 201–216.

[68] J. Pamić, B. Tomljenović, D. Balen, Geodynamic and petrogenetic evolution of Alpine ophiolites from the central and NW Dinarides: an overview, *Lithos*, **65** (2002), pp. 113–142.

[69] W. F. McDonough, S.-s. Sun, The composition of the Earth, *Chem. Geol.*, **120** (1995), pp. 223–253.

[70] S. Patrascu, M. Bleahu, C. Panaiotu, Tectonic implications of paleomagnetic research into Upeer Cretaceous magmatic rocks in the Apuseni Mountains, Romania, *Tectonophysics*, **180** (1990), pp. 309–322.

[71] E. Márton, M. Tischler, L. Csontos, B. Fügenschuh, S. Schmid, S., The contact zone between the ALCAPA and Tisza-Dacia megatectonic units of Northern Romania in the light of new paleomagnetic data, *Swiss J. Geosci.*, **100** (2007), pp. 109–124.

[72] S. A. M. Brown, A. H. F. Robertson, Evidence for Neotethys rooted within the Vardar suture zone from the Voras Massif, northernmost Greece, *Tectonophysics*, **381** (2004), pp. 143–173.

[73] J. A. Pearce, Trace element characteristics of lavas from destructive plate boundaries, in: *Andesites: Orogenic Andesites and Related Rocks*, R. S. Thorpe (ed.), John Wiley & Sons, Chichester, U.K., 1982, pp. 525–548.

[74] L. C. Patino, M. J. Carr, M. D. Feigenson, Local and regional variations in Central American arc lavas controlled by variations in subducted sediment input, *Contrib. Miner. Petrol.*, **138** (2000), pp. 265–283.

[75] M. J. Defant, M. S. Drummond, Derivation of some modern arc magmas by melting of young subducted lithosphere, *Nature*, **347** (1990), pp. 662–665.

[76] J. Ferrière, A. Stais, Nouvelle interprétation de la suture téthysienne vardarienne d'après l'analyse des séries de Péonias (Vardar oriental, Hellénides internes), *Bull. Soc. Géol. France*, **166** (1995) pp. 327–339.

НОВ ПОГЛЕД НА ОФИОЛИТИТЕ ОД ИСТОЧНАТА ВАРДАРСКА ЗОНА: КРАТКА СИНТЕЗА НА ГЕОЛОГИЈАТА И ГЕОХЕМИСКИТЕ ПОДАТОЦИ

Блажо Боев[1*], Vladica Cvetković[2], Dejan Prelević[2], Kristina Šarić[2], Иван Боев[1]

[1]Универзитет „Гоце Делчев“, Штип, Република Македонија
[2]Faculty of Mining and Geology, University of Belgrade, Belgrade, Serbia

Во оваа студија се објавуваат и синтетизираат геолошките и геохемиските податоци за источно вардарските офиолити, вклучувајќи ги и најпознатите појави од Јужните Апусенски Планини во Романија до врвот на полуостровот Халкидики во Грција. Овие збирни геолошки податоци укажуваат на тоа дека источновардарските офиолити во најголем дел се изградени од магматски секвенци, со многу мала застапеност на карпите во обвивката. Члeновите на магматската секвенца се карактеризираат со присуство на поголема количина кисели и интермедијарни вулкански и интрузивни карпи. Староста на овие офиолити е одредена палеонтолошки и радиометриски и податоците укажуваат на тоа дека источновардарските офиолити се

формирале како краткотрајно океанско подрачје кое било активно пред горен кимериски период. Присутен е релативно слаб адакитски афинитет во интраофиолитските кисели и интермедијарни карпи во многу предели од Источновардарскиот регион.

Ова може да се земе како доказ дека на младата и жешка плоча се појавила субдукција, најверојатно со претходно ширење на гребенот. Се предлага палео-тектонската реконструкција од четири фази. Таа вклучува: а) рана/средна јурска северо-североисточна субдукција на западновардарската океанска плоча; б) формирање на среднојурски вулкански лак и тесен задлачен басен на океанскиот појас на Источновардарската зона; в) средно-/горнојурско започнување на субдукција на Источновардарската зона над оската на гребенот, г) комплексно и хетерогено поставување на офиолитите на Источновардарската зона. Податоците кои се достапни даваат релативно јасна слика за потеклото и еволуцијата на офиолитите на Источновардарската зона. Сепак, за да се овозможи подобро разбирање на сите аспекти на еволуцијата, треба да одговориме на дополнителни прашања кои се однесуваат на вистинската структурна поврзаност на делови на офиолитите на Источновардарската зона во Србија, вистинската природа на субдукцијата која е причинител на задлачното ширење на кората (интраокеанско наспроти субдукција под континентот?) и целосното значење на адакитските својства на карпите во пределите на источен вардарски регион надвор од Демир Капија.

Клучни зборови: офиолити; субдукција; задлачен басен; Тетис; Балкански Полуостров

ПРИЛОЗИ, Одделение за природно-математички и биотехнички науки, МАНУ, том **39**, бр. 1, стр. 69–74 (2018)
CONTRIBUTIONS, Section of Natural, Mathematical and Biotechnical Sciences, MASA, Vol. **39,** No. 1, pp. 69–74 (2018)

Received: March 16, 2018
Accepted: May 14, 2018

ISSN 1857–9027
e-ISSN 1857–9949
UDC: 634.11:631.532
DOI: 10.20903/csnmbs.masa.2018.39.1.120

Original scientific paper

DISTRIBUTION OF ROOT SYSTEM AT APPLE CV. GRANNY SMITH GRAFTED ON DIFFERENT DWARFING ROOTSTOCKS

Viktor Gjamovski[1*], Marjan Kiprijanovski[2], Tosho Arsov[2]

[1]Institute of Agriculture, Ss. Cyril and Methodius University, Skopje, Republic of Macedonia
[2]Faculty of Agricultural Sciences and Food, Ss. Cyril and Methodius University, Skopje, Republic of Macedonia
e-mail: v.gjamovski@zeminst.edu.mk

This paper analyses the distribution of root systems of nine dwarf apple rootstocks (M.9 T 984, M.9 T 337, Jork 9, Mark 9, Budagowski 9, M.9 EMLA, Pajam 1, Pajam 2 and Supporter 4). All rootstocks were grafted with apple cultivar Granny Smith. The study was performed in the experimental orchard established in the Prespa region (Resen, R. Macedonia). The experimental orchard was established in 2004, with a planting distance 3.5 m x 1.5 m. At the end of the 7th growing season following characteristics were evaluated: length and weight of the fine (fibrous) and coarse roots, and depth distribution of the root system. Among the evaluated rootstocks statistically significant differences in total length of the fine roots were not found. Between different rootstocks the results for total length of coarse roots showed more variability. In general, even 89% of the total length of root system belonged to fine roots, and the highest percentage (35%) was located at depths of 20 to 40 cm. Trees grafted on Mark 9 rootstock had the highest value for total root length, while the smallest values were registered on those grafted on Pajam 1 rootstock. Trees grafted on Supporter 4 rootstock had the greatest weight of the root system, while the smallest one was found on rootstock Budagowski 9.

Key words: apple; rootstocks; root system; depth distribution

INTRODUCTION

The root systems of fruit trees have a heredity-determined pattern. However, the some environmental factors like soil, climate, presence of a shallow hard rock or groundwater, as well as the cultural practices applied, can induce important changes in the root system distribution in soil [1–3].

Knowledge of the quantity, quality and distribution of roots is useful in agricultural production to provide information on the location of fertilizer application, tree spacing, intercrops, soil management and irrigation [4]. The development of root system is primarily affected by its origin (rootstock and variety combination), soil and climate conditions, and applied cultural practices. Atkinson et al. [5] and Atkinson [6] point out that the length of root systems of apples directly depends on the planting distance and the type of the rootstock.

According to Fante Júnior et al. [7] the assessment of such factors as the volume of soil explored, root length and root activity is a difficult task, and great difficulties are encountered in any sampling technique, including the time spent, limited information obtained and great variability of results. According to Vasconcelos et al. [8] a perfect method for evaluating roots does not exist because the suitability of a method for the evaluation of the root system depends on the *in situ* conditions.

The ratio between the tree root system and the aerial system in grown fruit trees is relatively constant within the same soil, regardless of the cultivar and rootstock. In general, the tree root is approximately 25–30% of the total tree mass in intensive orchards [9], and most of the roots are distributed within the 25–100 cm depth in temperate climate and mineral soils [10].

According to De Silva et al. [11] the main component of the root system of trees are fine roots (diameter < 2 mm) through which trees made the absorption of water and nutrients.

The objective of this study is to show the effects of various dwarfing apple rootstocks on distribution of the root system of Granny Smith apple cultivar under the specific conditions of the apple growing region of Prespa, South-Western Macedonia.

MATERIAL AND METHODS

The research was carried out in the experimental orchard located in the South-Western part of the Republic of Macedonia (Region of Lake Prespa). According to Scheffer's and Schachtschabel's classification, the soil is a texture class clay loamy soil, which is characterized by a very suitable texture. The root system distribution of the rootstocks M.9 T 984, M.9 T 337, Jork 9, Mark 9, Budagowski 9, M.9 EMLA, Pajam 1, Pajam 2 and Supporter 4 was evaluated using the scion cultivar Granny Smith. The trees were planted in 2004 at a spacing of 3.5 m × 1.5 m and were trained to slender spindle system. The experiment has been arranged in randomized block design with four replications of five trees per plot. The orchard is equipped with drip irrigation system. The study was carried out in 2010 (the 7th growing season). The development of root system, its length and weight was determined by digging of the model trees, according to the method of trench. From each different rootstock, 4 representative trees with similar vigor of the crown were selected. From each tree the digging of ¼ of the total predicted area of the root system, differently positioned, was done. The size of the trench was 1,25 m × 0,75 m, or a half of the distance between rows and a half of the distance between the trees. The distribution and development of the root system were followed at 3 different depths: from 0–20 cm; 20–40 cm and 40–60 cm.

The differences between rootstocks were evaluated by ANOVA analysis through General Linear Model (GLM) procedure. After GLM analyses, post hoc comparison of means was calculated by LSD. Results were expressed at the $P < 0.05$ level of significance.

RESULTS AND DISCUSSION

In Table 1 and Figures 1 and 2, the data of the length and distribution of the root system in the evaluated rootstocks are given. By analyzing the data on the length and distribution of the root system in the evaluated rootstock (Table 1, Figure 1, Figure 2), it can be concluded that there were no statistically significant differences in the total length of the fine roots between the evaluated rootstocks. The largest length of the fine roots was recorded in the rootstock Mark 9 (23947.2 cm), and the lowest in the rootstock Pajam 1 (15270.4 cm). A greater variability between rootstocks was observed in the length of the coarse roots (> 3 mm). The highest value for the total length of coarse roots was measured in the rootstock Supporter 4 (3617.6 cm). It was statistically significantly higher than in the rootstock Budagowski 9 (1017.6 cm).

Table 1. Length of the root system of different dwarfing rootstocks in Granny Smith apple trees (cm)

Rootstock	Soil depth (cm)							
	Fine roots (< 3 mm)				Coarse roots (> 3 mm)			
	0–20	20–40	40–60	Total	0–20	20–40	40–60	Total
M.9 T 984	6030.4^{b}	10273.6^{a}	4584.0^{a}	20888.0^{a}	435.2^{cd}	1417.6^{ab}	600.0^{bc}	2452.8^{ab}
M.9 T 337	7814.4^{ab}	8009.6^{a}	5467.2^{a}	21291.2^{a}	1236.8^{a}	1086.4^{ab}	577.6^{bc}	2900.8^{a}
Jork 9	8785.6^{ab}	9433.6^{a}	5092.8^{a}	23312.0^{a}	1051.2^{abc}	1534.4^{ab}	489.6^{bc}	3075.2^{a}
Mark 9	12672.0^{a}	7363.2^{a}	3912.0^{a}	23947.2^{a}	1033.6^{abc}	1486.4^{ab}	486.4^{bc}	3006.4^{a}
Budagowski 9	5604.8^{b}	6124.8^{a}	4945.6^{a}	16675.2^{a}	280.0^{d}	560.0^{b}	177.6^{c}	1017.6^{b}
M.9 EMLA	6812.8^{ab}	10088.0^{a}	5756.8^{a}	22657.6^{a}	484.8^{bcd}	1200.0^{ab}	1403.2^{a}	3088.0^{a}
Pajam 1	5044.8^{b}	5843.2^{a}	4382.4^{a}	15270.4^{a}	529.6^{bcd}	708.8^{ab}	1115.2^{ab}	2353.6^{ab}
Pajam 2	5926.4^{b}	6585.6^{a}	4611.2^{a}	17123.2^{a}	667.2^{abcd}	1489.6^{ab}	737.6^{abc}	2894.4^{a}
Supporter 4	8166.4^{ab}	8216.0^{a}	6171.2^{a}	22553.6^{a}	1110.4^{ab}	1640.0^{a}	867.2^{abc}	3617.6^{a}
Average	**7428.6**	**7993.1**	**4991.5**	**20413.2**	**435.2**	**1417.6**	**600.0**	**2452.8**

Values followed by the same letter in a column were not statistically different according to LSD test ($P < 0.05$).

In all the examined rootstocks, the largest length of the fine and coarse roots was recorded at a depth of 20 to 40 cm, with average values of 7993.1 cm, and 1417.6 cm, respectively. It is in line with the results of Arsov [11] who examined the distribution of the roots of the Jonagold apple variety grafted on M9 rootstock.

An exception to this statement is the data for the fine roots of the Mark 9 rootstock. The root length at the depth from 0 to 20 cm was greater in relation to the length at the depth from 20 to 40 cm (Figure 1). These data correlated with literature data that indicate a shallow development of the root of this rootstock and its susceptibility to drought.

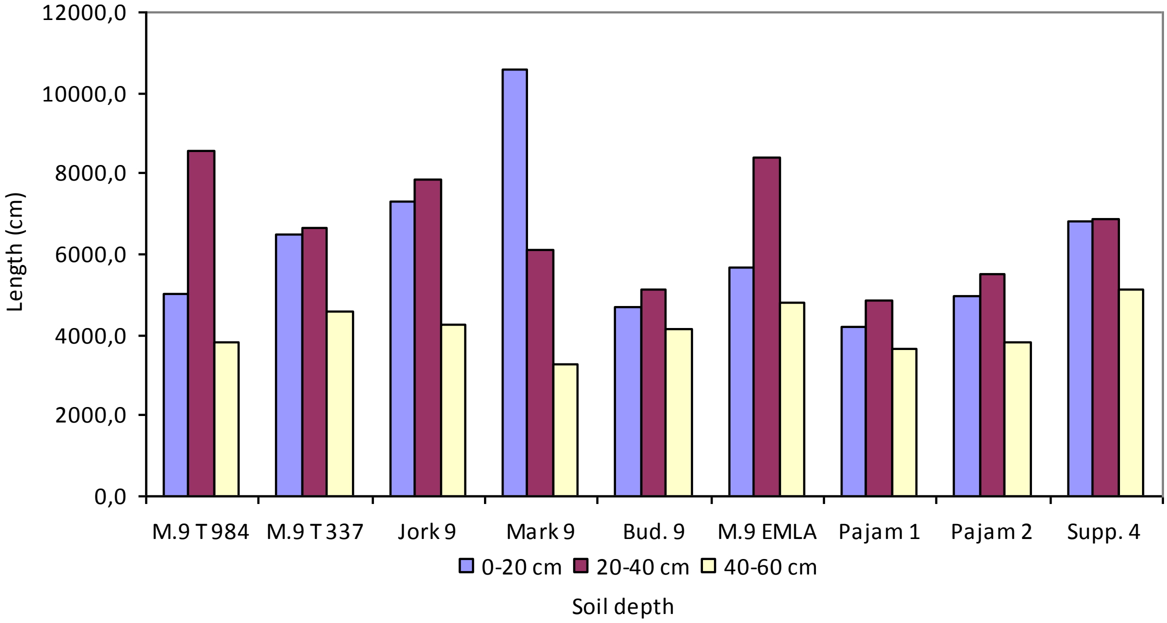

Figure 1. Vertical distribution of the fine roots of different dwarfing rootstocks in Granny Smith apple trees

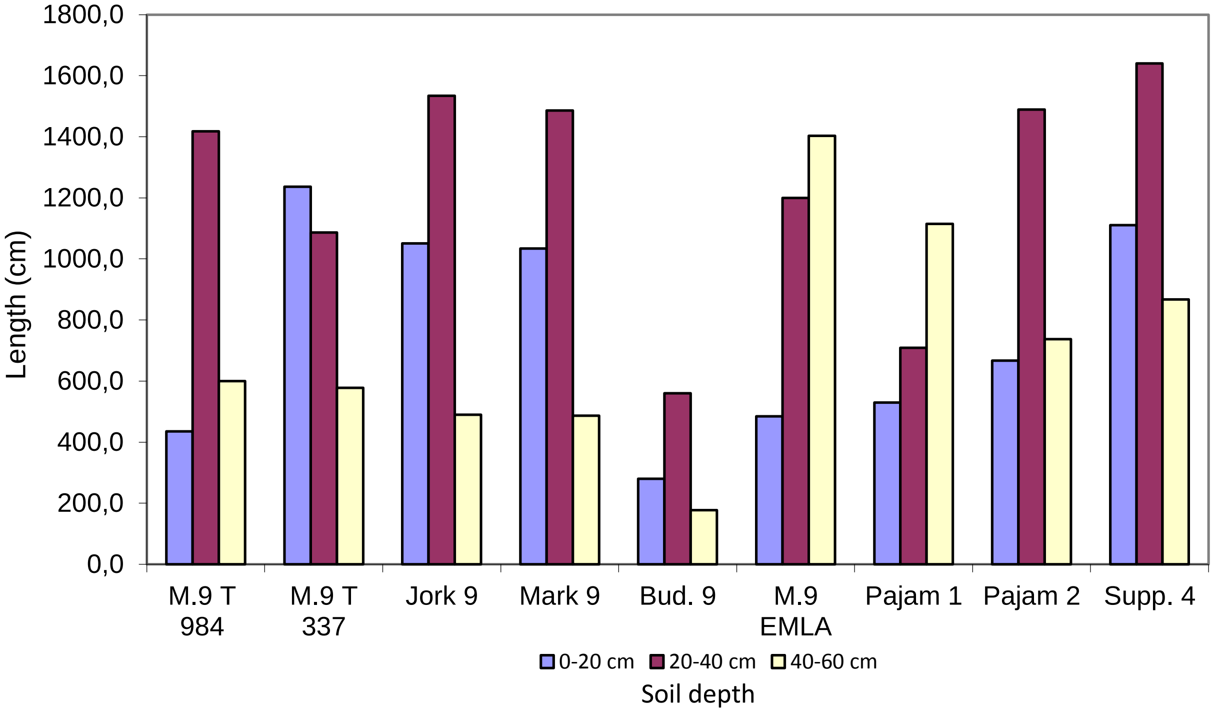

Figure 2. Vertical distribution of the coarse roots of different dwarfing rootstocks in Granny Smith apple trees

According to the data on distribution of different types of roots in different soil depths (Figure 3), it can be concluded that even 89% of the total length of the root system belongs to the fine roots and the largest percentage of them (35%) was located at a soil depth of 20 to 40 cm.

The data on the weight of the fine and coarse roots of the evaluated rootstocks, depending on the depth of the soil layer are given in Table 2. In all evaluated rootstocks the highest weight of the fine roots was registered at soil depths between 20 and 40 cm, except in the rootstock Mark 9 where weight of the fine roots in the first soil layer was higher. The highest total weight of the fine roots was found in Jork 9 rootstok (347.9 g), while the smallest one was found in Pajam 1 rootstok (182.3 g). Statistically significant differences between the rootstocks concerning the total weight of the fine root were not detected.

Expectedly, the highest weight of the coarse roots in all evaluated rootstocks was found at the depth of the soil layer from 0 to 20 cm, which on average was 349.8 g. According to the total values, the Supporter 4 rootstock had the highest weight of coarse roots (1344.4 g), statistically significantly higher than those in the Budagowski 9 rootstock, which had the lowest value (146, 7 g) for this parameter.

According to Arsov [12], the total weight of the fine roots in M9 rootstock grafted with Jonagold apple variety growth on the planting distance of 4 × 1.5 m was 573.6 g, and of the coarse roots it was 2397.4 g. This data correlates with the data obtained in this research.

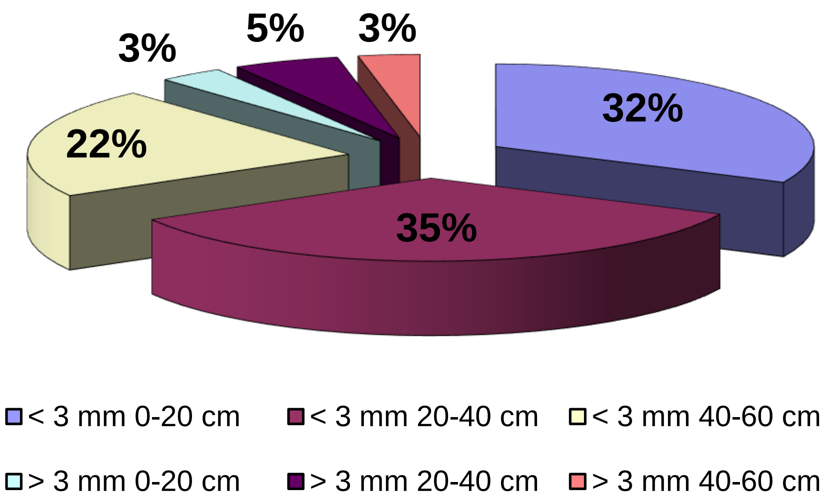

Figure 3. Length and depth distribution of total root system on various dwarfing apple rootstocks in Granny Smith apple trees

Table 2. Weight of the root system of different dwarfing rootstocks in Granny Smith apple trees (g)

Rootstock	Fine roots (< 3 mm)				Coarse roots (> 3 mm)			
	Soil depth (cm)							
	0–20	20–40	40–60	Total	0–20	20–40	40–60	Total
M.9 T 984	89.4[ab]	148.5[a]	52.3[a]	290.2[a]	148.2[b]	333.8[a]	124.2[abc]	606.2[ab]
M.9 T 337	108.5[ab]	128.2[a]	67.1[a]	303.7[a]	737.0[a]	351.1[a]	65.7[bc]	1153.7[a]
Jork 9	136.6[ab]	151.0[a]	60.3[a]	347.8[a]	253.6[ab]	436.0[a]	56.9[bc]	746.6[ab]
Mark 9	165.1[a]	105.0[a]	40.7[a]	310.7[a]	276.4[ab]	308.8[a]	87.5[bc]	672.7[ab]
Budagowski 9	60.7[b]	93.0[a]	42.5[a]	196.1[a]	96.0[ab]	32.7[b]	17.9[c]	146.7[b]
M.9 EMLA	89.6[ab]	126.7[a]	75.2[a]	291.5[a]	98.1[b]	333.2[a]	276.7[a]	708.0[ab]
Pajam 1	52.9[b]	63.9[a]	65.5[a]	182.3[a]	345.8[ab]	173.7[a]	184.1[abc]	703.7[ab]
Pajam 2	84.2[ab]	102.9[a]	67.9[a]	255.0[a]	509.3[ab]	451.6[a]	188.2[abc]	1149.1[a]
Supporter 4	120.7[ab]	112.9[a]	75.4[a]	309.0[a]	683.7[a]	456.3[a]	204.4[ab]	1344.4[a]
Average	**100.9**	**114.7**	**60.7**	**276.3**	**349.8**	**319.7**	**133.9**	**803.4**

Values followed by the same letter in a column were not statistically different according to LSD test (P < 0.05).

CONCLUSIONS

The mass and the length of the root system, and its horizontal and vertical layout are important elements in determining the planting distance, as well as for applying agro-technical measures in the orchard.

Between the nine economically most important rootstocks evaluated in Prespa region statistically significant differences were not found . The highest root length in all investigated rootstocks was found at the soil depths between 20 and 40 cm. An exception to this is the root system of the trees on Mark 9 rootstock where the highest length was found at the first soil depth (0-20 cm). Total root lengths were the highest in the trees on Mark 9, Supporter 4 and Jork 9 rootstocks, while the lowest values were registered in the trees on Pajam 1 and Budagowski 9 rootstocks. The trees grafted on Supporter 4 had the highest weight of coarse roots, while the lowest one was found in the trees grafted on Budagowski 9 rootstock.

REFERENCES

[1] V. A. Kolesnikov, *The Root System of Fruit Plants*, WASCHNIL Press, Moscow, 1971.

[2] O. Tudosescu, P. Parnia, Tree root architecture depending on rootstock and cultivar in apple (in Romanian), *Lucr. St. ICPP*, **II**, Pitesti, Romania, (1975), pp. 189–200.

[3] S. Stan, M. Cotorobai, Influence of growth regulators on tree rooting system in apple (in Romanian), *Lucr. St. ICPP*, **X**, Pitesti, Romania, (1983), pp. 137–142.

[4] A. A. Fracaro, F. M. Pereira, Distribuição do sistema radicular da goiabeira ‘Rica’ produzida a partir de estaquia herbácea, *Revista Brasileira de Fruticultura*, v. **26**, n. 1 (2004), pp. 183–195.

[5] D. Atkinson, D. Naylor, G. A. Coldrick, The effect of tree spacing on the apple root system, Horticulture Research, **16** (1976), pp. 89–105.

[6] D. Atkinson, The Distribution and Effectiveness of the Roots of Tree Crops, *Hort. Rev*., **2**, (1980), pp. 424–490.

[7] L. Fante Junior, K. Reichardt, L. A. C. Jorge, S. Crestana, Distribuição do sistema radicular do milho em terra roxa estruturada latossólica: I. Comparação de metodologias, *Scientia Agricola*, v. **51**, n. **3** (1994), pp. 513–518.

[8] A. C. M. Vasconcelos, A. A. Casagrande, D. Perecin, L. A. C. Jorge, M. G. A. Landell, Avaliação do sistema radicular da cana-de-açúcar por diferentes métodos, *Revista Brasileira de Ciência do Solo*, v. **27**, n. **3**, (2003), pp. 849–858.

[9] M. M. Westerwood, *Temperate-Zone Pomology*, Freeman & Company, W. H., 1978, New York.

[10] A. Negrila, *Pomology*, *Didactica si Pedagogica*, Bucharest, 1971.

[11] N. De Silva, A. J. Hall, D. S. Tustin, P. W. Gandar, Analysis of distribution of root length density of apple trees on different dwarfing rootstocks, *Annals of Botany*, **83** (1999), pp. 335–345.

[12] T. Arsov, *Intensive systems in apple growing*, PhD, Ss. Cyril and Methodius University Skopje, Faculty of Agricultural Science and Food, (2009), p. 94.

ДИСТРИБУЦИЈА НА КОРНОВИОТ СИСТЕМ КАЈ СОРТАТА ЈАБОЛКО ГРЕНИ СМИТ КАЛЕМЕНА НА РАЗЛИЧНИ СЛАБОБУЈНИ ПОДЛОГИ

Виктор Ѓамовски[1*], Марјан Кипријановски[2], Тошо Арсов[2]

[1]Земјоделски институт, Универзитет „Св. Кирил и Методиј“, Скопје, Република Македонија
Факултет за земјоделски науки и храна, Универзитет „Св. Кирил и Методиј“,
Скопје, Република Македонија,

Во трудот се содржани резултатите од споредбени испитувања на девет слабобујни подлоги за јаболко (M.9 T 984, M.9 T 337, Jork 9, Mark 9, Budagowski 9, M.9 EMLA, Pajam 1, Pajam 2 и Supporter 4), калемени на сортата грени смит, во однос на развојот и дистрибуцијата на корeновиот систем. Испитувањата се извршени во 7-та вегетациска година на овошките во експериментален овоштарник лоциран во регион на Преспа во Р Македонија. Овоштарникот е подигнат во 2004 година, со садење на овошките на растојание од 3,5 m × 1,5 m. Беа евалуирани следните карактеристики: должина и тежина на обраставачките (влакнести) и скелетните коренчиња и дистрибуција по длабочина на кореновиот систем. Анализирајќи ги добиените податоци, заклучуваме дека помеѓу испитуваните подлоги не постојат статистички разлики во вкупната должина на обраставачките коренчиња. Во резултатите за вкупна должина на скелетните коренчиња е забележана поголема варијабилност меѓу подлогите. Во принцип дури 89% од вкупната должина на кореновиот систем отпаѓа на обрастувачките коренчиња, а највисокиот процент (35%) коренчиња се наоѓаат на длабочина од 20 до 40 cm. Овошките на подлогата Mark 9 имаат највисока вредност на вкупната должина на коренот, а најмалата оние кои се пресадени на Pajam 1. Овошките на подлогата Supporter 4 имаат најголема тежина на корeновиот систем, додека најмала тежина имаат тие на Budagowski 9.

Клучни зборови: јаболко; подлога; коренов систем; дистрибуција на корен

INSTRUCTIONS FOR AUTHORS

The journal *Contributions*, *Section of Natural, Mathematical and Biotechnical Sciences* is an official publication of the Macedonian Academy of Sciences and Arts. It is published twice a year. The journal publishes **original scientific papers, short communications, reviews, professional papers** and **educational papers** from all fields of:

natural sciences – physics, chemistry, biology, geography, geology;
mathematical sciences – mathematics, informatics;
biotechnical sciences – agriculture and food, forestry.

This journal also publishes, continuously or occasionally, the bibliographies of the members of the Macedonian Academy of Sciences and Arts, book reviews, reports on meetings, information on future meetings, important events and dates, and various headings which contribute to the development of the corresponding scientific field.

The **original scientific papers** report unpublished results of completed original scientific research. Experimental data should be presented in a way that enables reproduction and verification of analyses and deductions on which the conclusions are based. The manuscripts should normally not exceed 6000 words.

The **short communications** should contain completed (but briefly presented) results of original scientific research. The manuscripts should normally not exceed 2000 words.

The **reviews** are submitted at the invitation of the Editorial Board. They should be critical surveys of an area in which preferably the author himself is active. The reviews can be longer than typical research articles but should generally be limited to 10000 words including references, tables and figures.

The **professional papers** report on useful practical results that are not original but help the results of the original scientific research to be adopted into scientific and production use. Manuscripts should normally not exceed 4000 words.

The **educational papers** report on the activities in the laboratory and classroom and the needs of the community of educators in all mentioned fields. Manuscripts should normally not exceed 4000 words.

Submission of manuscripts

The authors bear the sole responsibility for the content of the contributions. It is assumed that by submitting their paper the authors have not violated any internal rules or regulations of their institutions related to the content of the contributions. Submission of a paper implies that it has not been published previously, that it is not under consideration for publication elsewhere, and that, if accepted, will not be published elsewhere in the same form, in English or in any other language, without the written consent of the Publisher.

A cover letter must accompany the manuscript submission. It should contain full names of all authors and their affiliation, the manuscript title and the name and contact information for the corresponding author. Please provide e-mail address and phone number. For submission, please send an electronic version of the manuscript (in MS Word) at: smalinovska@manu.edu.mk

Preparation of manuscripts

Prepare the entire manuscript in double-space typing, on numbered pages of A4 format with margins of 2.5 cm on each side. Do not use footnotes.

The papers should be written in the shortest possible way and without unnecessary repetition. The original scientific papers, short communications, professional papers and reviews should be written in English. An Abstract and list of key words in Macedonian must accompany each manuscript. For contributions by authors who are not speakers of Macedonian, the above data will be provided by the Editorial Board.

The manuscript should contain: title, authors names and addresses, abstract, key words, introduction, experimental or theoretical background, results and discussion, acknowledgement (if desired) and references.

Title. It should be brief and informative but should define the subject of the manuscript. It should include most of the key words.

Authorship. List the first and last name of each author. Omit professional and official titles. Give the complete mailing address of each author. For the corresponding author include an e-mail address and a phone number. The name of the corresponding author should carry an asterisk.

Abstract. Each manuscript should be provided with an abstract of about 100–150 words. It should give the aim of the research, methods or procedures, significant results and conclusions. Define any abbreviations used in the abstract. The text of the abstract should contain as many key words as possible.

Key words. Up to 5 key words or phrases should be given separately to facilitate indexing and on-line searching.

Introduction. The most important previous results related to the problem in hand should be reviewed avoiding a detailed literature survey but clearly pointing to the place of the research in hand within the general area of scientific knowledge. The aim and importance of the research should be clearly stated.

Experimental section. This section should contain a description of the materials used and methods employed in form which makes the results reproducible, but without detailed description of already known methods.

Manuscripts that are related to theoretical studies, instead of experimental section should contain a sub-heading *theoretical background* where the necessary details for verifying the results obtained should be stated.

Results and discussion. The authors should discuss their findings, postulate explanations for the data, elucidate models and compare their results with those of other works. Irrelevant comparisons and speculations unsupported by the new information presented in the manuscript should be avoided. The conclusions should be not given separately but included in this section. In special cases a separate section containing conclusions could be included.

Tables. They should be given with a suitable caption and should be numbered consecutively with Arabic numerals. Footnotes to tables should be typed below the table and should be referred to by superscript lowercase letter. Each table should be typed on a separate sheet. The correct position of the tables should be marked on the manuscript.

Figures. Figures (photographs, diagrams and schemes) should be numbered consecutively with Arabic numerals in order to which they mentioned in the text. They should accompany the manuscript but should not be imbedded in the text. Each figure should be clearly marked with the figure number and the first author's name. All figures should have captions that should be supplied on a separate sheet. Correct position of the figures should be marked on the manuscript. The size of the symbols for the physical quantities and units as well as the size of the numbers and letters used in the reduced figures should be comparable with the size of the letters in the main text of the paper. Each figure or group of figures should be planned to fit, after appropriate reduction, into the area of either one or two columns of text. The maximum finished size of a one-column illustration is 8.0 cm and that of a two-column illustration is 17.0 cm width. Make sure you use uniform lettering and sizing of your original artwork. All figures should be printed on a high quality printer or graphics plotter. Figures should be also sent in electronic form as TIFF or JPG files with minimum 300 dpi or higher resolution.

Color illustrations in print can be included only at the author's expense.

Units. The SI (Systeme Internationale d'Unites) for quantities and units should be used throughout the whole text. In marking the axes, the symbol, of the corresponding quantity (in italics) should be **divided** by the unit of this quantity. If nomenclature is specialized, nomenclature section should be included at the end of the manuscript, giving definitions and dimensions for all terms.

The **names of chemical substances** should be in accordance with the IUPAC recommendations and rules or *Chemical Abstract* practice.

The results of elemental analyses of organic compounds should be given in the following form:

Anal. $C_{12}H_{16}O$ (176.26).

Calc'd: C 81.77; H 9.15; O 9.08 %.

Found: C 81.63; H 9.36; O 9.01 %.

When a large number of compounds have been analyzed, the results should be given in tabular form.

Formulas and equations. Chemical equations should be balanced and numbered consecutively along with mathematical equations or other mathematical expressions. All of them should be marked with Arabic numerals in parenthesis in the right hand margin. The use of equation editor (Word) for typesetting the equations is recommended. Strokes (/) should not be used instead of parentheses.

Acknowledgement. Financial support, advice or other kinds of assistance can be included in this section.

References. Literature references should be numbered and listed in order of citation in the text. They should be selective rather than extensive with the exemption to review articles. Avoid references to works that have not been peered-reviewed. Citation of a reference as "in press" implies that it has been accepted for publication. Abbreviations of the titles must follow the internationally accepted practice.

The surname (not first name and/or initials) of one or two authors may be given in the text, whereas in case of more than two authors they should be quoted as, for example, Julg *et al.* [1]. In the list of references the citation should be as follows:

Journals:

[1] J. Zhang, X. Wang, H. Xie, Phonon energy inversion in graphene during transient thermal transport, *Phys. Lett*. A, **377** (2013), pp. 721–726.

[2] G. Jovanovski, P. Makreski, B. Šoptrajanov, B. Kaitner, B. Boev, Minerals from Macedonia, *Contributions, Sec. Math. Tech. Sci*., MANU, **XXVI**, 1 (2005), pp. 7–84.

[3] A. Čarni, M. Kostadinovski, V. Matevski**,** Species composition and syntaxonomic consideration of two communities of the Drabo-Cardaminion hirsutae in the southern part of the Republic of Macedonia, *Acta Bot. Croat*., **62** (2003), pp. 47–56.

[4] D. Dimovski, A geometric proof that boundary links are homotopically trivial**,** *Topology Appl.*, **29** (1988), pp. 237–244.

[5] F. C. Oliveira, Á. C. Collado, L. F. C. Leite, Autonomy and sustainability: An integrated analysis of the development of new approaches to agrosystem management in family-based farming in Carnaubais Territory, Piauí, Brazil, *Agr. Syst.*, **115** (2013), pp. 1–9.

Books:

[1] J. A. Roels, *Energetics and Kinetics in Biotechnology*, Elsevier Biomedical Press, Amsterdam, New York, Oxford, 1983.

[2] H. Chum, M. Baizer, *The Electrochemistry of Biomass and Derived Materials*, ACS Monograph 183, American Chemical Society, Washington, DC, 1985, pp. 134–157.

[3] J. W. Finley, G. A. Leveille, Macronutrient substitutes, in: *Present Knowledge in Nutrition*, E. K. Ziegler, L. J. Filer Jr. (Eds), ILSI Press, Washington DC, 1996, pp. 581–595.

[4] Gj. Filipovski: *Characteristic of the Climatic and Vegetational Soil Zones in the Republic of Macedonia*, Macedonian Academy of Sciences and Arts, Skopje, 1996.

Scientific meetings:

[1] M. S. Steel, Creating woodlands for wildlife and people in Scotland, *18th Commonwealth Forestry Conference; Restoring the Commonwealth's Forests: Tackling Climate Change*, Edinburgh, Scotland, 2010, Book of Abstracts, p. 3.

Note that the *full titles* of the cited papers should be included.

For the web references, as a minimum the full URL should be given. Any further information, if available (author names, dates, reference to a source publication, etc.) should also be given.

Editorial process

Receipt of manuscripts. The received manuscript is read and examined for conformity to these Instructions to Authors. Failure to meet the criteria outlined will result in return of the manuscript for correction before evaluation.

Peer review/evaluation. Papers received by the Editorial Board are sent to two referees (one in the case of professional and educational papers). Identities of the reviewers will not be released to the authors. The review process is expected to be complete within 3 months, but conflicting recommendations and other unpredictable events may cause some delay.

The comments and recommendations of the referees and the Editorial Board are sent to the authors for further action. The authors are allowed 30 days to undertake revisions and return the corrected text to the Editorial Board. The final decision on acceptance or rejection is made by the Editorial Board. This decision, together with any relevant reasons, will be send to the corresponding author.

Publication process. The accepted manuscript is again checked for conformation to the Instructions to Authors and to ensure that all necessary paperwork is present. Any areas that are identified as problematic will be addressed by the Editorial Board in consultation with the corresponding author. The papers will be prepared for publication by a professional copy editor responsible for ensuring that the final printed work is consistent in form and style.

Galley proofs. A galley proof is sent to the corresponding author. It should be checked very carefully and must be returned within 2 days of receipt. The proof stage is not the time to make extensive corrections, additions, or deletions.

Reprints. The corresponding author will receive, free of charge, 20 reprints of the paper published in the *Contributions*. Additionally he will receive a complementary copy of the journal.